CONTROL AND METHODS FOR PV INVERTER MINIATURIZATION

by

Hamidreza Jafarian

A dissertation submitted to the faculty of
The University of North Carolina at Charlotte
in partial fulfillment of the requirements
for the degree of Doctor of Philosophy in
Electrical Engineering

Charlotte

2017

Approved by:

____
Dr. Babak Parkhideh

____
Dr. Johan Enslin

____
Dr. Robert Cox

____
Dr. Maciej Noras

ABSTRACT

HAMIDREZA JAFARIAN. Control and methods for PV inverter miniaturization. (Under the direction of DR. BABAK PARKHIDEH)

Analyzing the price of PV generation systems in different market sectors shows that the portion of inverter cost and Balance of System (BoS) are increased due to advent of new PV module technologies and dramatic cost reduction in PV module production in recent years. The BoS cost for residential PV systems changed from 15% to 24% between the 2009 and 2012. The same trend can be seen in other power level sectors such as commercials and utility level PV generations. After 2012, due to investment on new PV inverter architectures the BoS cost share reduced to 20% at beginning of 2016, but still there is a large room for improvement. Therefore, it is critical to come up with an architecture that can revolutionize the PV generations in different power levels, to reduce the inverter cost and BoS costs.

The available grid-tied PV inverter technologies can be classified in two main categories such as central PV inverter systems and module-integrated PV inverter systems. However, the balance of system and inverter cost are still a major part of PV inverter systems' cost. The main goal of this dissertation is to design and implement a decentralized control scheme for the grid-tied AC-stacked PV inverter architecture which is expected to be more cost effective than others due to different cabling structure, connection and physical implementation of the system. The Decentralized control scheme allows the inverter miniaturization, because there is no need for wideband communications. In addition, this architecture because of lower counts of components, has the potential to be miniaturized and have high power density if it can be implemented in a decentral manner.

This dissertation will study this architecture for the first time and analyze the feasibility and stability of decentralized Hybrid Current/Voltage-mode Control (HCVC) scheme for this architecture with minimum communication requirements using the Relative Gain Array (RGA) approach. Based on RGA analysis, it is shown for the first time that a fully decentralized control architecture with no communication between inverters can regulate the output power properly and generate the maximum power from PV modules with minimum mismatch losses.

Moreover, novel grid integration and smart inverter functions such as reactive power support and background harmonics mitigation, are designed and implemented and analyzed for this architecture. The reactive power control method and background harmonics mitigation methods introduced in this thesis have the main advantage of maximizing the operation margin for increasing the system stability during nominal operating condition and during disturbances such as partial shading, gird voltage sag and swell and frequency disturbances.

Controller robustness analysis and evaluating the impact of components inaccuracies on robust operation of this decentralized control scheme are also provided in this dissertation. Robustness analysis is crucial, especially for distributed architectures where subsystems are regulated with local measurements. The Smart Inverter Robustness Index (SIRI) is introduced as a comprehensive tool for evaluating the robust operation of grid-tied PV inverter systems and the impact of component inaccuracies on robustness of AC-stacked PV inverter system is studied.

The proposed control methods and architectures in this research have been verified using mathematical modeling and analysis, off-line simulation in Matlab/Simulink, Controller

Hardware-in-the-Loop (CHiL) and lab-scale experimental setup. All prove the effectiveness of proposed methods during symmetrical conditions, asymmetrical conditions and fault conditions.

DEDICATION

I dedicate this dissertation to my late father, my mother,

my wife, my sister and brother for their endless love and support.

BIOGRAPHY

The author, Hamidreza Jafarian was born in Mashhad, Iran. He received his B.Sc. degree with honors in Electrical Engineering from Amirkabir University of Technology (Polytechnic Tehran), Tehran, Iran. He received his first M.Sc degree in Electrical Engineering from Ferdowsi University of Mashhad, Mashhad, Iran and the second M.Sc degree in Electrical Power Engineering from the Institute of Power Electronics and Electrical Drives of RWTH-Aachen University, Aachen, Germany. In 2013, he started to pursue his PhD in Electrical Engineering in University of North Carolina at Charlotte, Charlotte, NC. In the summer of 2014, he was an intern at SineWatts Inc, NC, working on design and development of a module-level PV inverter architecture. In the summer of 2015, he was an intern at Plexim Inc. MA, working on development of different offline simulation, processor-in-the-loop and hardware-in-the-loop models. Since May 2017, he has joined WiTricity Co. as a Staff Scientist working on the design and development of control schemes for wireless power chargers for electric vehicles. Hamidreza is also a recipient of several awards including the best oral presentation in APEC 2017. His research interests are power electronics control, grid integration of renewable energies and energy storage systems.

ACKNOWLEDGEMENTS

I would like to start by acknowledging that this dissertation would not have been possible without unmatched mentorship and extraordinary support provided by my advisor, Dr. Babak Parkhideh. I doubt I can ever show enough gratitude for his thoughtful mentorship and guidance and his confidence in my abilities. He taught me to become an independent researcher by thinking out of the box. I hope to be privileged to benefit from his mentorship and collaboration throughout my future career.

I would like to express my deep appreciation to my committee members, Dr. Johan Enslin, Dr. Robert Cox, and Dr. Maciej Noras for their valuable suggestions and feedbacks which helped me during my PhD research.

It has been a great pleasure to work with the SineWatts, Inc, Plexim Inc. and WiTricity Corporation. Working in these premier companies provided me with a unique opportunity to collaborate with the great experts in power electronics. I would like to thank my mentors and supervisors for their support, Dr. Shibashis Bhowmik, Dr. Beat Arnet, Mr. Steve Ganem, Mr. Aldo D'Amico, and Dr. Milisav Danilovic.

During my four years of research at Energy Production and Infrastructure Center (EPIC), I had a special opportunity to make great friends that I would like to thank them all. I would like to thank my lab mates, especially, Dr. Deepak Somayajula, Dr. Iman Mazhari, Mr. Mehrdad Biglarbegian, Mr. Shariar Nibir, Mr. Soheil Yousefi, Mr. Namwon Kim, Mr. Steve Banasik, Mr. Daniel Evans, and Mr. Saurabh Trivedi.

Outside work, I have been blessed with continued support and love of my family and I am forever thankful for having them in my life. Last but not the least, I would like to thank my love and my best friend, *Sara Shahbazi*, for her endless caring, understanding, encouragement and love. Without her support, presenting this work was not possible. My heartfelt gratitude.

TABLE OF CONTENTS

LIST OF TABLES

LIST OF FIGURES

CHAPTER 1: INTRODUCTION

Growing environmental concerns and energy independence have led to increase of penetration of renewable energy systems into power networks. Wind and photovoltaic energy are the major renewable sources of electricity production, which is 67.1% of renewable power capacity worldwide at the end of 2015 [1]. Particularly, solar PV systems received significant research attention due to the advent of new technologies and cost reduction. In 2015, the solar PV capacity growth rate worldwide was 28.2%, the highest among all sources of energy [1]. However, increasing integration of PV systems may violate the grid standards and requirements. For example, in high penetrated PV networks, due to the intermittent nature of solar PV generations, power supplied by PV generation may not match with power demand and potential overloading or voltage rises can appear at power network buses [2-5]. The suggested solution for this issue is the requirement of participation of PV inverter systems in voltage regulation through reactive power control [2, 6]. Other Possible problems in networks with high penetrated PV generations are harmonic emission of injected current [7, 8], network resonance [9, 10], false islanding detection [11], overloading of network equipment that should be considered [12]. Consequently, new standard regulations are needed to achieve safe and reliable operation of power networks using renewable energies.

1.1 Motivation

Analyzing the price of PV generation systems in different market sectors shows that the portion of inverter cost and Balance of System (BoS) cost are increased due to advent of new PV module technologies and dramatic cost reduction in PV module production in recent years [1]. Therefore, it is critical to come up with a new architecture that can transforms the PV power plant implementation, to reduce the inverter cost and BoS costs.

Different PV inverter architectures have been introduced such as central technologies like central inverters, string inverters and string inverter with DC power optimizer, and panel level architectures like micro-inverter which could reduce the cost share of inverter and BoS. However, the balance of system and inverter cost are still a major part of PV inverter systems. The main goal of this dissertation is to design and implement a decentralized control scheme for AC-stacked PV inverter architecture, shown in Figure 1.1 which is expected to be more cost effective than others due to different cabling structure, connection and physical implementation of the system. Decentralized control scheme allows the inverter miniaturization, because there is no need for wideband communications. In addition, this architecture because of lower counts of components, has the potential to be miniaturized and have high power density if it can be implemented in a decentral manner. This dissertation will study this architecture for the first time and analyze the feasibility and stability of decentralized Hybrid Current/Voltage-mode Control (HCVC) scheme for this architecture with minimum communication requirements. Moreover, grid integration and smart inverter functions such as reactive power support and harmonics mitigation are designed and implemented and analyzed for this architecture to improve the performance of AC-stacked PV inverter systems in the future electrical networks with high penetrated Distributed Generations (DG).

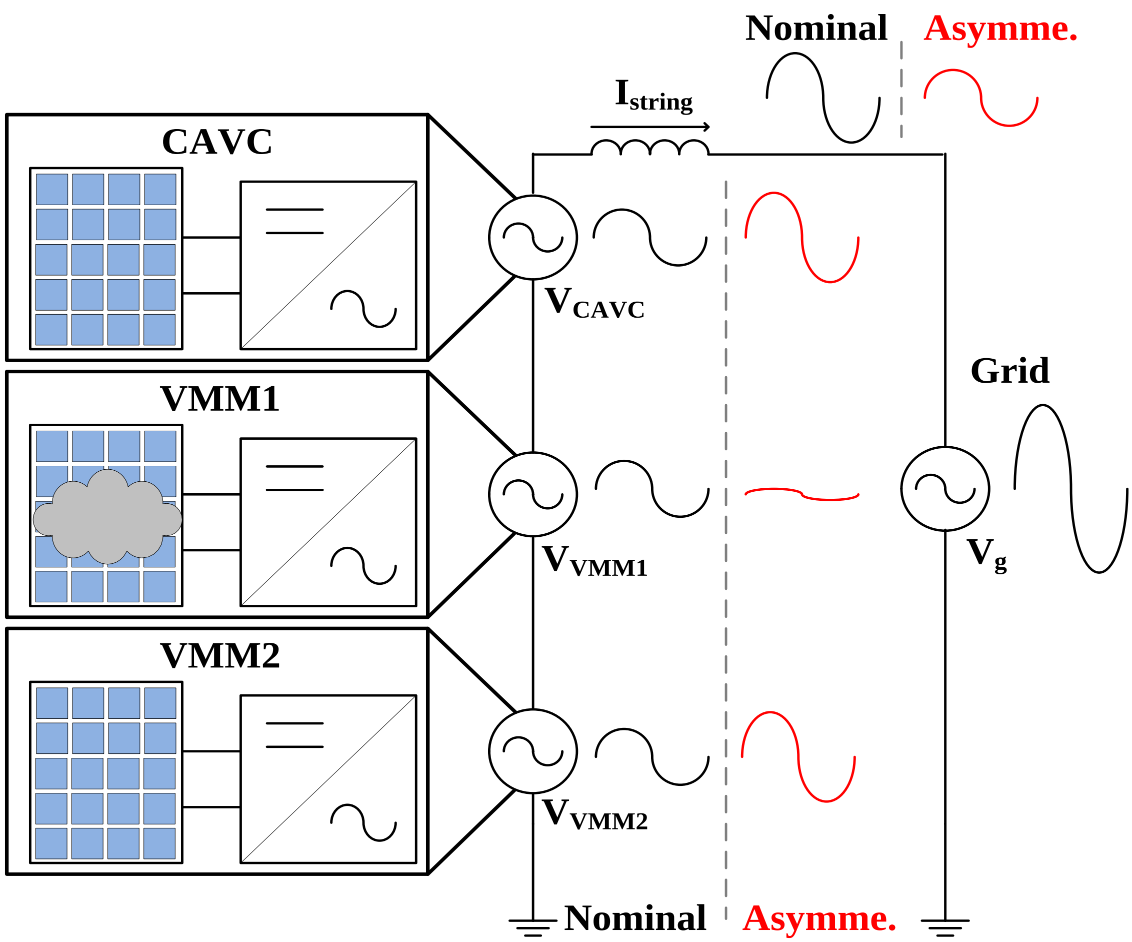

Figure 1.1. AC-stacked PV inverter architecture schematic.

1.2 Aim and Outline

Based on the motivation provided in the previous section, the aims of this research are:

- Available inverter architectures are briefly described and the main advantages and drawbacks of those configuration are explained.
- Grid-tied AC-stacked PV inverter architecture as a version of Cascaded H-bridge (CHB) PV inverter is described.

- Available control schemes for cascaded h-bridge inverters and AC-stacked PV inverters are reviewed and the popular control methods are classified based on implementation of different stages of controller.
- Feasibility of decentralized control algorithm for AC-stacked PV inverter architecture is proved, utilizing Relative Gain Array (RGA) approach.
- Based on RGA analysis, Hybrid Current/Voltage Control (HCVC) method is introduced and feasibility of this control scheme is verified using mathematical analysis.
- Effectiveness of the proposed HCVC method is verified by simulation results in different conditions such as nominal operating condition, full string shading, partial shading, grid disturbances etc.
- To further verify the HCVC method, an experimental test-bed is developed and performance of HCVC control method is evaluated in different conditions such as nominal operating condition, string shading, partial shading, grid disturbances and etc.
- Feasibility of controlling the PV string voltage phase by one inverter in the string is shown with mathematical analysis and vector diagrams.
- Single-member Phase Compensation (SmPC) method is introduced to control the output power of AC-stacked PV inverter system with minimum communication requirement.
- Effectiveness of the proposed SmPC method is verified by simulation results in different conditions such as unity power factor, lagging, leading and different irradiances.

- SmPC method performance is further verified using experimental results in different active and reactive power conditions.
- Smart inverter functionalities and new strategies for implementing such functions are introduced.
- The impact of grid background harmonics on performance of the current control of AC-stacked PV inverter system is analyzed using mathematical analysis and output impedance in frequency domain.
- Two control methods for mitigating the impact of grid background harmonics on current controller of HCVC are introduced and performance of these methods are evaluated using mathematical modeling and output impedance analysis in frequency domain.
- The effectiveness of proposed Single-member Phase Compensation (SmPC) and All-member Phase Compensation (AmPC) are verified using simulation results in Simulink.
- A Control Hardware-in-the-Loop (CHiL) test-bed is developed to better analyze the effectiveness of SmPC and AmPC methods and their performances are compared in detail in different grid voltage harmonics and disturbances.
- A new index called Smart Inverter Robustness Index (SIRI) is introduced to evaluate the robust operation grid-tied PV inverters
- Impact of components variation due to environmental condition, aging and manufacturing inaccuracies on robust operation of grid-tied PV inverters is studied.

- Impact of inaccuracies on robust operation of string PV inverters and AC-stacked PV inverter is compared using SIRI index and statistical analysis using Monte Carlo sampling method and Latin Hypercube Sampling (LHS).

1.3 Key Contributions

- ✓ AC-stacked PV inverter architecture has been modelled in this dissertation. The non-linear model consists of detailed PV module with one diode and shunt resistor. The performance of open-loop and closed loop model has been studied during different grid conditions.
- ✓ The feasibility of decentralized control method has been proven by Relative Gain Array approach for symmetric and asymmetric conditions and the best possible input/output pairing sets have been identified to decouple the system to decentralize controlled subsystems.
- ✓ The primary HCVC control scheme, has been extended with all the practical constraints such as PV module non-linear characteristics and grid integration requirements, such as reactive power support, harmonic mitigation, voltage support etc.
- ✓ Decentralized HCVC method has been implemented in simulation, in CHiL and in experimental setup and the performance of proposed control architecture has been proven in nominal condition and different fault conditions.
- ✓ The control robustness of the architecture has been evaluated by a proposed novel index called Smart Inverter Robustness Index. The SIRI takes into the account the physical inaccuracies in general and relates them to the system level performance

including conversion efficiency, total harmonics distortion, power factor compliance and MPPT effectiveness.

- ✓ Smart inverter functions have been designed and implemented for this architecture. Single-member Phase Compensation (SmPC) method has been introduced and analyzed for reactive power compensation of this inverter which can be extended to other smart inverter functions like harmonics support.
- ✓ The impact of grid voltage background harmonics on the performance of current controller of grid-tied PV inverters has been evaluated using impedance analysis in frequency domain. Two different methods for mitigating the impact of background harmonics have been introduced and their performances are compared using simulation and experimental results.

CHAPTER 2: GRID-TIED AC-STACKED PV INVERTER ARCHITECHTURE

2.1 Introduction

In this chapter, different configurations of grid-tied PV inverter systems are introduced and analyzed. Cascaded multilevel inverters as one of the most popular architectures in recent years is explained and different control schemes which proposed for this architecture in the literature are presented and evaluated in this chapter. Finally, AC-stacked PV inverter architecture which is a version of cascaded multilevel inverters is introduced. In section 2.2, available PV inverter architectures are classified to central and module-integrated configurations. Cascaded multi-level inverter and its operation principle is presented in section 2.3. Available control schemes for this architecture are analyzed in detail in section 2.4. Finally, AC-stacked PV inverter architecture, which is studied in this dissertation, is introduced in section 2.5.

2.2 PV Inverter Configurations

Different PV inverter configurations have been introduced to convert the solar energy to AC power that can be used for electrical loads and also in integration to electrical network. These configurations are shown in Figure 2.1. Available technologies shown in this figure can be classified into two main categories, central architectures and module-integrated architectures.

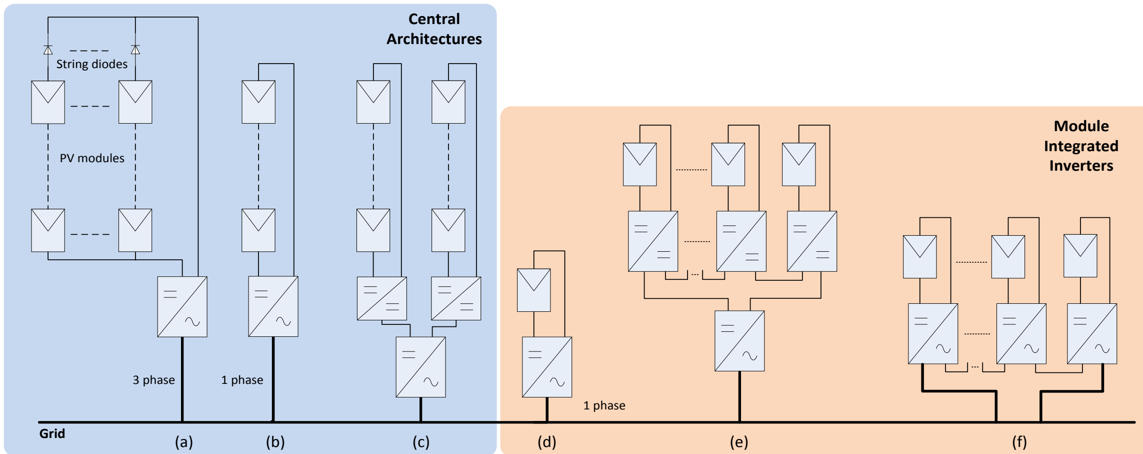

Figure 2.1. Grid-tied PV inverter configurations.

Central inverter architecture which is presented in Figure 2.1.(a), has the advantages of high efficiency power conversion and low hardware cost per watt. In this architecture, proper number of PV modules are connected in series to build up required voltage for grid connection with no extra boosting stage. Strings of PV panels are connected through string diodes as shown in Figure 2.1.(a). The resulting large PV generator is connected to the input of a central inverter. a central inverter is typically in three-phase but there are some examples of single phase central inverter. Central inverter is typically a full-bridge with IGBTs, BJTs or even wide bandgap MOSFETs. This inverter consists of power decoupling capacitors at the input and a low pass filter at the output. Installation of this architecture is time consuming, costly and requires significant engineering and construction effort which increases Balance of System (BoS) cost. Central architecture lacks flexibility in its configuration due to a central controller for regulating the system. High mismatch losses and missing individual Maximum Power Point Tracking (MPPT) are other disadvantages of this architecture [13].

String and multi-string inverters shown in Figure 2.1.(b) and Figure 2.1.(c) are classified in the central architecture category. These architectures are more flexible and expandable configurations. In these architectures, there is no parallel connection between PV module strings. Therefore, smaller inverters can be used for direct connection of each PV string. This mitigate the parallel diode losses and also the mismatch losses due to partial shading will be reduced since maximum power of each PV string is controlled separately [13, 14]. The multi-string inverters utilize separate DC/DC converters for performing MPPT operation for each PV string which reduces the mismatch losses. Moreover, this topology allows the connection of inverters with different power ratings and PV modules with different *(I-V)* characteristics. Main drawback of this architecture is that the multi-string inverter always needs two power conversion stages which leads to higher conversion losses [15].

Micro-inverters shown in Figure 2.1.(d) is the first module-integrated architecture which is discussed here. This configuration consists of a module-level PV inverter directly interfaced to the grid. Because of the individual PV panel maximum power point tracking operation, this architecture has minimum mismatch losses. The main drawback of this configuration is the required boost conversion stage for grid integration which increases conversion losses and also increase the price per watt [16, 17].

The configuration shown in Figure 2.1.(e), is similar to the one in Figure 2.1.(c), but the DC/DC power optimizer converter is applied to the individual PV panels. Therefore, in this architecture, we also have minimum mismatch losses but it required two power conversion stages which are lossy and decreases the overall efficiency [18].

Finally, cascaded DC/AC inverter is illustrated in Figure 2.1.(f). This architecture and AC-stacked PV inverter architecture which will be studied in this dissertation, have absorbed attention of researchers in academia and industry due to its unique characteristics in recent years. This architecture has the advantage of panel-level MPPT operation. AC-stacked architecture can utilize only one power conversion stage which further increase the PV system efficiency [19]. The critical requirement for this architecture is properly designed decentral controller which can reduce the BoS cost significantly will be studied in detail in next chapters.

2.3 Cascaded Multi-level PV Inverters

The general idea of multilevel inverters is to generate a sinusoidal voltage waveform from distinct levels of voltages, generally acquired by isolated voltage sources. As the number of levels increases, the output voltage waveform adds more steps, producing a staircase wave which approaches the sinusoidal wave with minimum harmonic distortion. Among this group of converters, Neutral-Point Clamped (NPC) converters, Flying Capacitor (FC) converter and Cascaded H-Bridge (CHB) converters are the most popular ones [20]. There has been a significant amount of research interest in the cascaded multilevel inverter or cascaded H-bridge (CHB). This architecture is one of the commercial topologies of multilevel configurations which is suitable for PV application due to capability of connection of each PV panel to an H-bridge and series connection of the output of each level for AC voltage build up [21]. This topology and its control schemes are investigated in detail in the following sections.

2.4 Control Schemes

As it is mentioned in previous sections, with the momentous rise in generation of electrical energy using PV systems, attention to grid-tied PV inverter architectures is also increasing in recent years. Different PV inverter architectures have been proposed which were introduced in section 2.2. Cascaded DC/AC converters, and in particular cascaded H-bridge multi-level converters, have gained significant research interest, especially in recent years [20-23]. In multi-level cascaded H-bridge inverters, DC voltages can be controlled independently, which increases the system efficiency during partial shading condition or other sources of asymmetric operation such as PV panel aging, dust accumulation or even utilizing different types of PV panels in a string [22]. In addition, this topology can utilize semiconductors with lower voltage ratings because of the series connection of the inverters. Finally, this topology has a high degree of freedom for controlling the output current, increasing the robustness and reliability of grid-tied PV systems [20, 21]. This research investigates a novel AC-stacked grid-tied PV inverter topology, which is similar to a cascaded DC/AC configuration. However, proposed inverter architecture includes some novel characteristics that differentiate it from cascaded H-bridge multilevel inverters [19, 24].

For all market segments, the PV inverter control scheme is a critical part of the inverter configuration. This becomes increasingly demanding as smart inverter functionalities are mandated and inverters must provide more dynamic performance and advanced functionalities to improve the grid stability [25-27]. Proper control design for these configurations can improve performance and reliability of the system. In recent years, there has been a great deal of research on control of PV inverters [20-22, 28-31].

Grid-tied DC/AC converter controllers are responsible for extracting maximum power from the PV modules and injects optimum active and reactive power to the grid. Because of the important role they play, design and development of a novel controllers which control the output power with high power quality and capability of maintaining the performance in fault conditions, have attracted the attention of researchers in recent years [32]. Different variety of control algorithms are introduced to control the grid-tied cascaded H-bridge PV inverters [20, 21, 31, 33-38]. Despite the distributed nature of the cascaded H-bridge configuration, most of the proposed control schemes for this design are centralized, requiring a huge amount of communications among inverters specially for controlling the output current.

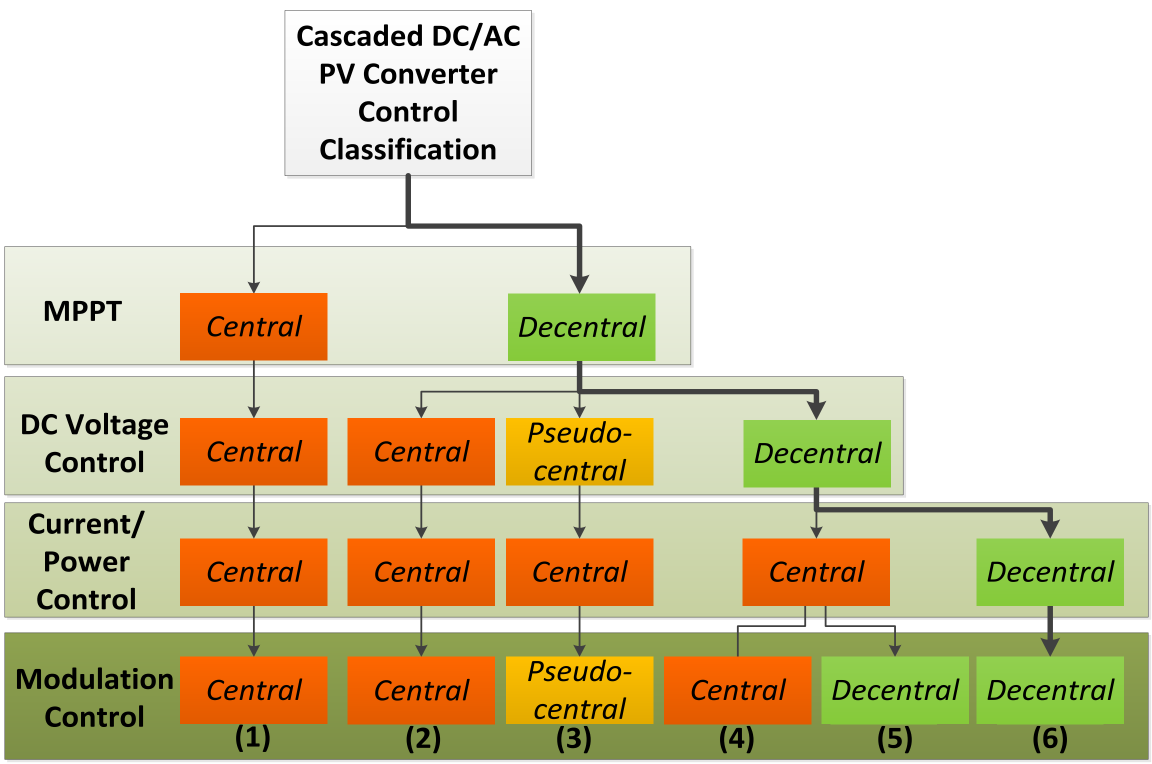

Figure 2.2. Control schemes for cascaded H-bridge classification

As can be seen in Figure 2.2, all the proposed control schemes for this architecture consist of four different control stages which are Maximum Power Point Tracking (MPPT) control, DC bus voltage control, output current/power control, PWM switching signal generation. The first proposed control algorithm in this figure is a four-stage central control system. An example of this control algorithm is a dual-inverter, connected to two identical PV strings which controlled by four levels of central controllers [39-41]. However, as it can be seen in Figure 2.2, most of the proposed control schemes utilize decentralized MPPT control to minimize mismatch losses. DC voltage controller of these inverters can be centralized, pseudo-centralized or decentralized. As it is shown in control scheme (2), if the DC voltage controller is implemented centrally, the output current/power controller and modulation index controller are also central. Examples of this control strategy are presented in [30, 33, 42-45]. In an example of this control scheme, two central predictive control methods for regulating output current and power are introduced to improve the performance and reduce output current harmonic distortion content [45]. This control scheme consists of a decentralized MPPT control stage for each PV panel. Using the DC voltage references of this stage, the absolute DC-bus voltage error is calculated centrally and compensated with a central PI controller. In the next stage, using predictive model, the output current and voltage are controlled and finally PWM modulation indices are built. A similar control strategy with a new central modulation approach and combination of staircase and unipolar PWM, is introduced in [45]. In another example, after independent MPPT controllers, a central double-loop controller is utilized to regulate the output power of the PV array. For central PWM generation and the power weighting PWM generation, central information is distributed among inverters based on individual PV power weighting factors [42]. In a similar work, the sum of DC-link voltages after MPPT controllers is controlled by a PI controller and a current controller applied to the summation of the active and non-active current references for generating modulation indices [43]. Resonant controllers have been also used in some articles to control the output current [44, 45].

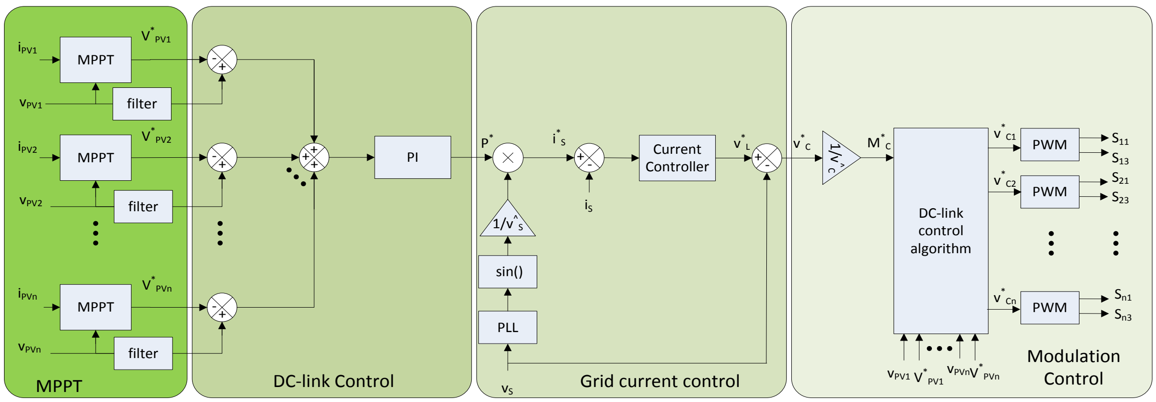

Figure 2.3. Example of a control scheme with central DC voltage control, central current/power control and central PWM generation.

Pseudo-central DC voltage control strategy (control scheme (3) in Figure 2.3) is popular in the recent literature [20, 21, 46-49], in these control schemes the sum of DC-link voltages is controlled to generate the output current reference for the next control stage [20]. The control scheme in [20] which attracted notable attention is presented in Figure 2.4. In this control scheme, decentralized MPPT control level extracts the maximum power from each PV panel with minimum mismatch losses. In DC voltage control stage, (n-1) inverters control their own DC voltage locally with no external information and one central controller is applied for controlling the DC voltage of one inverter using the information of DC voltage references of all inverters, which is called pseudo-central DC voltage controller in this dissertation. Output current of the system is controlled centrally and similar pseudo-central approach has been utilized for generating individual inverter PWMs. In similar schemes, the reference of the central current controller can be the output of the pseudo-central DC voltage control section [47] or the summation of the non-active current reference and DC-link voltage controller outputs [46]. The output of the current/power controller should be subtracted by summation of the other modulation indices to build the modulation index of the master inverter [48, 49] and (n-1) modulation indices are the direct outputs of DC-link voltage controllers. In the next chapters, it is shown that to control the output current, information from one inverter is enough and there is no need to use the summation of the output of DC-link voltage controllers.

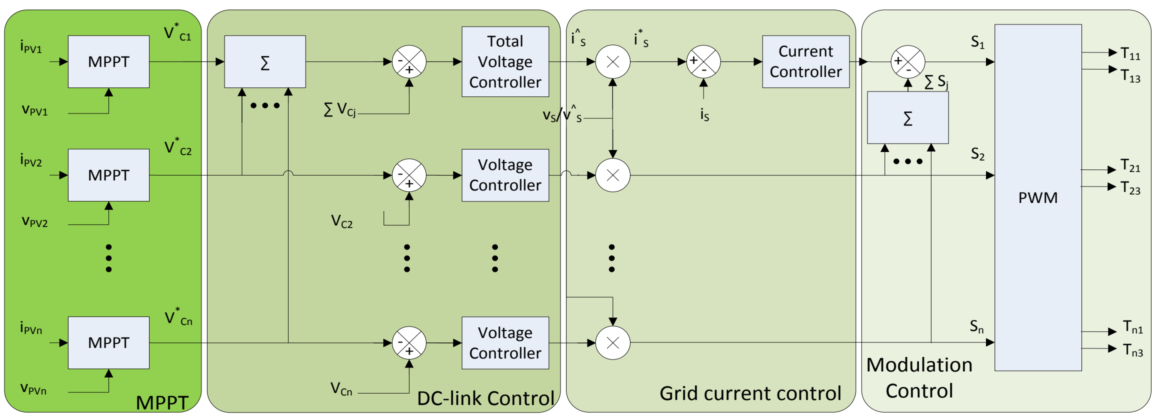

Figure 2.4. An example of control scheme with decentral MPPT control, pseudo-central DC-voltage control, central current control and pseudo-central PWM generation.

More attention to the diagram presented in Figure 2.2 shows that the output current/power controllers are implemented centrally in all the studies. However, the reference for this central controller can be built by summation of the individual reference powers, generated by decentralized DC-link voltage controllers, control schemes (4) and (5) [31, 50-54]. If the d-q controller is implemented, this information is the d-component of the reference output current. The q-component of the output current is an external command which is sent to the central regulator [54]. In the final stage, the output of the central current controller is injected to central Phase Shifted PWM and Level Shifted PWM modulators to generate gate signals for all inverters [31]. However, modulation indices can be generated locally from distributed PS-PWM modulators to increase inverter system reliability [50, 53].

This dissertation, to the best of the author's knowledge, for the first time proposes and mathematically proves the feasibility of fully decentralized control scheme for grid-tied module-level PV inverter architecture. The control scheme presented in this research is shown with bold lines in Figure 2.4. In this control architecture, all the four control stages are decentralized.

2.5 AC-stacked PV Inverter Architecture

The AC-stacked PV inverter architecture studied in this thesis is a novel distributed cascaded inverter topology, suitable for PV applications such as standalone or grid-tied. In this architecture, shown in Figure 2.5, a few module-level PV inverters are connected in series and operate cooperatively to maintain the grid connection requirements. Each inverter member provides the maximum power point from each PV panel to minimize the mismatch losses. This configuration and its tangible advantages were introduced in [19]. The proposed panel-level configuration, similar to cascaded H-bridge architecture, has the benefit of utilizing low-voltage semiconductor devices such as MOSFETs. These can switch at much higher frequencies than high voltage switches like IGBTs. However, this configuration, unlike a cascaded H-bridge, is an AC-stacked configuration with no intentional phase shifting and a fully decentralized control scheme, implementing high frequency switching. However, if controlled with central or pseudo-central methods, the control signal must be transferred using a much higher bandwidth communication method, which in practice limiting the converter switching frequency [24].

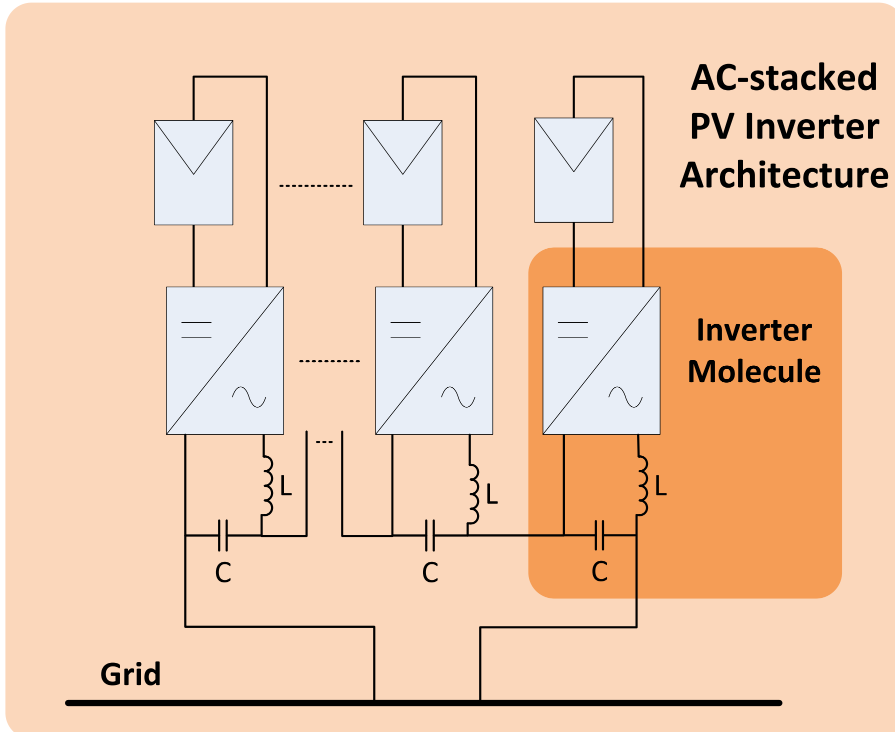

Figure 2.5. AC-stacked PV inverter architecture schematic

From a control implementation point of view, AC-stacked PV inverter architecture is a distributed architecture where each inverter generates a sinusoidal output voltage and current. Therefore, it has the benefit of using a fully distributed control scheme as presented and analyzed in this thesis. By utilizing a fully decentralized control system, there is no need to transmit high frequency signals such as measurements and controller outputs over wire or wirelessly. As a consequence, inverter switching speed can be increased as much as the semiconductors' Safe Operating Area (SOA) allows. This can help to shrink PV inverter size and increase power density.

On the other hand, completely decentralized panel-level architecture reduces the hardware costs such as large cables and expensive isolation and it can also reduce the installation costs such as trenching, foundation etc. Therefore, Balance of System (BOS) costs are much lower compared to central architectures or even panel-integrated architectures like micro-inverters which due to high output voltage requires expensive cables with insulation.

CHAPTER 3: DECENTERALIZED CONTROL SCHME DESIGN FOR AC-STACKED PV INVERTER ARCHITECURE

3.1 Introduction

In this chapter, a decentralized control scheme is proposed for AC-stacked PV inverter architecture introduced in previous chapter. The approach is to generate the detailed mathematical model of AC-stacked system. the second step is to determine the best pairing input/output sets for decomposing the multi-input multi-output system to decentralized subsystems. To do so, the Relative Gain Array (RGA) method is used to evaluate the strength of interconnection between inputs and outputs of AC-stacked model. Using RGA values the best subsystems will be determined and required controllers are designed for those subsystems.

The rest of this chapter is organized as follow. First RGA method and its advantages are introduced in section 3.2. In section 3.3 a nonlinear model of grid-tied AC-stacked PV inverter system with three inverters in a string is presented. Section 3.4 provides decentralized control design approach.

3.2 Relative Gain Array

To analyze the feasibility of the decentralized control scheme and to determine the best input and output pairs for the system decomposition and design the control scheme, the first step is to measure the interaction of inputs and outputs. There are few methods to measure the coupling and interaction between inputs and outputs of MIMO systems. The two main methods to quantify the degree of directionality and the level of interactions are condition number and Relative Gain Array (RGA). RGA method is the most popular and effective method [55, 56]. The RGA of a non-singular transfer function matrix measures the degree of coupling or interaction between inputs and outputs of a multi-input multi-output (MIMO) system. This method was introduced by Bristol in 1966 [57] which is very effective to analyze static coupling of MIMO systems. Several applications of RGA method have been reported including bidirectional power transfer systems [58], three phase grid-connected NPC inverter control design [59], HVDC controller design [60], as well as two loop controller design of buck-SEPIC converter for power management [61]. Bristol, claimed for a MIMO system, in which u_i and y_j are a pair of input and output that we want to control the output y_j with the input u_i, there are two extreme cases to be considered for the interaction analysis:

1. Other subsystems and control loops are open: All other inputs are constant. In such a condition which is illustrated in Figure 3.1, If there is a step change in the input u_i this change can be seen in both outputs as (3.1) and (3.2).

$$\Delta y_j = \Delta u_i \times G_{ij} \tag{3.1}$$

$$\Delta y_i = \Delta u_i \times G_{ii} \tag{3.2}$$

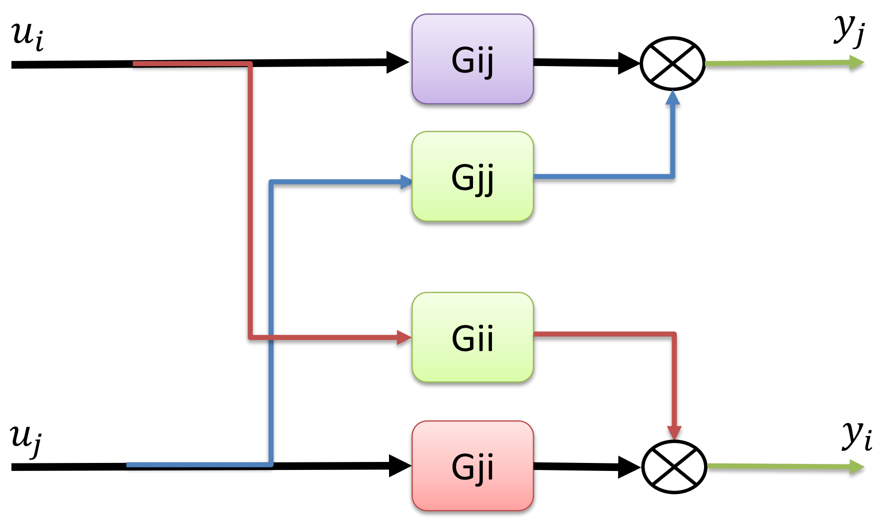

Figure 3.1. The extreme case #1, where all control loops are open.

2. Other subsystems and loops are perfectly controlled. This means all other outputs are constant. In the other word, any variation of other inputs doesn't have impact on these outputs. For instance, in the block diagram shown in Figure 3.2, the perfectly closed loop for the loop $r_j y_i$ means that the loop completely damped the external disturbances from u_i and changes in u_i would not have any impact on y_i. Therefore, in this case equations (3.1) and (3.2) can be rewritten as (3.3) and (3.4).

$$\Delta y_j = \Delta u_i \times G_{ij} + \Delta u_j \times G_{jj} \tag{3.3}$$

$$\Delta y_i = 0 \tag{3.4}$$

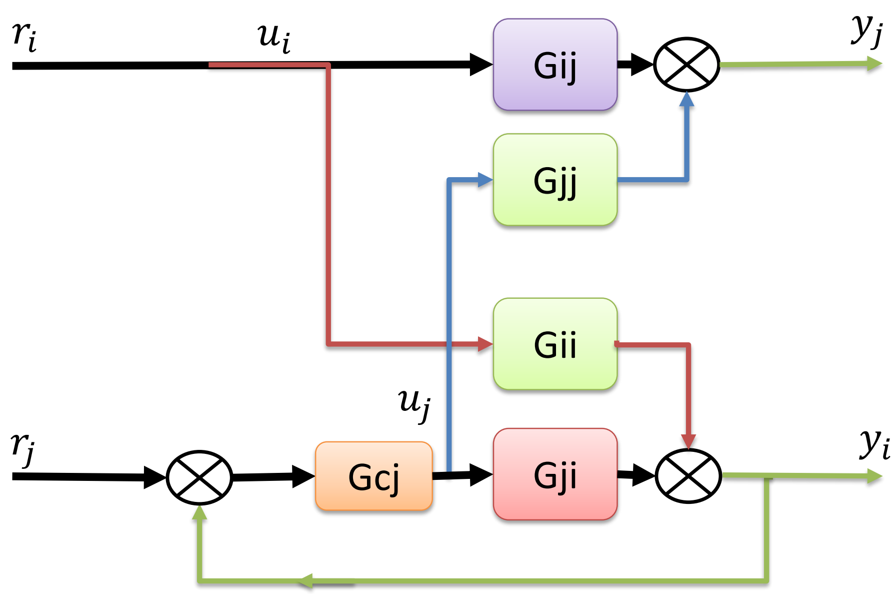

Figure 3.2. The extreme case #2 where all the other control loops are perfectly closed.

Therefore, it can be derived for these two extreme cases:

All the other loops open: $\left(\dfrac{\partial y_j}{\partial u_i}\right)_{u_k=0,k\neq i} = g_{ji}$ (3.5)

All the other loops are perfectly closed $\left(\dfrac{\partial y_j}{\partial u_i}\right)_{y_k=0,k\neq j} = \hat{g}_{ji}$ (3.6)

Bristol showed that for a pair of input-output u_i and y_j the Relative Gain Array is defined as (3.7).

$$\lambda_{ji}(s) = \left(\frac{g_{ji}}{\hat{g}_{ji}}\right) \tag{3.7}$$

When the static RGA gains of a control system acquired, the suitable input-output pairs can be selected to decompose a large system to decentralized sub-systems. The RGA of a nonsingular square matrix G can be calculated by (3.8).

$$RGA(G) = \Lambda(G) = G \times (G^{-1})^T \tag{3.8}$$

In this Equation, × denotes element-by-element product. The RGA equation presented in (3.8) can only analyze the system in steady state and cannot comment on dynamic interactions of inputs and outputs. Therefore, modified method called Dynamic Relative Gain Array (DRGA) is introduced by replacing static gains in (3.8) with transfer functions in (3.9) [56, 62].

$$DRGA\big(G(s)\big) = \Lambda\big(G(s)\big) = G(s) \times (G(s)^{-1})^T \tag{3.9}$$

Dynamic RGA is modified to be applicable for general MIMO systems such as systems with integrators and differentiators [63].

$$DRGA\big(G(j\omega)\big) = \Lambda\big(G(j\omega)\big) = \lim_{s \to j\omega} \left\{ G(j\omega) \times (G(j\omega)^{-1})^T \right\} \tag{3.10}$$

The RGA formula presented in (3.8) is a version of (3.10) where ω is close to zero $(\omega \to 0)$ and system is in steady state.

(3.8)-(3.10) are derived to calculate RGA of systems with square transfer matrix with equal number of inputs and outputs. For systems with non-square transfer matrix where number of inputs and outputs are not equal, such as AC-stacked PV inverter system studied in this chapter, these equations can be rewritten as (3.11)-(3.13).

$$RGA(G) = \Lambda(G) = G \times (G^{+})^T \tag{3.11}$$

$$DRGA\big(G(s)\big) = \Lambda\big(G(s)\big) = G(s) \times (G(s)^{+})^T \tag{3.12}$$

$$DRGA\big(G(j\omega)\big) = \Lambda\big(G(j\omega)\big) = \lim_{s \to j\omega} \left\{ G(j\omega) \times (G(j\omega)^{+})^T \right\} \tag{3.13}$$

where $^{+}$ means the Moore-Penrose pseudo-inverse [56]. In this thesis, DRGA method for non-square systems is used to define the best input-output pairs for decomposing AC-stacked PV inverter system to some decentralized sub-systems.

The two well-known pairing rules related to RGA analysis which are used in this study for rearranging the system are introduced here [55]:

1. For decomposing the system to decoupled subsystems for decentralized control design, it is preferable to pair input and output pairing sets with the relative RGA gains closer to 1. In such a system, the resultant subsystem is less affected by other loops when the gain is closer to 1, which means there is negligible coupling effects between control loops.
2. Avoid pairing variables with negative relative RGA gains, since there is significant interaction between control loops and decomposed MIMO system would be unstable.

This method is utilized in this dissertation for evaluating the strength of interconnection between inputs and outputs of AC-stacked PV inverter system. Based on RGA and DRGA analysis the AC-stacked PV inverter system is decomposed to three subsystems and corresponding controllers are designed.

3.3 Inverter Modelling

In this section, first, a mathematical model of the proposed grid-tied PV inverter architecture is derived. Since the AC-stacked PV inverter architecture is a distributed configuration, to be able to analyze all characteristics of this architecture in conditions such as partial shading, the model should consist of at least three inverter members to see the impact of disturbances in one inverter in at least two different healthy inverters. However, number of inverters in a string for this architecture depends on the grid voltage, PV panel characteristics and desirable nominal efficiency and operating margin. For example, for 120V grid voltage system, considering minimum DC voltage of PV panels not lower than 25V, the minimum required number of inverters is seven. Because a mathematical model of a system with seven inverters has no significant technical differences compared to the three-inverter system, an AC-stacked PV inverter system with three inverters is analyzed in this section which is shown in Figure 3.3.

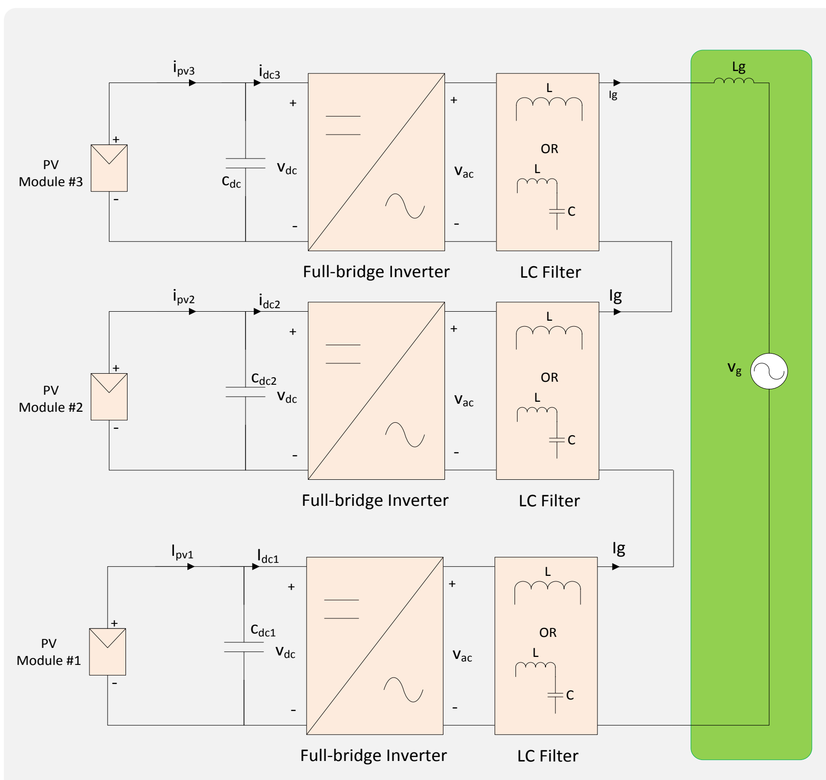

Figure 3.3. Three-member AC-stacked PV inverter system

$$x = \begin{bmatrix} x_1 & x_2 & x_3 & x_4 & x_5 \end{bmatrix}^T = \begin{bmatrix} V_{dc1} & V_{dc2} & V_{dc3} & I_d & I_q \end{bmatrix}^T$$

$$\begin{aligned} u &= \begin{bmatrix} u_1 & u_2 & u_3 & u_4 & u_5 & u_6 \end{bmatrix}^T \\ &= \begin{bmatrix} m_{d1} & m_{q1} & m_{d2} & m_{q2} & m_{d3} & m_{q3} \end{bmatrix}^T \end{aligned} \tag{3.14}$$

$$y = \begin{bmatrix} y_1 & y_2 & y_3 & y_4 & y_5 \end{bmatrix}^T = \begin{bmatrix} V_{dc1} & V_{dc2} & V_{dc3} & I_d & I_q \end{bmatrix}^T$$

where:

$V_{dc1}, V_{dc2}, V_{dc3}$	input DC voltages of individual inverters *(V)*
m_{d1}, m_{d2}, m_{d3}	d-component of modulation indices
m_{q1}, m_{q2}, m_{q3}	q-component of modulation indices
I_d	d-component of output current injected to the grid *(A)*
I_q	q-component of output current injected to the grid *(A)*

The dynamic nonlinear model of this system consisting three inverters is developed by introducing the state variables, inputs and outputs. The inputs of this system are modulation indices of inverters and outputs are DC voltages and the output string current. The system states are also DC voltages and the output string current.

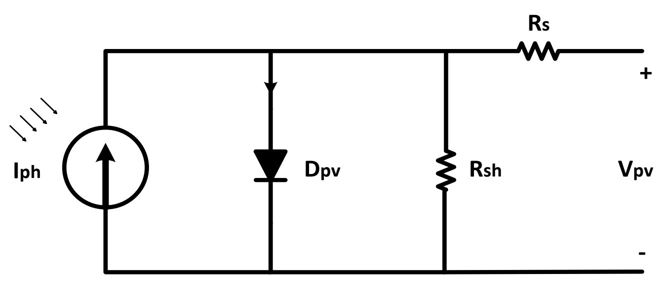

Figure 3.4. PV panel model.

In this equation, d-components and q-components are the adopted Park transformation for single-phase system. In this system, a precise equivalent circuit consisting of a diode and a shunt and series resistors for each PV module is utilized which is shown in Figure

3.4. Since the series resistor is small, it is neglected in this study. The dynamic nonlinear model can be presented by following five nonlinear differential equations:

$$\begin{cases} \dot{x}_1 = \left(\dfrac{I_{sc1} I_{r1}}{I_{r\max 1}} - \left(\dfrac{I_{sc1}}{e^{\left(k_c V_{oc1} / N_{s1}\right)} - 1} \right) \left(e^{\left(x_1 / V_{t1} n N_{s1}\right)} - 1 \right) - \dfrac{x_1}{R_{sh1}} \right) \Big/ C_{dc1} - \dfrac{x_4 u_1}{C_{dc1}} - \dfrac{x_5 u_2}{C_{dc1}} \\ \dot{x}_2 = \left(\dfrac{I_{sc2} I_{r2}}{I_{r\max 2}} - \left(\dfrac{I_{sc2}}{e^{\left(k_c V_{oc2} / N_{s2}\right)} - 1} \right) \left(e^{\left(x_2 / V_{t2} n N_{s2}\right)} - 1 \right) - \dfrac{x_2}{R_{sh2}} \right) \Big/ C_{dc2} - \dfrac{x_4 u_3}{C_{dc2}} - \dfrac{x_5 u_4}{C_{dc2}} \\ \dot{x}_3 = \left(\dfrac{I_{sc3} I_{r3}}{I_{r\max 3}} - \left(\dfrac{I_{sc3}}{e^{\left(k_c V_{oc3} / N_{s3}\right)} - 1} \right) \left(e^{\left(x_3 / V_{t3} n N_{s3}\right)} - 1 \right) - \dfrac{x_3}{R_{sh3}} \right) \Big/ C_{dc3} - \dfrac{x_4 u_5}{C_{dc3}} - \dfrac{x_5 u_6}{C_{dc3}} \\ \dot{x}_4 = -\dfrac{x_1 u_1}{L_g} - \dfrac{x_2 u_3}{L_g} - \dfrac{x_3 u_5}{L_g} - \omega x_5 + \left(\dfrac{V_g}{L_g} \right) \\ \dot{x}_5 = -\dfrac{x_1 u_2}{L_g} - \dfrac{x_2 u_4}{L_g} - \dfrac{x_3 u_6}{L_g} + \omega x_4 \end{cases} \tag{3.15}$$

$$V_t = \frac{kT}{q} \tag{3.16}$$

$$k_c = \frac{q}{knT} \tag{3.17}$$

where:

N_{s1}, N_{s2}, N_{s3}	Number of series connected solar cells in PV modules
$I_{sc1}, I_{sc2}, I_{sc3}$	Short circuit currents of PV modules (A)
I_{r1}, I_{r2}, I_{r3}	Solar irradiations of PV modules (W/m2)
$I_{r\max 1}, I_{r\max 2}, I_{r\max 3}$	Maximum solar irradiations of PV modules (W/m2)
q	Electron charge (C)
$V_{oc1}, V_{oc2}, V_{oc3}$	Open circuit Voltages of PV modules (V)
V_g	Grid voltage (V)

$R_{sh1}, R_{sh2}, R_{sh3}$	Shunt resistance of equivalent circuits of PV modules (Ω)
$C_{dc1}, C_{dc2}, C_{dc3}$	DC-link capacitors (F)
k	Boltzmann's constant (J/K)
n	Ideality factor of diodes
T	Environment Temperature (K)
L_g	Grid inductance (H)
ω	Frequency $\left(\frac{rad}{s}\right)$

In order to derive the small signal state space model, the system is linearized and solved around a nominal operating point. In this study, nominal operating point is a condition in which all the inverters are working at the Maximum Power Point (MPP) at the nominal irradiance and the system is symmetric assumed that inverters are identical and there is no shading in the system. By linearizing the equation set in (3.15) around operating point which is presented in Table 3.1, this system can be expressed in the standard state space form with six inputs and five outputs as follow:

Analyzing the linearized state-space system shows the symmetric system is controllable and observable. However, the open-loop grid-tied PV inverter system is unstable which is an inherent characteristic of all open-loop grid-tied inverters. In order to stabilize the system a proper controller is designed in this paper which is provided in the following section. The designed controller should be able to decouple the system to stable subsystems and maintains the stability of overall system. Design and analysis are provided in the following sections.

Table 3.1. AC-stacked PV inverter parameters' values at the operating points for mathematical modelling

Parameter Name	Symmetrical Condition
$V_{dc1}, V_{dc2}, V_{dc3}$	$31.2\ V$
I_{r1}, I_{r2}, I_{r3}	$1000 W/m^2$
T	$298\ K$
$C_{dc1}, C_{dc2}, C_{dc3}$	$10 mF$
L_1, L_2, L_3	$100 \mu H$
C_1, C_2, C_3	$20 \mu F$
ω	120π
f_{sw}	$40 kHz$
V_g	$\left(\frac{100}{2}\right) V_{rms}$
L_g	$50 \mu H$

$$
A=\begin{bmatrix}
\left(\dfrac{\dfrac{1}{R_{sh1}}+I_{sc1}q_1e^{\left(V_{dc1}q_1/\left(N_{s1}T_1k_1n_1\right)\right)}}{\left(N_{s1}T_1k_1n_1e^{\left(V_{oc1}q_1/N_{s1}T_1k_1n_1\right)}-1\right)}\right)\Big/C_{dc1} & 0 & 0 & -\dfrac{m_{d1}}{C_{dc1}} & -\dfrac{m_{q1}}{C_{dc1}} \\
0 & -\left(\dfrac{\dfrac{1}{R_{sh2}}+I_{sc2}q_2e^{\left(V_{dc2}q_2/\left(N_{s2}T_2k_2n_2\right)\right)}}{\left(N_{s2}T_2k_2n_2e^{\left(V_{oc2}q_2/N_{s2}T_2k_2n_2\right)}-1\right)}\right)\Big/C_{dc2} & 0 & -\dfrac{m_{d2}}{C_{dc2}} & -\dfrac{m_{q2}}{C_{dc2}} \\
0 & 0 & -\left(\dfrac{\dfrac{1}{R_{sh1}}+I_{sc1}q_1e^{\left(V_{dc1}q_1/\left(N_{s1}T_1k_1n_1\right)\right)}}{\left(N_{s1}T_1k_1n_1e^{\left(V_{oc1}q_1/N_{s1}T_1k_1n_1\right)}-1\right)}\right)\Big/C_{dc1} & -\dfrac{m_{d3}}{C_{dc3}} & -\dfrac{m_{q3}}{C_{dc3}} \\
-\dfrac{m_{d1}}{L_g} & -\dfrac{m_{d2}}{L_g} & -\dfrac{m_{d3}}{L_g} & 0 & -\omega \\
-\dfrac{m_{q1}}{L_g} & -\dfrac{m_{q2}}{L_g} & -\dfrac{m_{q3}}{L_g} & \omega & 0
\end{bmatrix} \tag{3.18}
$$

$$B = \begin{bmatrix} -\frac{I_d}{C_{dc1}} & -\frac{I_q}{C_{cd1}} & 0 & 0 & 0 & 0 \\ 0 & 0 & -\frac{I_d}{C_{dc2}} & -\frac{I_q}{C_{dc2}} & 0 & 0 \\ 0 & 0 & 0 & 0 & -\frac{I_d}{C_{dc3}} & -\frac{I_q}{C_{dc3}} \\ -\frac{V_{dc1}}{Lg} & 0 & -\frac{V_{dc2}}{Lg} & 0 & -\frac{V_{dc3}}{Lg} & 0 \\ 0 & -\frac{V_{dc1}}{Lg} & 0 & -\frac{V_{dc2}}{Lg} & 0 & -\frac{V_{dc3}}{Lg} \end{bmatrix} \tag{3.19}$$

$$C = \begin{bmatrix} 1 & 0 & 0 & 0 & 0 \\ 0 & 1 & 0 & 0 & 0 \\ 0 & 0 & 1 & 0 & 0 \\ 0 & 0 & 0 & 1 & 0 \\ 0 & 0 & 0 & 0 & 1 \end{bmatrix} \tag{3.20}$$

Analyzing the linearized state-space system shows the symmetric system is controllable and observable. However, the open-loop grid-tied PV inverter system is unstable which is an inherent characteristic of all open-loop grid-tied inverters. In order to stabilize the system a proper controller is designed in this paper which is provided in the following section. The designed controller should be able to decouple the system to stable subsystems and maintains the stability of overall system. Design and analysis are provided in the following sections.

3.4 Control Design

Since RGA analysis conveys important information about Multi Input Multi Output (MIMO) systems, the static RGA matrix of the nonlinear model of an AC-stacked PV inverter string consisting three inverters, modelled in previous section, is calculated and shown in a matrix in (3.21). The system inputs are represented as columns and system outputs are the rows of this matrix. In this study, the system operates in symmetric mode, where all three inverters and PV modules have similar operating conditions. Evaluating this RGA matrix shows the DC voltage of each inverter should be paired with d and q components of the same inverter modulation index denoted by *m*. For example, in the first row of this matrix, the RGA values show that V_{dc1} can be paired with m_{d1} because the corresponding RGA value is close to 1. It can also be paired with m_{q1} where the RGA is not close to 1, but it is positive and large enough, and significantly higher than the mostly-negative remaining values of this row. Since all three inverters are identical, the interactions between I_d and $m_{d1,d2,d3}$ are the same. Therefore, I_d can be paired with each of these control inputs. In this study, inverter #3 is selected to be paired with output current components. In practical conditions, where there is no exactly identical PV panels and inverters, the stronger inverter with more room for compensation for dynamic operation should be selected for controlling the output current.

$$
\begin{array}{ccc} \text{Subsystem \#1 (Inverter 1)(VMM1)} & \text{Subsystem \#2 (Inverter 2)(VMM2)} & \text{Subsystem \#3 (Inverter 3) (CAVC)} \end{array}
$$

$$
RGA(0) = \begin{array}{cc}
\begin{array}{cccccc} m_{d1} & m_{q1} & m_{d2} & m_{q2} & m_{d3} & m_{q3} \end{array} & \\
\begin{bmatrix}
1.0599 & 0.2910 & -0.1117 & -0.0273 & -0.1117 & -0.0273 \\
-0.1117 & -0.0273 & 1.0599 & 0.2910 & -0.1117 & -0.0273 \\
-0.1117 & -0.0273 & -0.1117 & -0.0273 & 1.0599 & 0.2910 \\
0.3501 & -0.1312 & 0.3501 & -0.1312 & 0.3501 & -0.1312 \\
0.0120 & 0.3203 & 0.0120 & 0.3203 & 0.0120 & 0.3203
\end{bmatrix} & \begin{array}{c} V_{dc1} \\ V_{dc2} \\ V_{dc3} \\ I_d \\ I_q \end{array}
\end{array} \qquad (3.21)
$$

Based on coupling analysis and RGA evaluation, a hybrid current/voltage-mode control scheme is proposed in this dissertation. The proposed hybrid controller is a fully decentralized control scheme, which consists of two different controllers for inverters, one inverter not only controls its own DC bus voltage and generates maximum power but also it controls the output current of the string and the other inverters are responsible to generate the maximum PV power and build the required output voltage for grid connection. In the other words, in the hybrid current/voltage-mode control scheme a subsystem is controlled by a two-loop cascade controller. The reason for designing a cascade control system is that increasing number of PV inverters in a string injects more uncertainty to the system, which can be controlled by two loop cascade control system.

This inverter not only controls its input DC voltage but also it is responsible to control the d-component of output current and compensate for transient voltage variations in the string and it is called the Current Administrator Voltage Compensator (CAVC) inverter. This inverter, as the voltage compensator, compensates for the voltage drop across the interfacing inductor during unity power factor operation. The output of inner current control loop in this inverter is the inverter modulation index which is the input of PWM generator. The PWM generator for this system can be bipolar, unipolar and hybrid. However, in this thesis, unipolar PWM generator is utilized that consists of one fast leg and one slow leg to minimize the conversion losses. The other two inverters which have smaller transient compensation capability only control their own input DC voltages and build up the output AC voltage for grid connection, these inverters are named Voltage Mode Members (VMM). The output of DC voltage control loop in VMM controllers is the amplitude of inverter modulation index which is applied to sinewave output of PLL and make the modulation index. PWM generator for VMMs are also unipolar as CAVC to minimize the conversion loss of the inverter architecture. In this architecture, each inverter receives the PLL information which is a heartbeat signal consists zero-cross information of the grid voltage. This information is provided through Power Line Carrier (PLC) to the individual inverter. Figure 3.5. shows this PV string architecture and the proposed decentralized control scheme.

By evaluating the steady-state closed-loop transfer function of the designed decentralized controller, interdependence between states can be analyzed. Steady-state analysis of the three-inverter system for nominal operating point is presented in (3.22). This closed-loop matrix shows the effectiveness of the decentralized controller. Since the parameters related to each state and its corresponding reference are very close to 1, the closed-loop system has a perfect reference tracking capability. In addition, evaluating the row related to I_d reveals an interesting fact about the strength of this control architecture. Although the reference of the d-component of the output current is generated from one inverter DC-link voltage controller, the other DC-link voltages have equal impact on this state. This means by controlling the current with only one inverter, we don't lose the impact of other inverters on the output power. This shows the feasibility of fully decentralized controller for AC-stacked PV inverters. In other words, we can control the output current by utilizing local measurements of one inverter which can be the strongest inverter in asymmetric conditions when inverters are not identical. The reason for this fact is that inverters are connected in series and the output current flows through all the inverters.

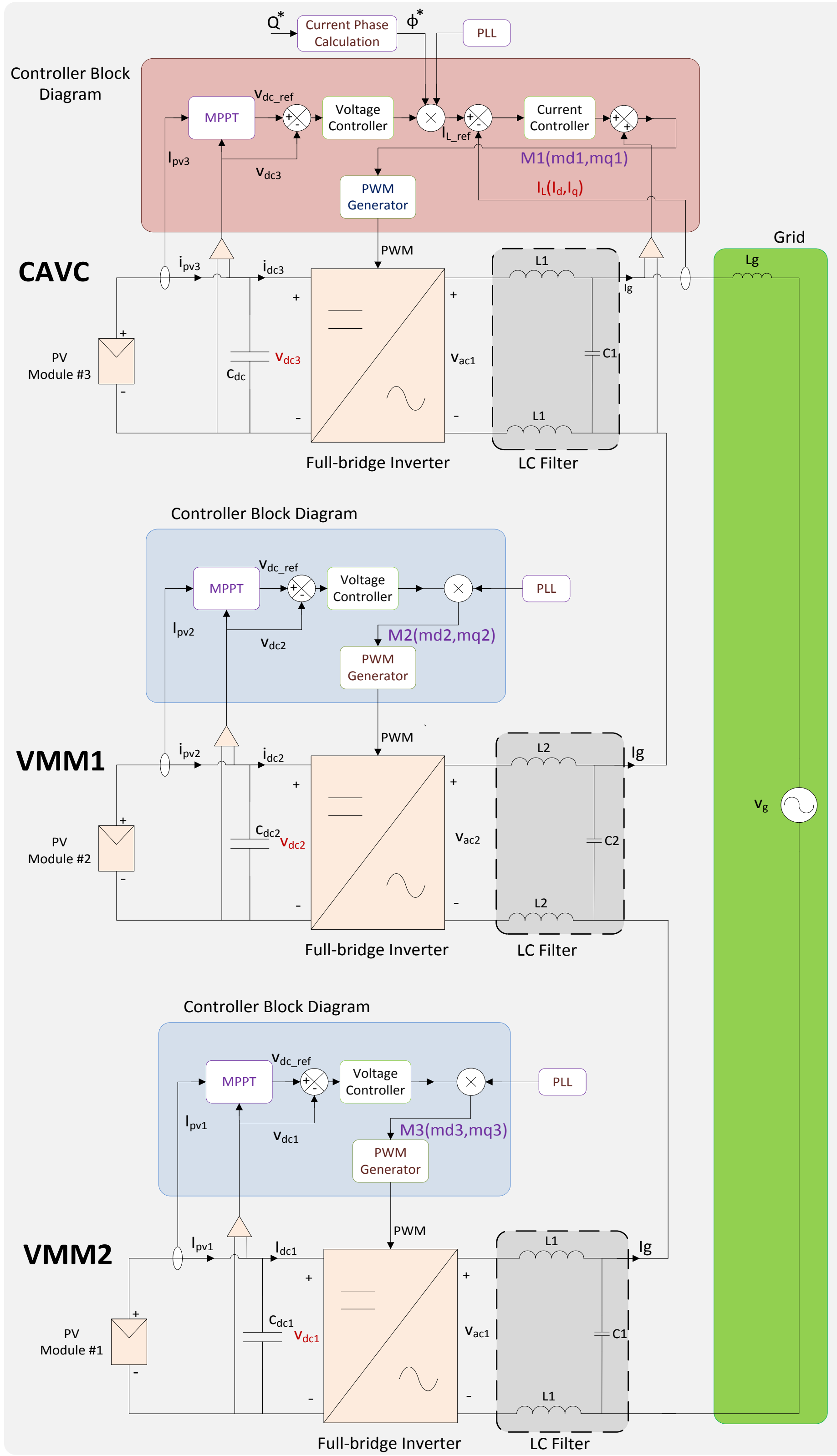

Figure 3.5. AC-stacked PV inverter architecture consisting of three module-connected inverters and proposed decentralized control scheme.

$$G_{CL-symmetric}(0) = \begin{array}{c} \begin{array}{ccccc} V_{dc1ref} & V_{dc2ref} & V_{dc3ref} & I_{qref} & V_g \end{array} \\ \begin{bmatrix} 0.9999 & 0.0000 & 0.0000 & 0.0000 & 0.0000 \\ 0.0000 & 0.9999 & 0.0000 & 0.0000 & 0.0000 \\ 0.0000 & 0.0000 & 0.9999 & 0.0000 & 0.0000 \\ 0.1505 & 0.1505 & 0.1505 & -0.0089 & -0.2973 \\ 0.0000 & 0.0000 & 0.0000 & 0.9999 & 0.0000 \end{bmatrix} \end{array} \begin{array}{c} \\ V_{dc1} \\ V_{dc2} \\ V_{dc3} \\ I_d \\ I_q \end{array} \quad (3.22)$$

It is desirable to have a completely damped and decoupled closed loop system where any disturbances such as step, impulse, etc. in a state should not affect other states. In other words, if an input reference of a subsystem changes, it should not affect other subsystems' outputs. Therefore, the MIMO system is completely decoupled and decentralized subsystems have no interconnection and coupling with each other. In this case, the decentralized controller has the best performance.

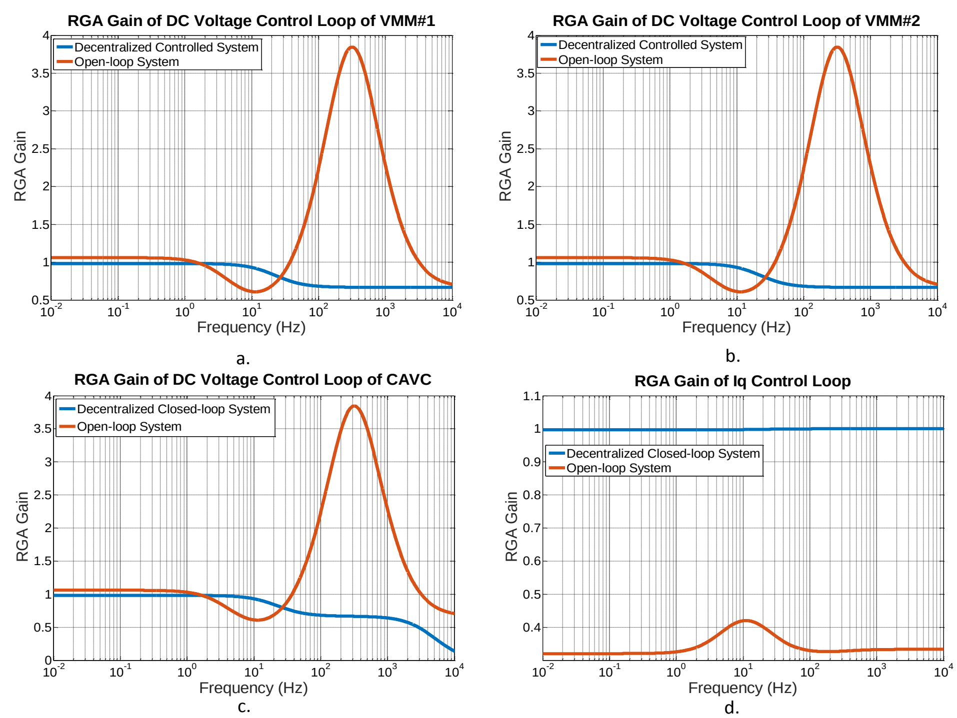

Figure 0.6. Dynamic RGA gains of input/output pairs for open-loop system and decentralized closed-loop system in frequency domain. a. VMM#1 DC voltage control loop. b. VMM#2 DC voltage control loop. c. Cascade control loop of CAVC. d. Q-component of string current control loop.

Steady state RGA analysis, presented in (3.21), provides intuitive information about the static behavior of the system. However, to analyze the dynamic coupling of the system, DRGA gains should be calculated for the system transfer function matrix in different frequencies. Frequency domain DRGA analysis, presented in Figure 0.6. shows that there is a dynamic coupling in the open-loop system. Decomposing the system by proposed decentralized control scheme reduces the dynamic coupling in the system significantly. Figure 0.6 compares DRGA values of the four input and output pairs for open loop and closed loop systems.

CHAPTER 4: SINGLE-MEMBER PHASE COMPENSATION METHOD

4.1 Introduction

In this chapter, a new decentralized control method is proposed for regulating the reactive power of AC-stacked PV inverter architecture, introduced in previous chapters. It is shown that for decentralized AC-stacked PV inverter system, the voltage drop across passive components are negligible and CAVC can compensate for this voltage drop individually. The rest of this chapter is organized as follow. The background of reactive power control of PV inverter system is provided first in section 4.2. In section 4.3, the Single-member Phase Compensation (SmPC) method is introduced and analyzed.

4.2 Background

Increasing integration of PV systems into power networks may violate the grid standards and requirements. For example, in PV networks with high penetration of PV systems, due to the intermittent nature of solar PV generations, the power supplied by PV generation may not match with power demand and potential overloading or voltage rises can appear at power network buses [2-4]. The suggested solution for this issue is the requirement of participation of PV inverter systems in voltage regulation through reactive power control [2, 64].

Available power grid codes are designed for network connection of PV systems into low penetrated PV networks. However, in high penetrated PV networks, PV inverters should participate more in providing ancillary services and smart inverter functionalities during normal operation and fault conditions. For instance, previous version of IEEE 1547 standard [65] forbidden reactive power support by PV inverter systems in Low Voltage (LV) grids to extract energy as much as possible from renewable energy sources [6]. However, the newly published amendment in 2014 [13] determines the PV inverter's reactive power control strategies for improving power quality and providing ancillary services.

Implementing different reactive power support strategies such as fixed reactive power, fixed power factor, power factor as a function of generated active power and reactive power in terms of local voltage, requires accurate and fast PF control capability of PV inverter control scheme and proper communication bandwidth for transferring supervisory control commands and grid information to individual inverters. These requirements are critical, especially for new distributed panel level architectures such as AC-stacked PV inverter systems in which required information should be sent to all the individual inverters. Therefore, despite the distributed nature of modular PV inverter architectures such as cascaded H-bridge, in all the proposed control schemes for these architectures, output active and reactive power are controlled centrally, as it was explained in detail in Chapter II. Central control of active and reactive power has an advantage that active and reactive power variation will not cause unbalanced in the system. Consider an AC-stacked PV inverter system consisting three inverters, Figure 4.1 shows how active and reactive power variation can change the string voltage and as a consequence, it can change the balance operation of the system. Figure 4.1.a shows the nominal operation condition of this system at unity power factor. If the active power changes, amplitude, and phase of string voltage change accordingly. However, if the system is not controlled centrally and reactive power information just is sent to inverter #3, this inverter will compensate for this variation and system will be unbalanced as shown in Figure 4.1.b. Implementing central control algorithm or providing string voltage information to all individual inverters can balance the system as it is illustrated in Figure 4.1.c. Later method requires significant communications bandwidth, particularly when a number of inverters in a string increases. Figure 4.1.d and Figure 4.1.e show the impact of PF variation on string voltage in the balanced and unbalanced system. In an unbalanced system, the output voltage of two inverters are equal in amplitude and phase, but they are not in phase with sting voltage. Therefore, the third inverter should compensate for the phase difference. In the balance system, all three inverters are equal in voltage amplitude, and phase and they are in phase with string voltage.

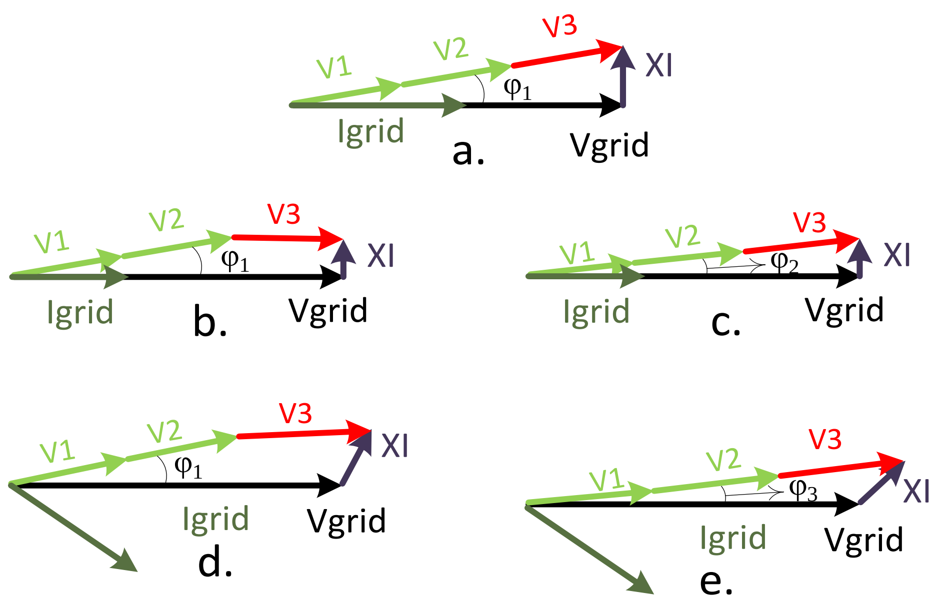

Figure 4.1. The impact of active and reactive power variation on string phase angle and symmetric operation of modular inverter system with central and decentral power control. a. Nominal operation at unity power factor and symmetric condition. b. Lower active power condition at unity power factor with decentral control and no data transfer to inverters, inverter #3 compensates for string phase change. c. Lower active power condition at unity power factor with central control and data transfer to inverters, balanced condition. d. Lagging condition when PF information is only sent to inverter #3. e. Lagging condition when PF information is sent to all inverters.

4.3 Single-member Phase Compensation Method for Reactive Power Control

In this section, I intend to show that first, the decentralized controller designed in the previous section can properly control the output reactive power and second, the impact of the active and reactive power of PV inverter system variations on balance of the system is negligible. Therefore, there is no need to send the reactive power command to VMM inverters and only one inverter is enough to receive this information.

For the control system designed in the previous section, it is desirable to have a damped and decoupled system where any disturbances such as step, impulse, etc. in a state would not affect other states. In other words, if an input reference of a subsystem changes, it should not affect other subsystems' outputs. Steady-state RGA analysis, presented in (3.22) (steady state RGA formula), provides intuitive information about the static behavior of the system. However, to analyze the dynamic coupling of this system, DRGA gains should be calculated for the system transfer function matrix in different frequencies. In order to analyze the effectiveness of controlling the reactive power of AC-stacked PV inverter system by one inverter, DRGA gain of the system which was modeled in Section II for Open-loop and closed-loop system are presented in Figure 4.2. As can be seen in this figure, DRGA gain of the open-loop system is lower than 0.5 which means there are dynamic couplings in the system. Decomposing the system by proposed decentralized control scheme reduces the dynamic coupling in the system significantly, and DRGA gains in a wide range of frequency domain are very close to 1.

Figure 4.2 shows that proposed decentralized control scheme in which one inverter controls reactive power can work properly in a wide range of frequencies. However, variations of reactive power will change the string voltage phase, and amplitude which can have an impact on VMM inverters and those inverters can detect the variation of power in the system.

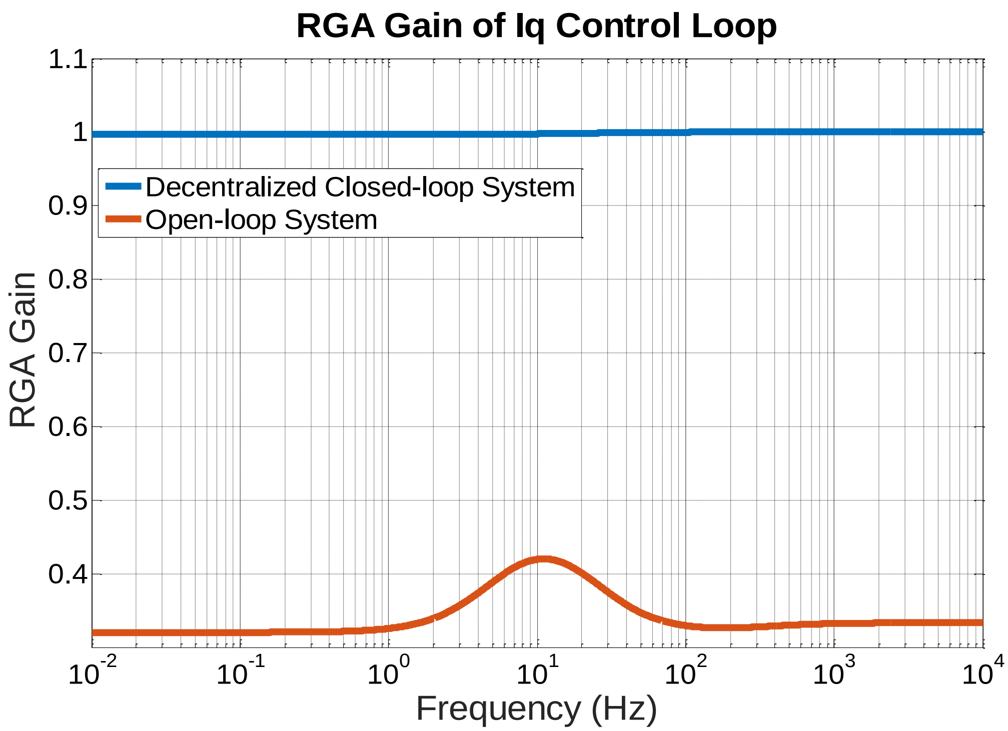

Figure 4.2. Comparison of DRGA gains of the control loop for the open-loop system and closed loop system in the frequency domain.

The proposed decentralized control scheme can enable the higher switching frequency, and therefore it can shrink the passive components in the system such as interface inductor. Utilizing small passive components makes the difference between grid voltage and string voltage negligible and consequently string voltage variation due to active and reactive power change is very small.

The negligible phase difference between grid voltage and string voltage is a unique advantage of the decentralized control scheme. If the phase difference between string voltage and grid voltage is small, there is no need to make the output voltages of VMM inverters aligned with string voltage. VMM inverters can be aligned with grid voltage. In other words, the communication requirement can be reduced, since phase information should be sent to only CAVC. In this strategy, CAVC can compensate for the voltage drop of interface inductor which is very small (less than 0.5%). This method which is introduced in this thesis is called Single-member Phase Compensation (SmPC). Figure 4.3 shows the vector diagram of AC-stacked inverter system utilizing decentralized controller.

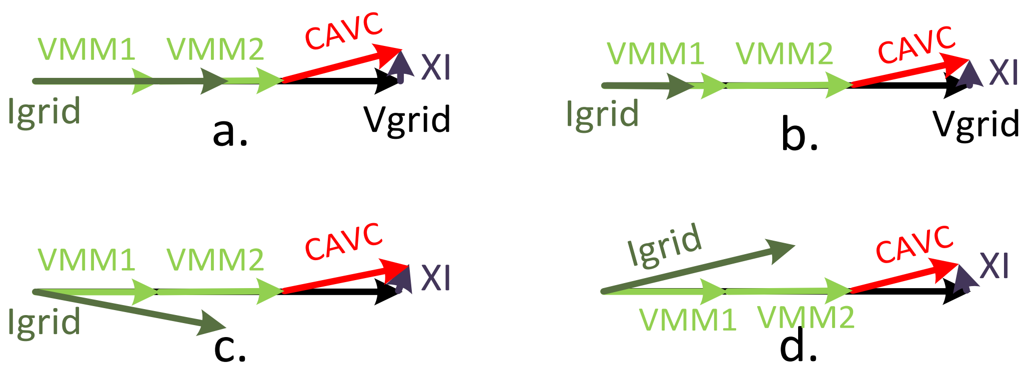

Figure 4.3. The impact of active and reactive power variation on string phase angle and symmetric operation of the system with decentralized controller and minimum communications. a. Nominal operation at unity power factor and symmetric condition. VMMs are in the same phase as grid and CAVC compensates for small voltage drop b. Lower active power condition at unity power factor with no data transfer to VMM inverters, CAVC compensates for smaller string phase shift. c. Lagging condition when PF information is only sent to CAVC. d. Leading condition when PF information is only sent to CAVC.

This figure shows the vector diagram of three-inverter AC-stacked PV inverter system which regulates the reactive power using the SmPC method. Therefore, VMM inverters don't receive string phase information, and they are aligned by grid voltage. Due to small passive components in the circuit, the voltage drop across these passive components is very small as it can be seen in Figure 4.3. Therefore, CAVC which compensates for the string voltage variation can compensate for this voltage drop. Since the overall impedance of passive components in the string is very small, by variation of active and reactive power, changing the amplitude and phase of the output voltage, the voltage drop across these passive components varies very small and therefore CAVC can compensate for these variations with negligible deviation from balance system. Figure 4.3.b shows the vector diagram of this system when the output active power is reduced. Figure 4.3.c and Figure 4.3.d presents the vector diagram of this system for lagging and leading output power, respectively. In lagging condition CAVC voltage is smaller than VMMs, and in leading condition, CAVC is larger than VMMs.

Figure 4.4 presents the impact of variation of active and reactive power on voltage amplitude of CAVC inverter. Figure 4.4.a. shows the impact of the size of interface inductor on variations of CAVC output voltage due to PF changes. In Figure 4.4.b, irradiance variation leads to output current variation which changes the voltage drop across the interface inductor. This curve shows the percentage of CAVC voltage variation to compensate for this change. AC-stacked PV inverter architecture using decentralized controller can operate at high switching frequencies which reduces the size of interface inductor significantly, assuming short circuit capability is not the problem. Based on Table 3.1, interface inductor for the system analyzed in this dissertation is $50\mu H$ which is significantly lower than similar architectures such as cascaded H-bridge presented in [20]. Figure 4.4.a. shows that for this system CAVC voltage compensation is less than 0.5%. To summarize, using decentralized control algorithm and SmPC reactive power control method presented in this paper, AC stacked PV inverter can operate at high switching frequencies which lead to small passive component requirement. Therefore, if the active and reactive power variation information is not sent to all the inverters, CAVC inverter can compensate for the string voltage variation which is less than 0.5% variation that is negligible.

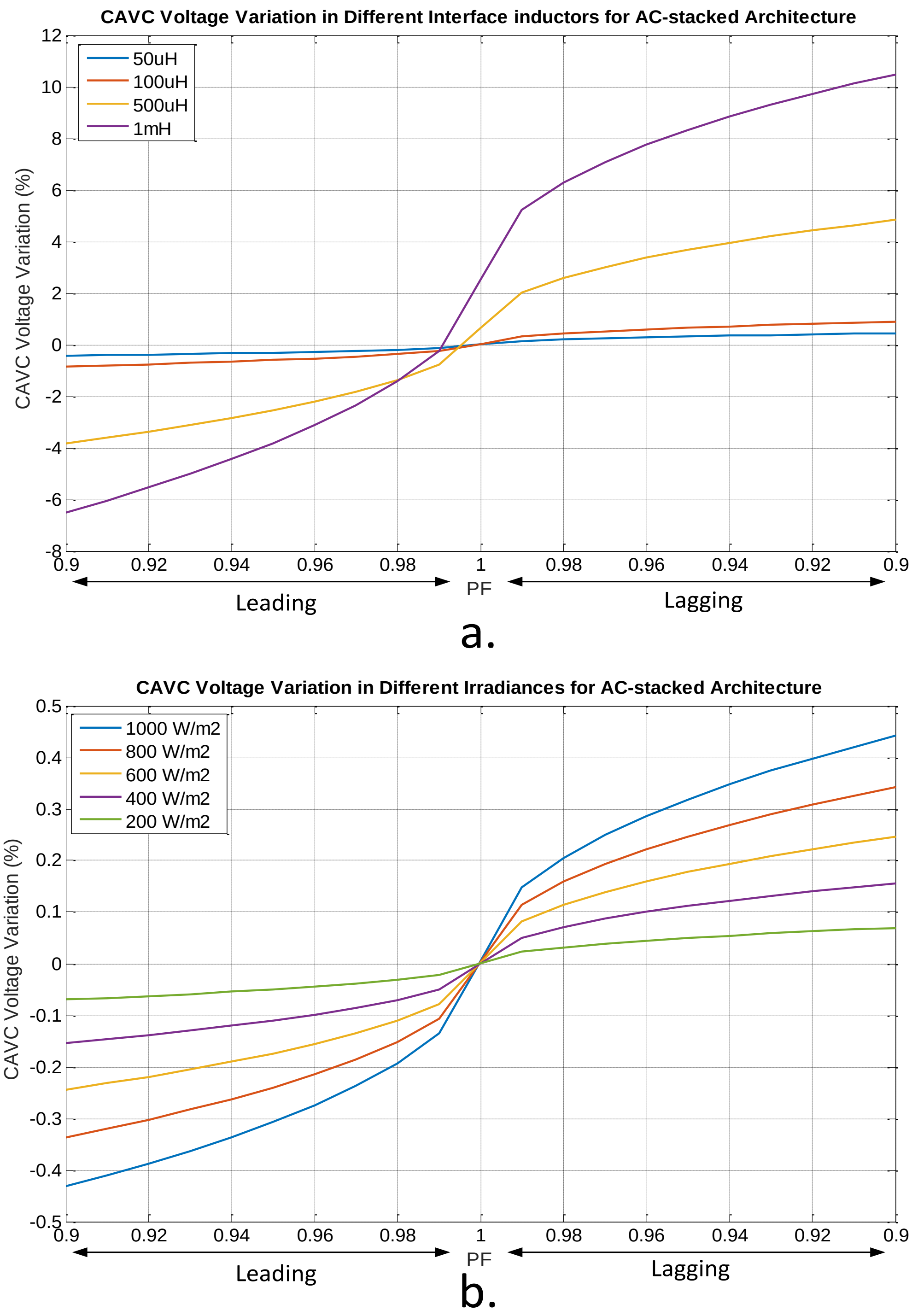

Figure 4.4. CAVC voltage variation due to active and reactive power changes. a. the impact of irradiance changes on CAVC voltage variations. b. the impact of interface inductor size on CAVC voltage variations in different PFs.

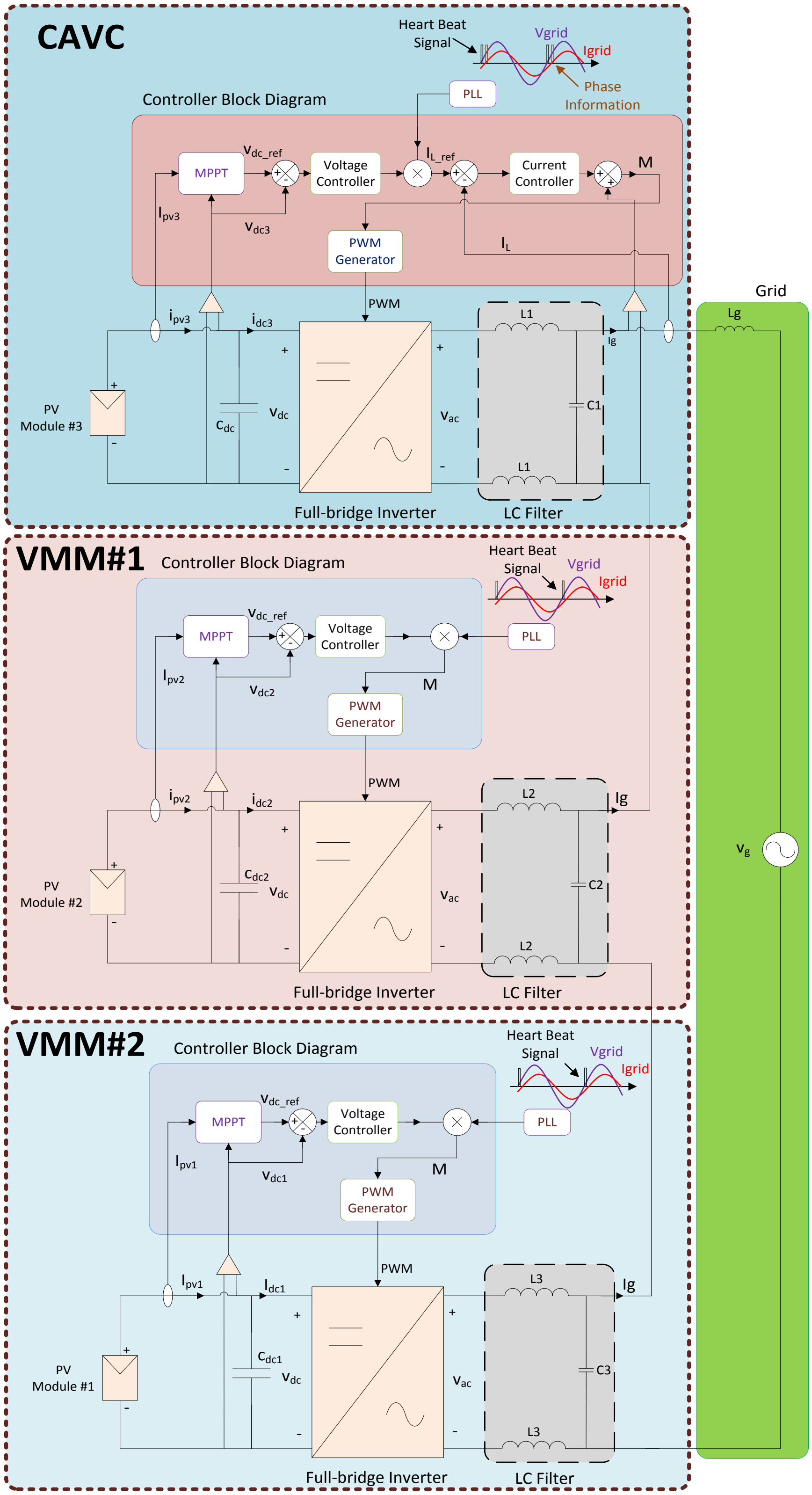

Figure 4.5. AC-stacked PV inverter architecture consisting of three module level inverters and proposed decentralized control scheme with SmPC strategy.

Considering SmPC method introduced in this chapter, the decentralized control scheme proposed in the previous chapter can be updated. The modified schematic of the AC-stacked PV inverter and decentralized control method with SmPC strategy is shown in Figure 4.5. As it can be seen in this figure, the heart beat signal which is zero-crossing information of grid voltage is sent to all string members including VMMs and CAVC. VMM inverters synchronized with this heart beat signal and aligned with grid voltage. On the other hand, CAVC member waits for the second information which is the command for zero-crossing of output current. The update rate of this information can be very slow, and it can be in several minutes or even few hours.

CHAPTER 5: BACKGROUND VOLTAGE HARMONICS MITIGATION

5.1 Introduction

PV power generation is intermittent in nature, and not properly matched to the load profile. As a result, large-scale integration of distributed PV generation challenges the power quality and stability of the grid [66, 67]. These challenges are exacerbated by constraining standards that govern the interconnection of PV into the grid system. The grid is responsible for providing regulated power at a high-quality standard to the load. This requires load following functions such as voltage and frequency regulation, and the supply of reactive power and harmonic currents [68]. In addition, adequate levels of energy storage and spinning reserve are required to absorb load transients, and respond to contingencies such as the tripping of a large generator. Some load-following functions such as voltage support, reactive power supply and harmonic mitigation can be achieved by appropriate control of the PV inverters [69, 70]. Other functions, such as frequency regulation support and spinning reserve can be addressed by coupling the PV inverter with energy storage capabilities. On the other hand, it is observed that the harmonic profile of the inverter system output current is affected by the variation in the harmonic profile of the background grid voltage [67, 71-73]. Therefore, it is very important to have a robust background harmonic mitigation control method for modern PV inverter architectures like AC-stacked PV inverters to deliver high quality power to the grid in different operation conditions [74].

Impact of renewable energy sources on grid voltage background harmonics, especially in networks with high penetrated Distributed Generations (DG) has been studied in [66, 75, 76]. On the other hand, distorted grid voltage at Point of Common Coupling (PCC) can impact on the generated current by distributed generations [67]. One of the main reasons of inverter current distortion in distorted grid is that the output impedance of the inverter provides a path for the grid harmonics. In order to mitigate the negative impact of background grid voltage harmonics and improve power quality using renewable energy sources, particularly PV inverters, two different methods have been proposed. One solution for mitigation of the impact of background harmonics on current control loop is the feedforward of grid voltage. This feedforward term can be as a full-feedforward scheme of the grid voltage [70, 77, 78], capacitor current feedforward [79] or band-pass filter feedforward [76]. This method due to increased susceptibility to the noises and the derivative terms in the feedforward link is not preferred. Moreover, providing grid voltage feedforward term requires a high bandwidth communication infrastructure for distributed architectures.

The second method is to increase the injected current control bandwidth which can also reduce the entire system stability. Different controllers such as proportional-integral (PI), proportional-resonant (PR) and harmonics compensators (HC) have been applied to mitigate for the steady state error in selected frequencies and to compensate for background grid voltage harmonics [71]. In order to avoid instability caused by these controllers, the current control loop should have a high enough bandwidth to cover the resonant frequency of these controllers [76, 80]. This method is more applicable for low voltage converters with high frequency switching and small PWM delay, that helps to achieve high bandwidth control loop [76].

This dissertation proposes two different strategies for implementing the grid harmonics suppression scheme for grid-tied AC-stacked PV inverters. Since the AC-stacked PV inverter architecture is a high frequency decentralized inverter, the proposed methods in this thesis are based on implementing selective PR controllers. AC-stacked PV inverter topology is the new modular panel level architecture which has been introduced in recent years which can convert solar energy to electricity with high efficiency and lower cost. This architecture and its tangible advantages was introduced in [19, 24]. As it is explained in the previous sections, unlike micro- and string-inverters that modularizes the power plant by power segments, the AC-stacked architecture, utilizes AC voltage optimization per-phase and per-string [29, 81][82]. Power optimization is performed at both the individual panel level and at the AC collector system level. To maximize the effectiveness of the proposed architecture each building block is controlled independently with no communication among themselves and minimum handshaking synchronization information with supervisory control [29].

In this section, two methods of implementation are investigated. In one method, a single inverter compensates for the background harmonics by utilizing additional PR controllers and in the second method all the inverters are participating in the harmonics mitigation. Feasibility and effectiveness of these two methods have been analyzed and verified by numerical analysis and hardware-in-the-loop experimental analysis.

The rest of this chapter is organized and presented as follow. Section 5.2 presents the AC-stacked PV inverter system and its control scheme. Details of proposed harmonic mitigation control schemes and mathematical analysis are proposed in Section 5.3 and section 5.4.

5.2 Current Control Strategy under Grid Voltage Background Harmonics

Figure 5.1 shows the AC-stacked PV inverter system. In this system, output of each inverter is filtered by a low-pass LC filter. In order to better analyze this system and study the impact of distorted grid voltage on this architecture, we should start with modelling of this system considering output impedance of the system.

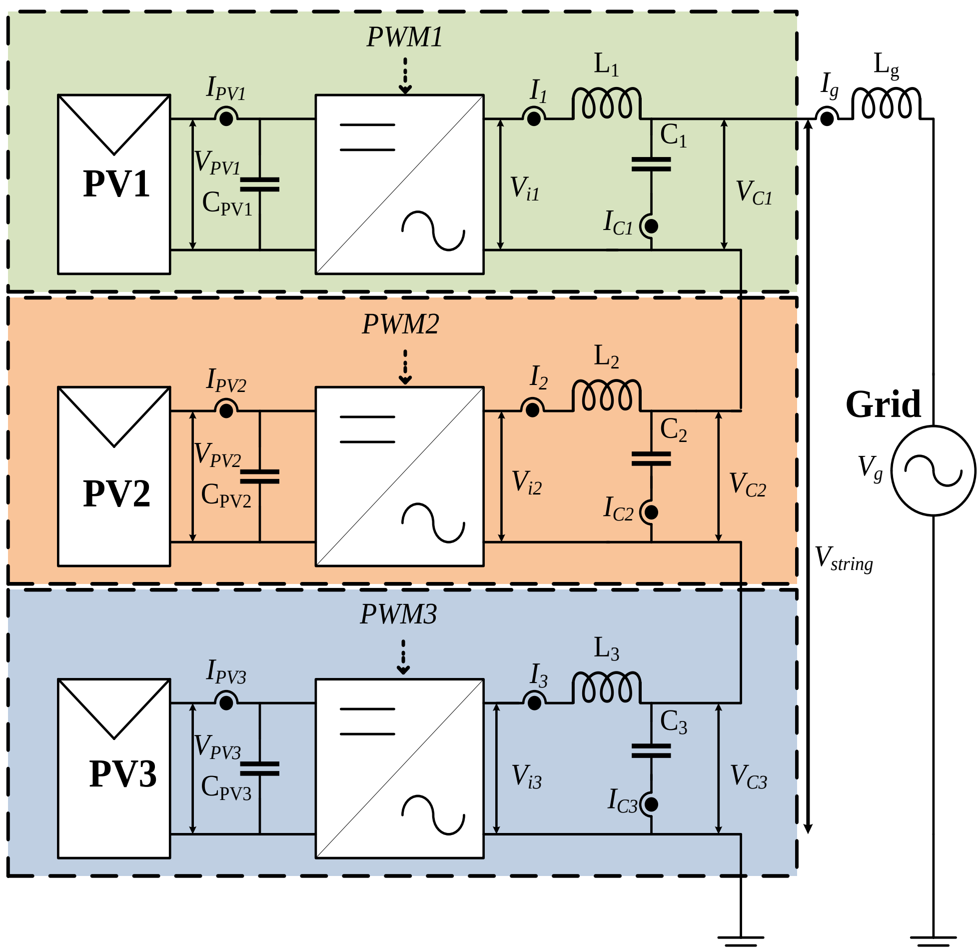

Figure 5.1. AC-stacked grid-tied PV inverter system consisting three inverters in a string.

To study the impact of grid voltage on output current of this inverter system, current control loop of this system should be studied. In the circuit presented in Figure 5.1, if DC-bus capacitors are large enough, it can be assumed that input DC voltage ripple is negligible. In addition, it is assumed that DC voltage control loops are much slower than current control loop and harmonics mitigation controllers. Therefore, for studying the current controller and background harmonics mitigation, we can assume the DC voltages are constant. The block diagram of this system is presented in the Figure 5.2.

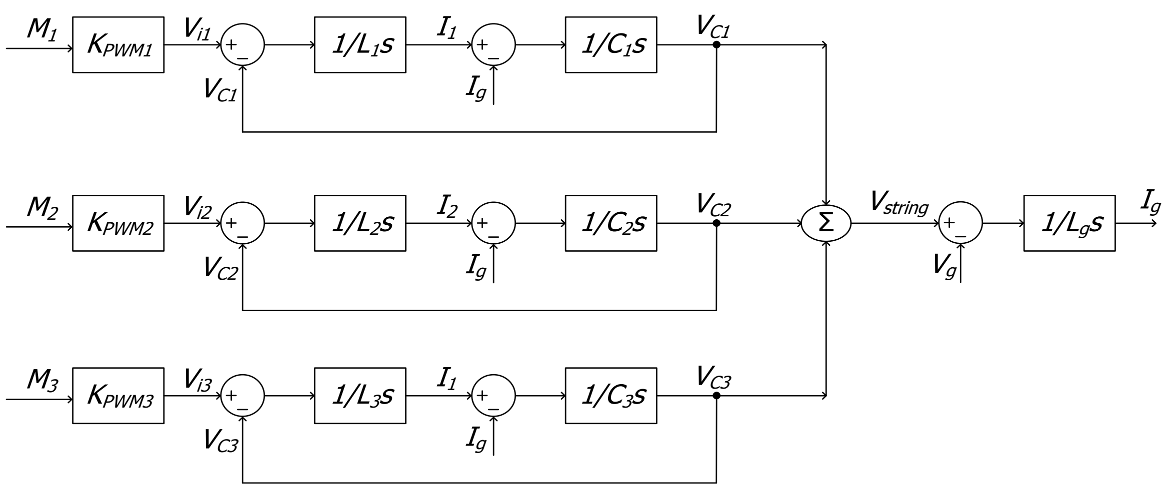

Figure 5.2. Single-phase AC-stacked grid-tied PV inverter block diagram.

where M is modulation index of each inverter, which is the input of each PWM generator. In this model, it is assumed that the switching frequency is high enough that PWM generator can be modelled as proportional gain (k_{PWM}) using average switching model. Based on block diagram presented in Figure 5.2, capacitor voltages and output current can be derived in (5.1) and (5.2), where V_{Cn} is the capacitor voltage of each inverter and I_g is the string output current. As can be seen, in the open loop model, output voltage of each inverter depends on the input modulation index of that inverter and also the output string current.

$$V_{Cn} = \frac{M_n K_{PWM}}{1 + L_n C_n s^2} - \frac{L_n s I_g}{1 + L_n C_n s^2} \tag{5.23}$$

$$I_g = \left(\sum_{n=1}^{3} V_{Cn} - V_g \right) \frac{1}{L_g s} \tag{5.24}$$

Combining these two equations and considering that the individual inverters consist of similar passive components which can represent as L_n, the transfer function of the string current can be formulated as:

$$\begin{aligned} I_g &= \frac{M_1 K_{PWM1}}{L_g L_n C_n s^3 + (3L_n + L_g) s} + \frac{M_2 K_{PWM2}}{L_g L_n C_n s^3 + (3L_n + L_g) s} \\ &+ \frac{M_3 K_{PWM3}}{L_g L_n C_n s^3 + (3L_n + L_g) s} - V_g \frac{1 + L_n C_n s^2}{L_g L_n C_n s^3 + (3L_n + L_g) s} \end{aligned} \tag{5.25}$$

In the HCVC control algorithm presented for this architecture, CAVC controls the current and remaining inverters build up the voltage for grid connection. Therefore, adding compensator to the first inverter which is assumed to be CAVC will change the block diagram of the system of Figure 5.3 to Figure 5.5 and Equation (5.3) will be changed to (5.4):

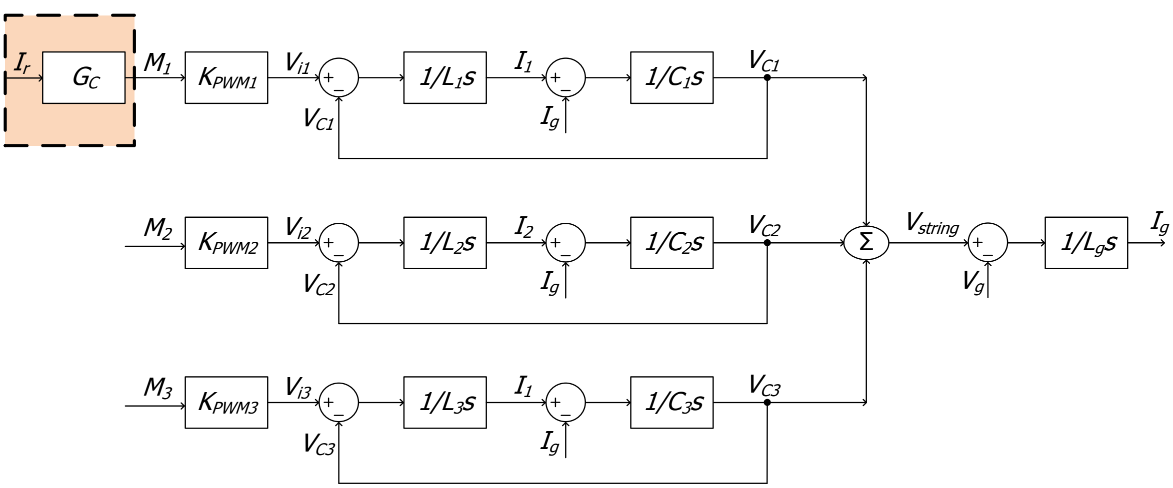

Figure 5.3. Block diagram of open loop

$$I_g = \frac{I_r G_c K_{PWM1}}{L_g L_n C_n \mathrm{s}^3 + (3L_n + L_g)\mathrm{s}} + \frac{M_2 K_{PWM2}}{L_g L_n C_n \mathrm{s}^3 + (3L_n + L_g)\mathrm{s}} + \frac{M_3 K_{PWM3}}{L_g L_n C_n \mathrm{s}^3 + (3L_n + L_g)\mathrm{s}} - V_g \frac{1 + L_n C_n \mathrm{s}^2}{L_g L_n C_n \mathrm{s}^3 + (3L_n + L_g)\mathrm{s}} \quad (5.26)$$

where I_r is the reference current and G_C is compensator which can be PI or PR controller presented in Equation (5.5) and Equation (5.6).

$$G_{CPI} = K_p + \frac{K_i}{\mathrm{s}} \quad (5.27)$$

$$G_{CPR} = K_p + \frac{K_r \mathrm{s}}{\mathrm{s}^2 + w^2} \quad (5.28)$$

Bode plots of this open-loop system considering PR compensator, PI compensator and no compensator are presented in Figure 5.4 with system parameters shown in Table 5.1. Since the bode plots are coincided including the cutoff frequency, so applying PI and PR controllers does not affect the stability of the system. On the other hand, PR controller has a big gain at fundamental frequency, which means it can track the AC-reference at this frequency without error.

Table 5.1. AC-stacked grid-tied system parameters

Parameter	Value	Symbol
Filter inductor	$300\mu H$	L_n
Filter capacitor	$200\mu F$	C_n
DC-bus capacitor	$100mF$	C_{PVn}
Interface inductor	$100\mu H$	L_g
PV voltage at MPP	$33.47V$	V_{MPP}

PV current at MPP	$7.63A$	I_{MPP}
PV power at MPP	$255W$	P_{MPP}
Grid voltage	$45Vrms$	V_g
Switching frequency	$36kHz$	f_{sw}

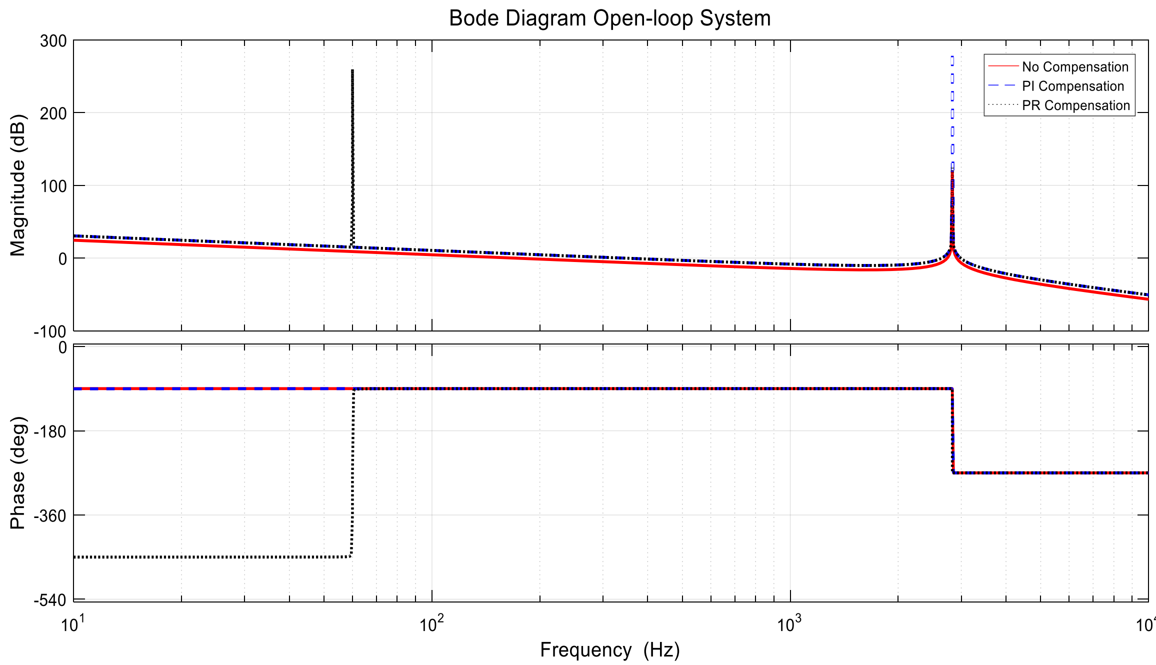

Figure 5.4. Bode plot of the open loop system with no compensation, PI compensator and PR compensator.

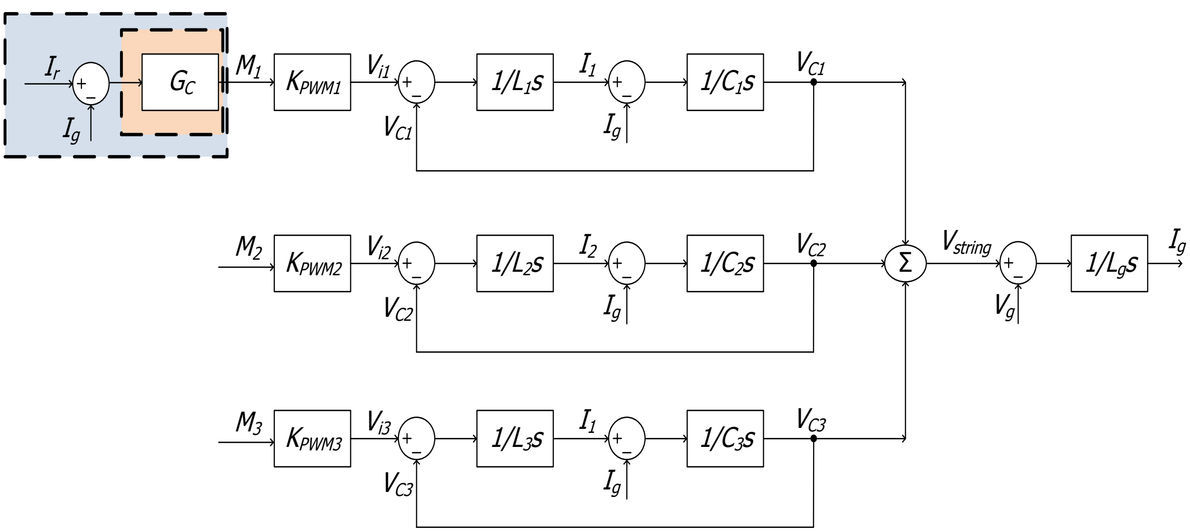

Figure 5.5. Closed-loop AC-stacked PV inverter model.

By adding the feedback term of the string current to the block diagram, the open-loop system will be changed to a closed loop system presented in Figure 5.5. In this case, Equation (5.23) for inverter #1 will be changed to Equation (5.29) and other two inverter transfer functions remain the same as Equation (5.23). Transfer function of string current to grid voltage for the closed loop system is presented in (5.30).

$$V_{C1} = \left(\frac{G_C K_{PWM}}{1 + L_n C_n s^2} \right) I_r - \left(\frac{K_{PWM} G_C + L_n s}{1 + L_n C_n s^2} \right) I_g \tag{5.29}$$

$$V_g = \left(\frac{L_g L_n C_n s^3 + K_{PWM} (G_C) + 3L_n s + L_g s}{1 + L_n C_n s^2} \right) I_g \tag{5.30}$$

5.3. Single-member Harmonics Compensation (SmHC)

The first harmonics compensation method proposed for this architecture in this dissertation is Single-member Harmonics Compensation, where only CAVC participates in mitigating the impact of background harmonics on the output current. In this method, separate resonant controllers are applied for compensation of selective harmonics and the reference for these controllers are zero to mitigate the selective harmonics. The outputs of the controllers are added to the modulation index for PWM generation. The block diagram of this method is presented in Figure 5.6. For this system, Equations (5.29) and (5.30) will convert to Equations (5.31) and (5.32), where $G_{PWM_{5th}}$ and $G_{PWM_{7th}}$ are PR controllers applied for mitigating the impact of background harmonics on 5th and 7th harmonics. Equation (5.33) shows the grid voltage disturbance to the string current which represents the grid impedance of the system with this control strategy.

$$V_{C1} = \left(\frac{G_C K_{PWM}}{1 + L_n C_n \, s^2} \right) I_r - \left(\frac{K_{PWM} (G_C + G_{PWM_{5th}} + G_{PWM_{7th}}) + L_n \, s}{1 + L_n C_n \, s^2} \right) I_g \qquad (5.31)$$

$$V_g = \left(\frac{L_g L_n C_n \, s^3 + K_{PWM} (G_C + G_{PWM_{5th}} + G_{PWM_{7th}}) + 3L_n \, s + L_g \, s}{1 + L_n C_n \, s^2} \right) I_g \qquad (5.32)$$

$$Z_g = G\left(\frac{V_g}{I_g} \right) = \left(\frac{L_g L_n C_n \, s^3 + K_{PWM} (G_C + G_{PWM_{5th}} + G_{PWM_{7th}}) + 3L_n \, s + L_g \, s}{1 + L_n C_n \, s^2} \right) \qquad (5.33)$$

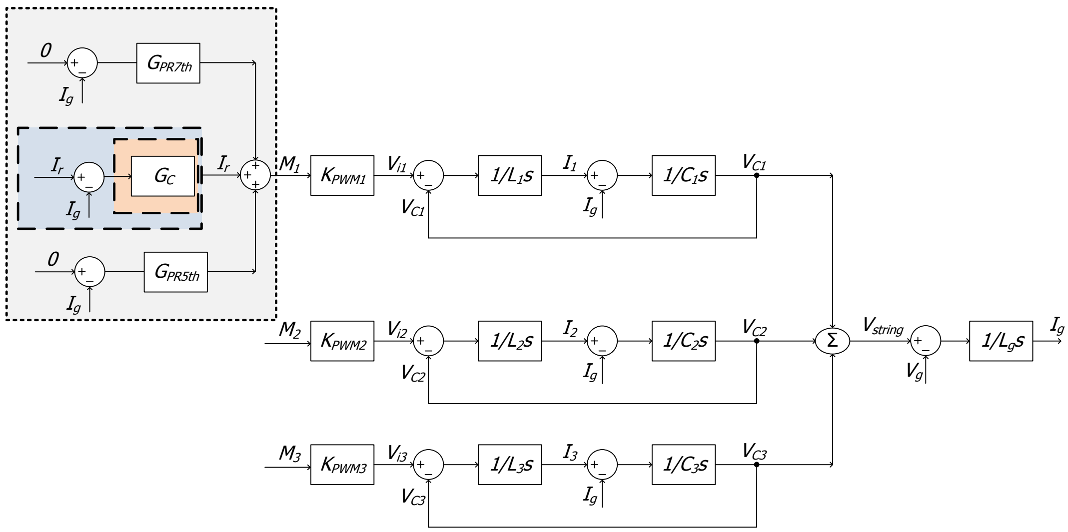

Figure 5.6. Block diagram of single-member harmonics mitigation strategy for AC-stacked PV inverter system.

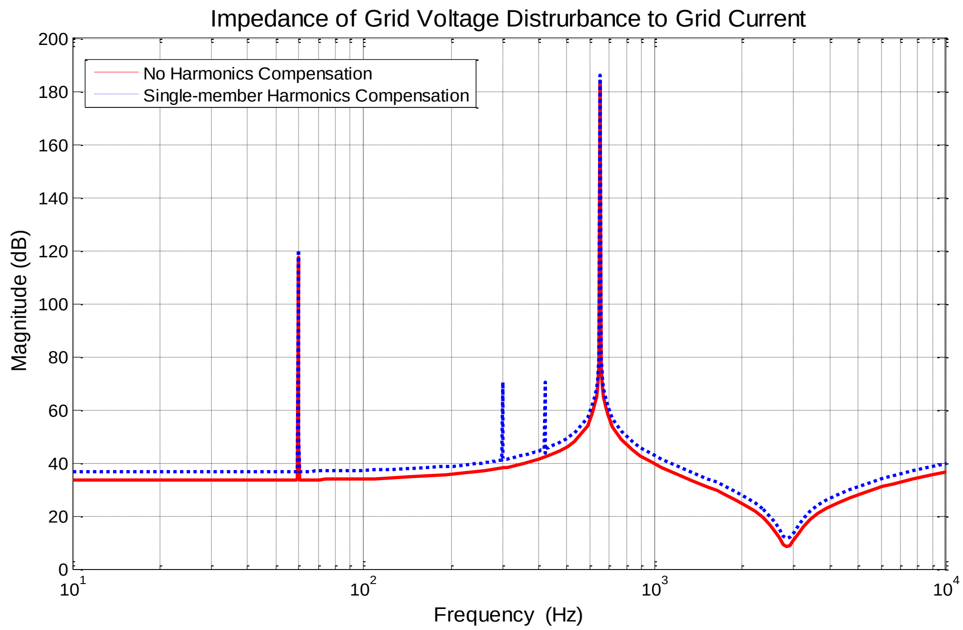

Figure 5.7. Grid voltage impedance to the output current with no harmonics mitigation and single-member harmonics mitigation method.

Impedance of grid voltage disturbance to the output current is presented in Figure 5.7. As you can see the in this plot, by adding PR controllers in SmHC method, the impedance of the system is increased in 5th and 7th harmonics. Therefore, the grid-voltage disturbance cannot impact on the string current. Evaluating the individual inverters impedances in Figure 5.8 shows that the high impedances at 5th and 7th harmonics are applied by CAVC inverter and VMM inverters are not participating in the harmonics mitigation as expected. This method will reduce the operation margin of CAVC because this inverter should utilize some part of its available operation margin for harmonics compensation. As a consequence, the operation margin of the whole system will be reduced which is the main constraint of this method.

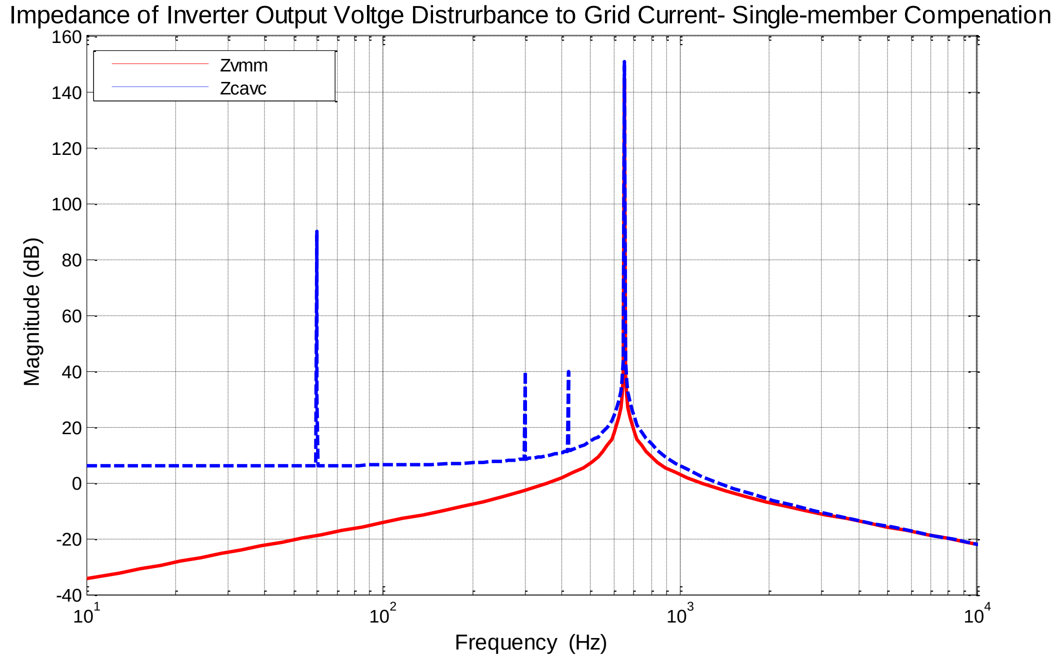

Figure 5.8. Impedance of individual inverter voltage disturbance to the string current in SmHC method.

5.4. All-member Harmonics Compensation (AmHC)

Because of the aforementioned constraint of SmHC method, the second method which is All-member Harmonics Compensation (AmHC) is proposed. In this method, not only CAVC mitigates the impact of selected background harmonics on the output current, but also VMMs will participate in this task. This method is applied with no communication requirements. Since the inverters are connected in series and the current is flowing through all the inverters and the output current measurements are available for all the inverters, all the individual inverters can detect the distorted output current autonomously and they can participate in harmonics mitigation. The block diagram of this inverter is presented in Figure 5.9.

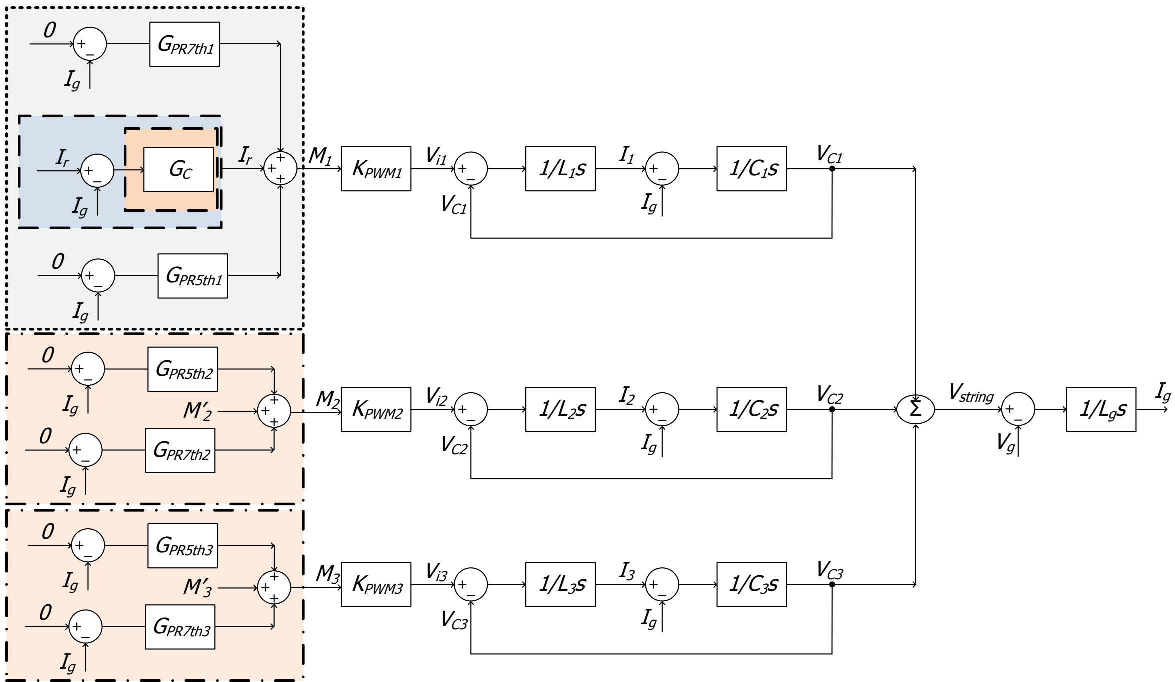

Figure 5.9. All-members Harmonics compensation method for AC-stacked PV inverter system.

Equations (5.31) and (5.32) will be changed to Equations (5.34) and (5.35) for AmHC method. Grid impedances of this method along with SmHC method and no compensation condition are presented in Figure 5.10. As can be seen, adding harmonics compensation to VMM inverters won't impact the stability of the system and the system will provide high impedance for attenuating the impact of selected harmonics on string current.

Individual inverter impedances in AmHC method are presented in Figure 5.11. As can be seen, in this method, VMM inverters are also participating in harmonics mitigation and providing high impedance for selective harmonics.

$$V_{C2} = \left(\frac{K_{PWM} M'_2}{1 + L_n C_n s^2}\right) - \left(\frac{\left(K_{PWM} G_{PWM_{5th}} + K_{PWM} G_{PWM_{7th}}\right) + L_n s}{1 + L_n C_n s^2}\right) I_g \tag{5.34}$$

$$V_g = \left(\frac{(G_C + G_{PWM1_{5th}} + G_{PWM1_{7th}} + G_{PWM2_{5th}} + G_{PWM2_{7th}})}{1 + L_n C_n \mathrm{s}^2} + \frac{L_g L_n C_n \mathrm{s}^3 + 3L_n \mathrm{s} + L_g \mathrm{s}}{1 + L_n C_n \mathrm{s}^2} + \frac{(G_{PWM3_{5th}} + G_{PWM3_{7th}})}{1 + L_n C_n \mathrm{s}^2} \right) I_g \tag{5.35}$$

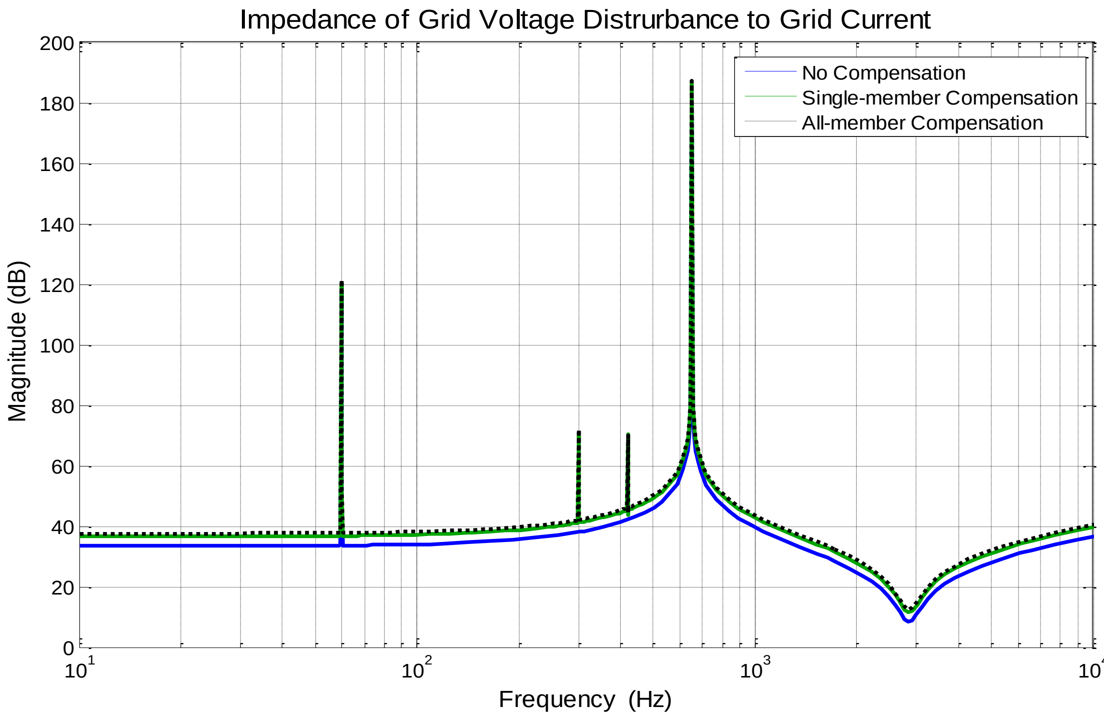

Figure 5.10. Grid voltage impedance to the output current with no harmonics mitigation, SmHC method and AmHC method.

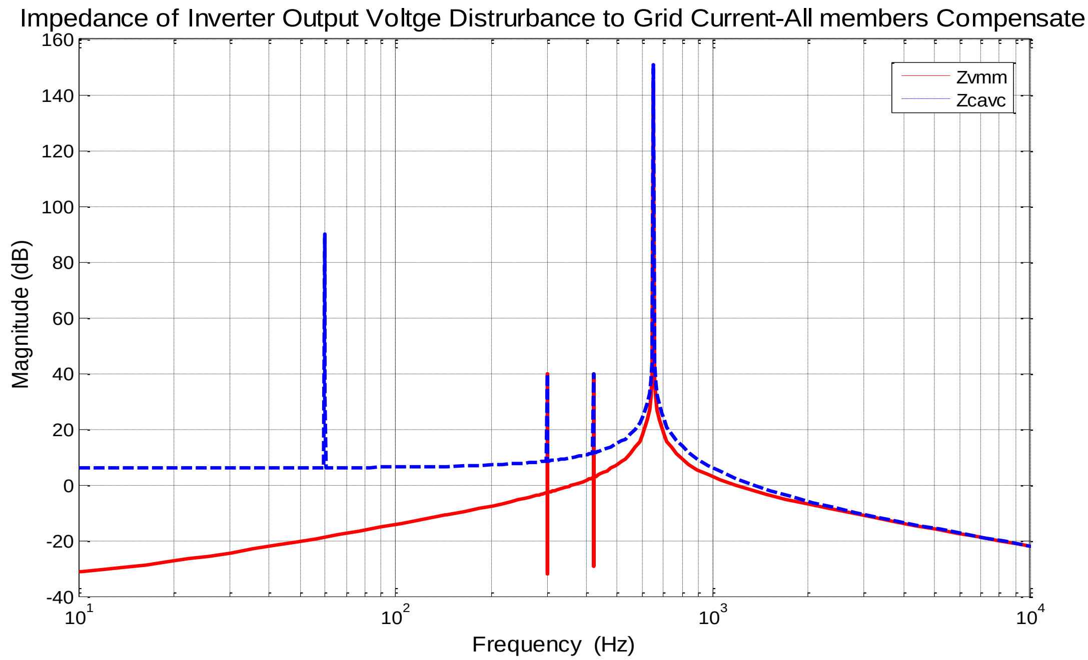

Figure 5.11. Impedance of individual inverter voltage disturbance to the string current in SmHC method

The detailed schematic of AC-stacked PV inverter system with decentralized control HCVC control scheme proposed in previous chapters with AmHC harmonics mitigation method proposed in this chapter is presented in Figure 5.12.

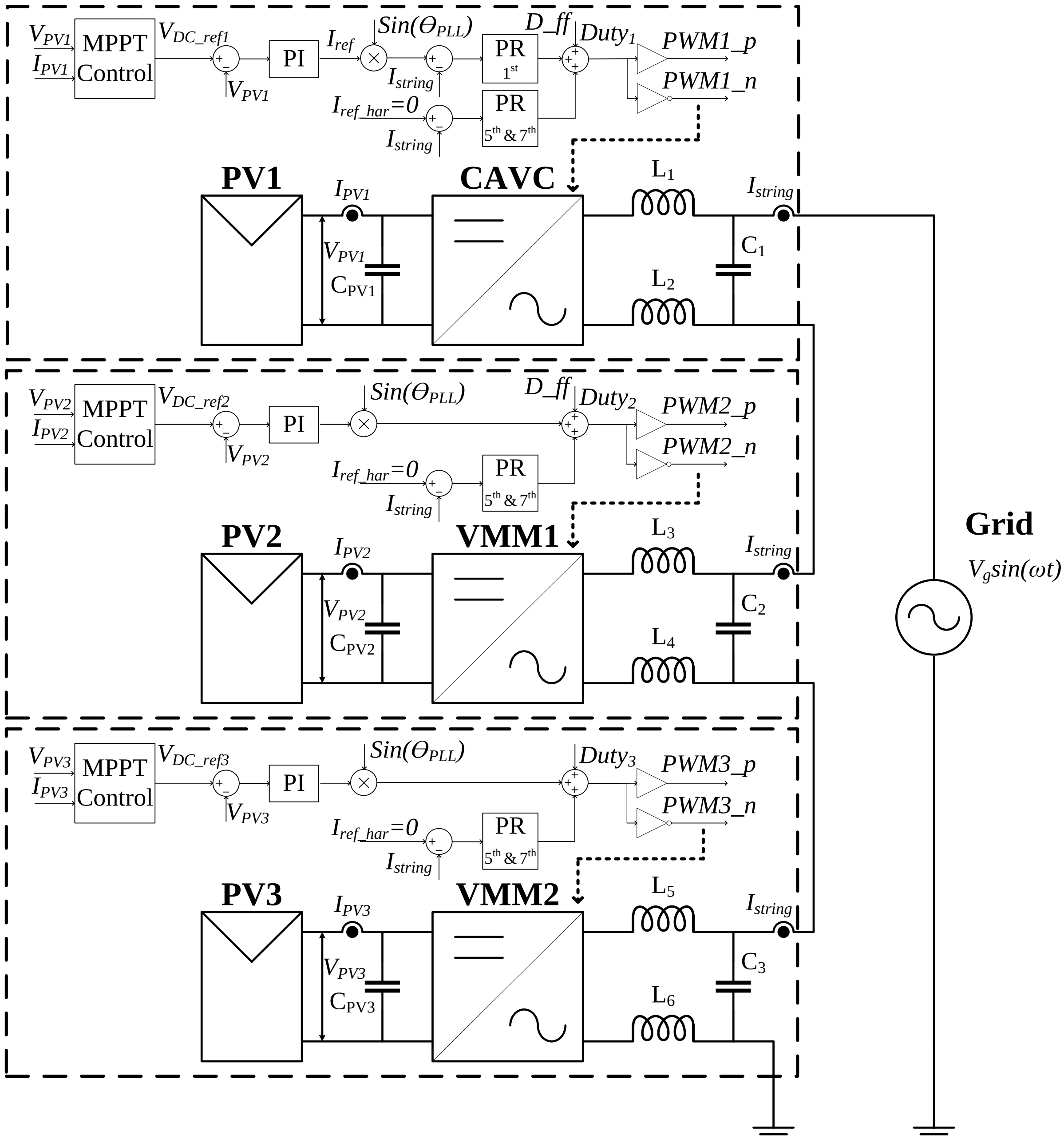

Figure 5.12. AC-stacked PV inverter schematic with decentralized controller and proposed All-member Harmonics Compensation control method.

CHAPTER 6: CONTROLLER ROBUSTNESS ANALYSIS

Increasing the integration of PV systems into distribution and transmission networks requires more reliable and more robust PV inverter architectures. A quantitative reliability and robustness assessment of Photovoltaic systems particularly grid-tied PV inverters is a critical requirement to assure reliable and robust PV generation. In this section, by proposing a comprehensive robustness index, reliability and robustness of the grid-tied AC-stacked PV Inverter architecture with decentralized HCVC control scheme are evaluated and the effect of variation, inaccuracies and environmental changes on reliability and robustness of PV inverters are analyzed.

6.1 Introduction

In recent years, cost reduction of PV modules and new power electronics technologies have led the capacity of solar PV systems to increase significantly in both distribution and transmission power networks [1]. However, traditional grid codes and standards are defined for power networks with low penetrated PV systems which should be reconsidered for highly penetrated networks. In high penetrated power networks, efficient and reliable operation of the system depends on robust operation of PV systems in which PV inverter plays a critical role. Therefore, PV inverter reliability and robustness should be considered and evaluated during design and operation of PV systems [4].

To provide comprehensive analysis of grid-tied PV inverter's robustness, there are multiple parameters that should to be considered such as: efficiency, Total Harmonic Distortion (THD), power factor (PF) compliance, Maximum Power Point Tracking (MPPT) accuracy.

In 2015, a new design tool was proposed to consider PV inverter reliability in design process of PV systems [83, 84]. Among all different performance parameters, efficiency has a great impact on reliability and robust operation of PV inverters which has been analyzed in the literature from the topologies and control based approaches [85-87]. However, inverter performance metrics such as efficiency do not only depend on topology and control scheme but also depend on characteristics of employed components such as passive components and sensing components [84, 86]. These characteristics can be varied based on different parameters such as manufacturing inaccuracies, environmental conditions and aging. The impact of physical variation of these components on efficiency of PV inverters has been analyzed in the recently published studies [84, 87-94].

On the other hand, efficiency is not the only parameter which has impact on robust operation of PV inverters. There are other characteristics such as Total Harmonic Distortion (THD), power factor compliance and Maximum Power Point Tracking (MPPT) accuracy that should be considered to have a comprehensive evaluation about inverter robustness [95, 96]. The impact of these performance characteristics on robust operation of PV inverters has been studied in previous literature separately.

- Conversion Efficiency: Conversion efficiency as the most important parameter was analyzed in the literature and it was considered as the only parameter which has impact on PV inverter robustness [84, 94]. Efficiency analysis of different PV inverter topologies and different semiconductor devices have been performed recently [91]. Moreover, the impact of control architecture on efficiency of low switching frequency PV inverter topologies is studied [92]. Impact of physical variation of main components of PV inverters on conversion efficiency was studied in [84] and results showed that European efficiency calculation should be modified for future high penetrated PV systems.

- Total Harmonic Distortion: Injection of harmonic distortion from inverters is a known fact which is more severe issue in networks with high penetrated PV generations. Numerous researches were conducted to mitigate these injected harmonics [2, 72, 74, 97]. This problem becomes more severe with increasing penetration of grid tied PV inverters to the network [93]. In recent years, several researches focused on attenuating the harmonic distortion of grid connected PV inverters output current [94, 97]. Physical variation of passive components is a parameter which has impact on harmonic distortion content and reliability of PV inverter systems in different operation conditions which should be analyzed.

- Power Factor Compliance: Reliable and robust operation of future power systems with highly penetrated PV systems asks for participation of PV inverter systems in ancillary services such as reactive power control which needs accurate power factor control on PV inverters [2, 6, 72]. Power factor control accuracy is highly dependent on manufacturing accuracy of physical components.

- Maximum Power Point Tracking Effectiveness: Accuracy of MPPT algorithm directly contributes in whole PV system efficiency which has critical impact on reliable and robust operation of PV systems. Previous studies showed that electrical component variation has a large impact on MPPT accuracy which can reduce the PV inverter robustness [98, 99]. The more analyses showed that MPPT effectiveness is highly dependent on environmental condition and component variations [98, 99].

In this section, a new performance metric which is called Smart Inverter Robustness Index (SIRI), is proposed to evaluate the robustness of grid-tied PV inverter systems considering conversion efficiency, THD, PF compliance and MPPT accuracy.

6.2 Smart Inverter Robustness Index

As mentioned above, a comprehensive grid-tied PV inverter robustness index should consist of efficiency, THD, PF and MPPT accuracy. For each of these parameters, there is a specific limit which shows the boundary of robust operation. Based on grid codes and standards, inverters should operate within these limits. For instance, according to IEEE-519-1992 standard, total harmonics voltage distortion on power system 69 kV and below was limited to 5.0% THD [100]. This limit was changed to 8% THD in the new IEEE-519-2014 [101]. Based on the same standards, there is 5% TDD limit for current distortion for systems rated 120 V through 69 kV.

The margin between measured parameter and the limit shows how far the system is operating from the boundary of robustness (1). Obviously, If the measured parameter is not within the robustness limit, the system would be un-robust.

$$margin_{THD} = k_{THD} - THD \tag{6.1}$$

In this equation THD is the measured THD of the inverter system and k_{THD} is the THD robustness limit. Similar to (6.1), we can calculate robustness margin for other parameters (6.2)-(6.4).

$$margin_{PF} = PF - k_{PF} \tag{6.2}$$

$$margin_{MPPT} = MPPT - k_{MPPT} \tag{6.3}$$

$$margin_{Eff} = Eff - k_{Eff} \tag{6.4}$$

In these equations k_{PF}, k_{MPPT} and k_{Eff} are robustness limits for power factor, MPPT accuracy and efficiency. The product of these margins gives us the combined robustness margin. However, because these margins can have different limits, each margin should be normalized in respect to the maximum margin possible to have all the margins in the same scale. The maximum margin for these parameters are shown in (6.5)-(6.8).

$$Max_{PFmar} = 1 - k_{PF} \tag{6.5}$$

$$Max_{MPPTmar} = 1 - k_{MPPT} \tag{6.6}$$

$$Max_{Effmar} = 1 - k_{Eff} \tag{6.7}$$

$$Max_{THDmar} = k_{THD} \tag{6.8}$$

Using maximum margins in (6.5)-(6.8) equations, we can normalize the equations (6.1)-(6.4) to (6.9)-(6.12).

$$Nor_{PFmar} = \frac{|PF - k_{PF}|}{1 - k_{PF}} \tag{6.9}$$

$$Nor_{MPPTmar} = \frac{MPPT - k_{MPPT}}{1 - k_{MPPT}} \tag{6.10}$$

$$Nor_{Effmar} = \frac{Eff - k_{Eff}}{1 - k_{Eff}} \tag{6.11}$$

$$Nor_{THDmar} = k_{THD} \tag{6.12}$$

Therefore, if we combine these four normalized indices in a single index, the resultant index would consider all the major characteristics of grid-tied PV inverters in with similar weighting factor. This combined normalized index can be seen in (6.13).

$$SIRI = Nor_{PFmar} \times Nor_{MPPTmar} \times Nor_{Effmar} \times Nor_{THDmar} \tag{6.13}$$

This index which is introduced in this thesis, is called SIRI. SIRI index is expanded in (6.14). In this index, if each normalized section is lower than one, it means the inverter system is not robust and the SIRI index would be -1. However, if the SIRI index is positive, it means the system is robust and the higher is the SIRI index the more robust is the inverter system. For robust systems, SIRI index can vary between 0 and 1 because all the characteristics are normalized and between 0 and 1. A system with SIRI index equal to 1 is an ideal system perfect PF control, no harmonics injection and 100% efficiency, which is not applicable in real life. On the other hand, a system with SIRI index of 0 operates at the boundary of robustness, where one or some of the parts of SIRI index is/are zero.

$$SIRI = \begin{cases} \dfrac{(PF - k_{pf})}{(1 - k_{pf})} \times \dfrac{(Eff - k_{Eff})}{(1 - k_{Eff})} \times \dfrac{((1 - THD) - (1 - k_{THD}))}{k_{THD}} \times \dfrac{(MPPT_{Eff} - k_{MPPT})}{(1 - k_{MPPT})}, \\ \qquad PF > k_{pf}, Eff > k_{Eff}, THD < k_{THD} or MPPT_{Eff} > k_{MPPT} \\ -1, \qquad PF < k_{pf}, Eff < k_{Eff}, THD > k_{THD} or MPPT_{Eff} < k_{MPPT} \end{cases} \tag{6.14}$$

6.3 Statistical Analysis

PV inverter operation and lifetime are highly dependent on performance of electrical components. One of the most important electrical components in modern PV inverters with distributed architecture and high frequency switching is a current sensing device. The performance of different current sensor technologies such as hall-effect, magneto resistor-based, and fluxgate current sensors with wide band of operational characteristics highly rely on manufacturing accuracy, variations of environmental conditions and changes in component's characteristics due to aging. Therefore, reliability and robustness of PV inverters will be affected respectively. Since physical variations is a consequence of the inherent randomness in electrical components, in order to analyze the impact of these uncertainties on performance of PV inverters, the system should be statistically analyzed. Different statistical analysis methods can be used for solving this problem, but as the most favorite one is Monte Carlo Sampling method. This method utilizes statistical analysis and random sampling experiments to provide approximate solutions for unformulated problems, which are random in nature and it is very difficult to solve [102]. Monte Carlo statistical analysis was utilized in the semiconductor industry to prove the feasibility of manufacturing of systems consisting several semiconductor devices. Similar approaches are expected to arrive when several components and devices work cooperatively together in a system such as PV inverters. Therefore, Monte Carlo method is widely applied for reliability and robustness analysis of PV inverters [86, 90, 95, 103, 104]. Monte Carlo analysis requires a large number of sampling points for solving big statistical problems with several uncertain variables. By using variance reduction techniques, the required number of sampling points can be reduced and consequently the simulation time reduced significantly [105]. A commonly used variance reduction method known as the Latin Hypercube Sampling (LHS) is a type of stratified Monte Carlo sampling algorithms, which used in this thesis. The LHS method not only reduces the required number of sampling points, but also improves the accuracy and confidence in the results [106]. In this method, cumulative distribution function is divided into few equally probable sub-sections and the equal number of sampling points are selected from these sub-sections. Therefore, this method by spreading sampling points can reduce the required points significantly [4, 107]. Figure 6.1 shows the advantage of Random Latin Hypercube Sampling (RLHS) method compare with Monte Carlo (MC) sampling method. As it can be seen in Figure 6.1.a, Monte Carlo method is a completely random method, which requires high number of sampling points to provide accurate results. In MC method, small number of sampling mostly gathered in the high probability areas and the analysis cannot provide a conclusive result. On the other hand, in RLHS method, the probability fun is divided to few equally probable areas and based on number of available samples few samples are selected from each area. In this way, sampling points are distributed in all over the function as can be seen in Figure 6.1.b.

In this dissertation, RLHS algorithm is used to model the impact of uncertainties of passive components and current sensing devices with minimum sampling points. Regarding the passive components variations, a sample size of 30 samples, was selected using RLHS method. Each physical variable is modeled with lognormal distribution function. Each of these variables was partitioned in five non-overlapping regions with equal probability. In each partition, six different values were selected randomly with respect to lognormal probability distribution. After selecting 30 values for each variable, 30 values obtained for all the passive components are randomly coupled with each other to build the random sets of values for passive component. Current sensor variations are modeled by a random scaling factor, which multiplied to sensor measurements and a random offset value is also added to the measurements. Robustness evaluation depends on SIRI index, which quantifies the robust operation of PV inverters.

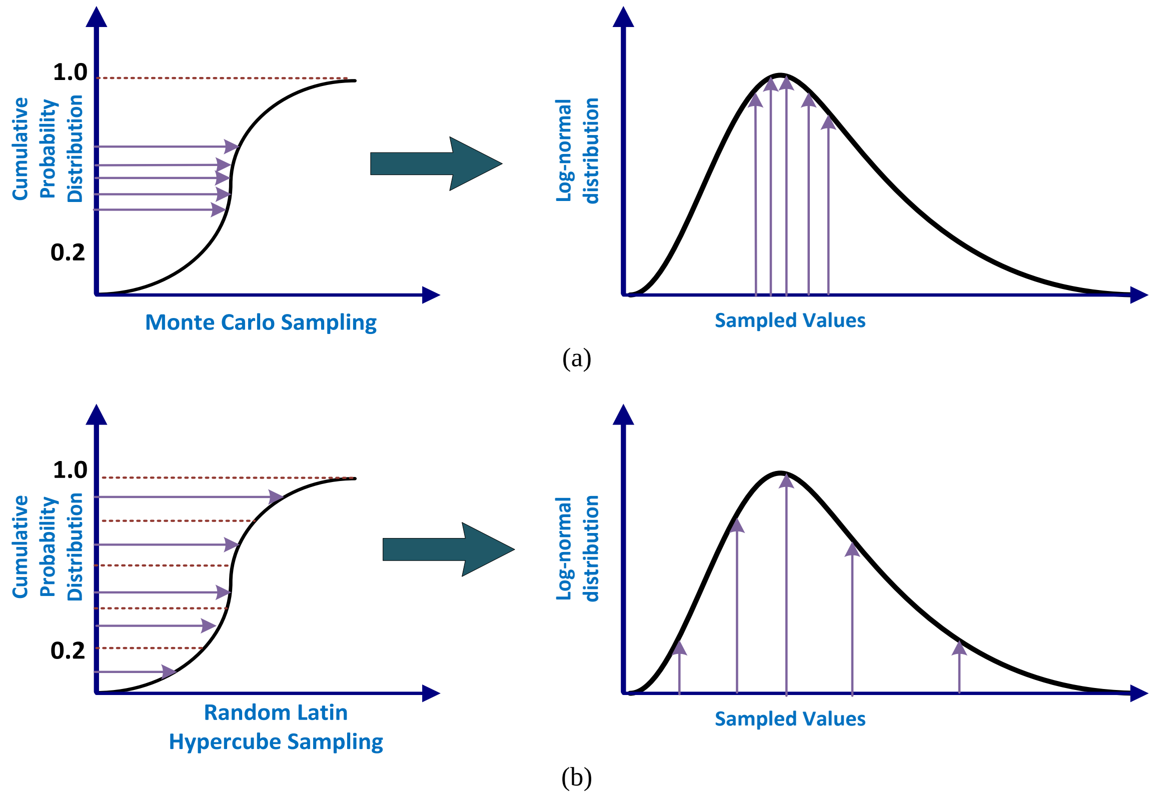

Figure 6.1. Impact of sampling methods on the required sampling points for statistical analysis. a. Monte Carlo Sampling (MC). b. Random Latin Hypercube Sampling (RLHS)

6.4 Case study

6.4.1 String Inverter

The schematic of a single-stage single-phase grid-tied strung PV inverter which is studied in this thesis is shown in Figure 6.2. A control scheme, consisting MPPT operation, DC voltage control and output current control, has been used to control this system. However, there are numerus inaccuracies which have impact on robust operation of this system. Some examples of these inaccuracies are shown in Figure 6.2, such as passive component variation due to manufacturing inaccuracies, aging and also sensing inaccuracies due to sensors manufacturing inaccuracies and digital control discretization like Analog to Digital Conversion (ADC) sampling and PWM sampling time. The focus of this thesis is on passive component inaccuracies and current sensing inaccuracies, which is highlighted as black in the figure.

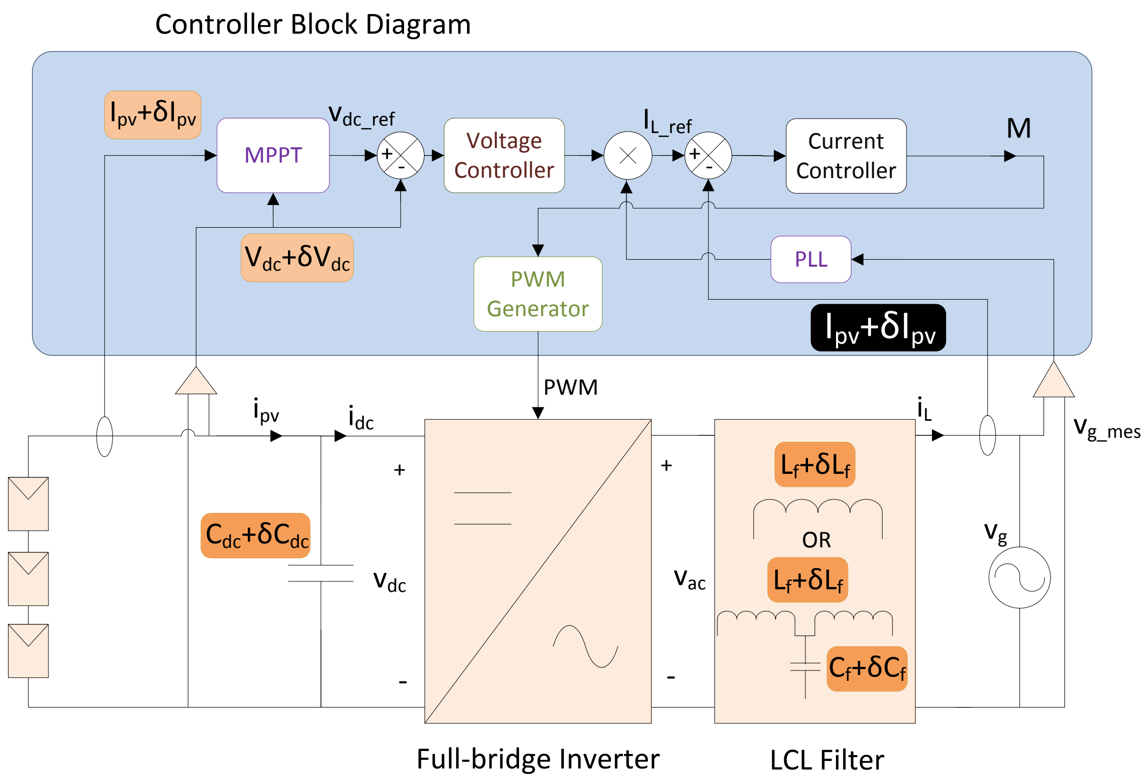

Figure 6.2. Grid-tied string PV inverter studied in this thesis, with passive component inaccuracies and sensing inaccuracies.

6.4.2. AC-stacked PV Inverter

By analyzing a single grid-tied inverter system and AC-stacked PV inverter system, the impact of cascading inverters on the robustness of AC-stacked PV inverter system will be evaluated in the following section. The power level of this system is equal to the single inverter system presented in the previous section. In this study inaccuracies of passive components and current sensors are studied. Based on HCVC method, only CAVC is responsible to control the output current and this inverter has a current sensor, which might have inaccuracy due to aging and environmental conditions. These inaccuracies affect the current measurement output by a scale factor, offset factor, and phase shift factor as shown in Figure 6.3.

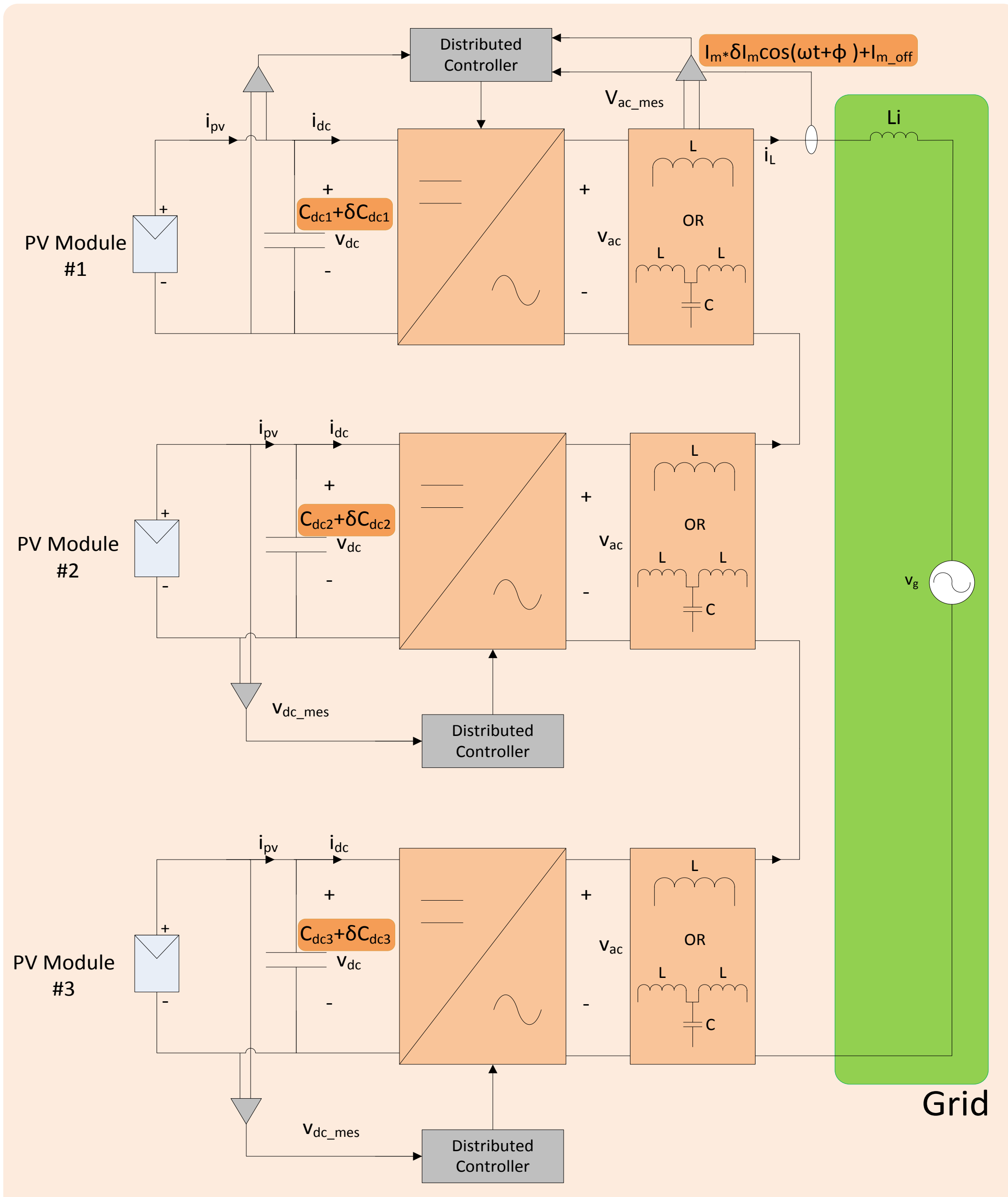

Figure 6.3. Grid-tied AC-stacked PV inverter architecture schematic with HCVC controller and with inaccuracies.

6.5 Results and discussions

In order to prove the effectiveness of proposed index and analyze the robustness of presented PV inverter systems, a Matlab Simulink model is built based on the schematics and the control schemes shown in Figure 6.2 and Figure 6.3. The input voltage of inverter is stabilized by a $50mF$ capacitor. The inverter switches are switching with speed of $80kHz$ and output voltage is filtered by an LC filter with designed values of $L = 150\mu H$ and $C = 50\mu F$. The Monte Carlo analysis and the Random Latin Hypercube Sampling (RLHS) have been used to study the impact of the physical variation on the operation of this system with minimum sampling points. In order to model the manufacturing inaccuracy of passive components, the lognormal distribution function with a mode equal to nominal value of the components is used. The mode of lognormal distribution functions can be calculated as below:

$$m = e^{\mu - \sigma^2} \tag{6.15}$$

where:

μ Mean of the distribution function
σ Standard deviation of the distribution function

To model the physical variations by RLHS method, the lognormal distribution function is divided into five regions with equal probability. The sampling selection method explained in section 6.2 is utilized for three passive components such as DC capacitor, filter capacitor and filter inductor. This study has been done for different standard deviations and constant mode value until a boundary for robust operation of the system is found. If in any run SIRI is not in its robust region the PV inverter string loses robust operation.

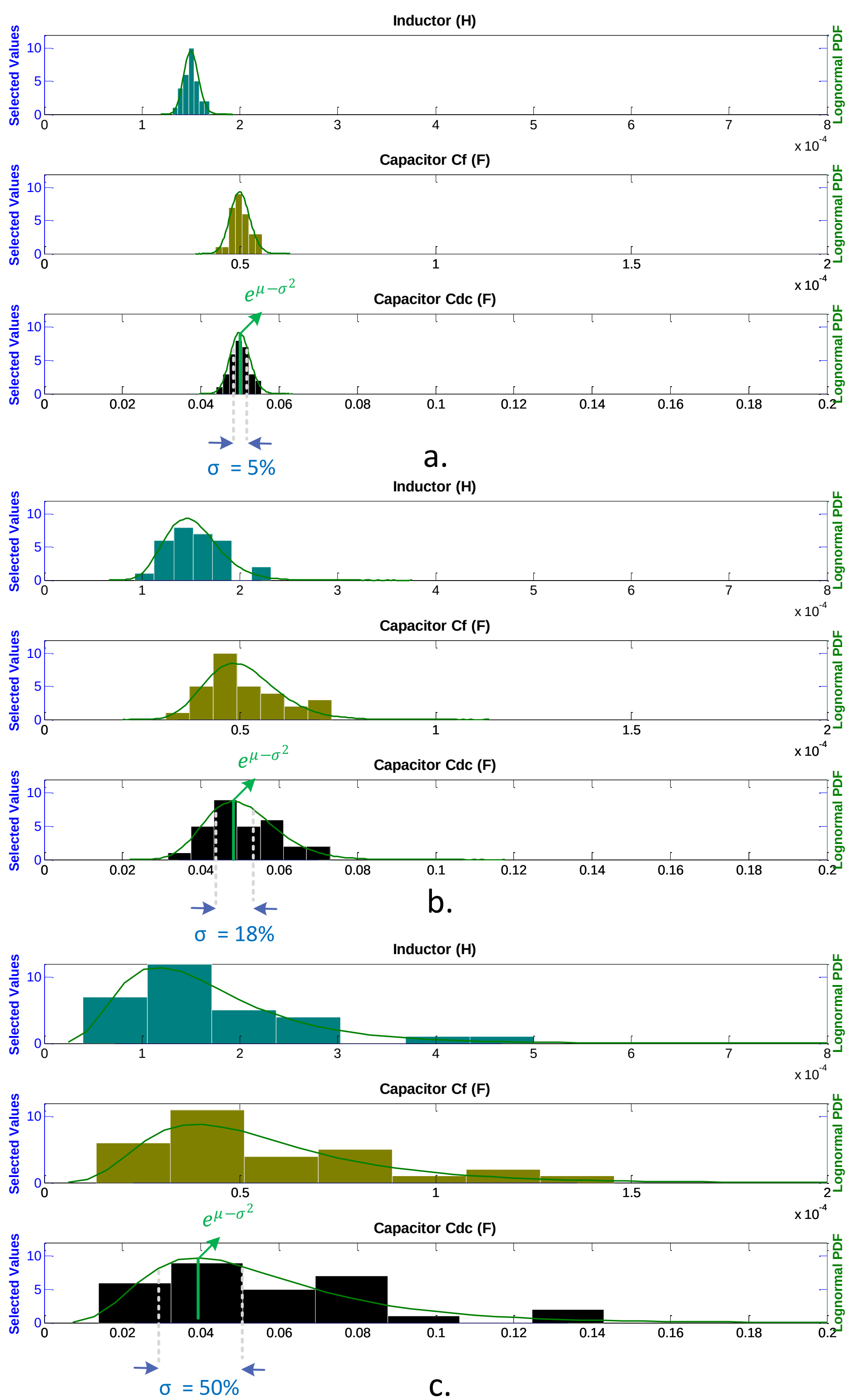

Figure 6.4. Selected passive components sampling sets for different standard deviations in the same scale, showing the distribution of sampling sets in different manufacturing inaccuracies a. 5% standard deviation (robust region) b. 18% standard deviation (boundary) c. 50% (un-robust region). The higher is the standard deviation, the more distributed is passive component values.

Figure 6.4 presents these sampling sets for three different standard deviations, 5% standard deviation which is inside robust region, 18% standard deviation which is the boundary of robust region and 50% standard deviation that is not robust. Figure 6.4 shows how by increasing manufacturing inaccuracy, the selected values are distributed and deviated from designed passive component values.

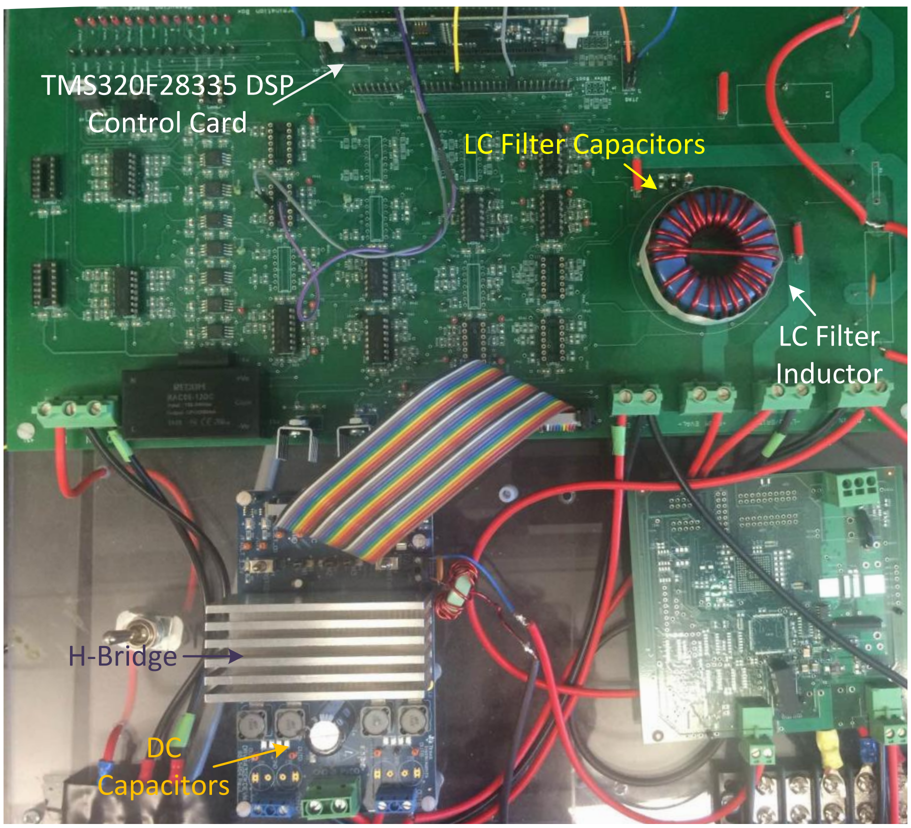

Figure 6.5. Lab-scaled single-phase single-stage PV inverter built for this study.

Verifying the proposed statistical analysis using experimental setup is almost impossible because of large number of sampling sets which requires huge variety of passive components with different manufacturing inaccuracies. Therefore, the feasibility of proposed analysis is verified by simulation analysis. However, in order to examine the accuracy of simulation setup an experimental test-bed has been designed and built which is shown in Figure 6.5. This inverter system is designed based on schematic of Figure 6.2 and inverter switching is controlled by a TMS320F28335 control card. Detailed quantitative evaluation of simulation and experimental system showed that the simulation system has the same performance as experimental test-bed in different operation conditions such as unity power factor, shading condition, and in different reactive power support situations. Figure 6.6 presents the exemplary results regarding the accuracy of the simulation model and experimental test-bed in symmetric condition with unity power factor. The comparison showed that simulation setup operation is very close to experimental test-bed with the error of less than 1%. Therefore, Simulation setup is used for all the statistical analysis in this thesis.

6.5.1. Passive Component Inaccuracies

In order to model the manufacturing inaccuracy and aging of passive components, the lognormal distribution function with a mode equal to nominal value of the components is used. To model the component variation due to manufacturing inaccuracies, aging and environmental conditions, the standard deviation of lognormal distribution function is changed. As can be seen in Figure 6.4, by increasing the standard deviation, the selected passive component values are deviated from the designed values. Table 6.1, presents the impact of manufacturing inaccuracy and aging of the DC capacitor on robustness of individual inverter at unity power factor. As can be seen in this table the boundary of robust operation is 39% standard deviation. Same study has been conducted on manufacturing inaccuracy of AC filter components and the results, presented in Table 6.2 shows that the boundary is 82% standard deviation. The next step is to study the robustness of PV inverter with combined DC capacitor and AC filter inaccuracies. The results presented in Table 6.3 and visualized in Figure 6.7, shows that the boundary of robustness is reduced to 18% standard deviation for combined inaccuracies.

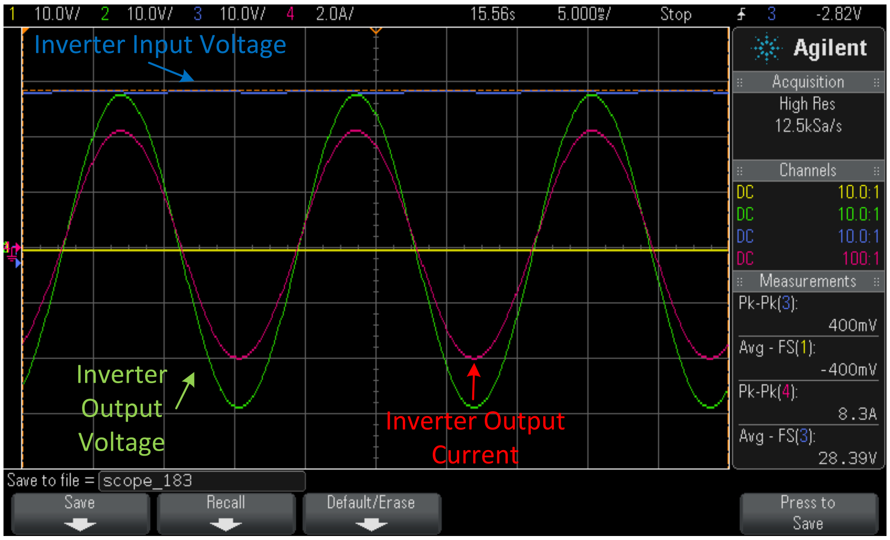

a.

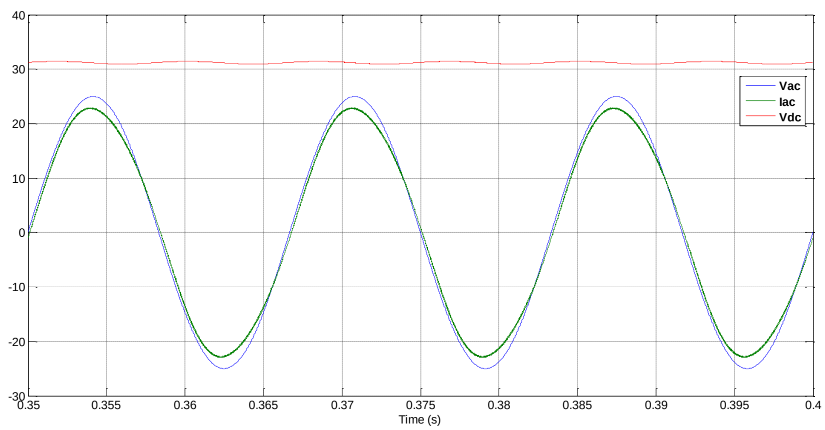

b.

Figure 6.6. Experimental setup verifies the performance of simulation system. a. Lab-scaled single-phase single-stage grid-tied PV inverter system operation with lowest physical variation b. Simulation of a real single-phase single-stage grid-tied PV inverter.

Due to self-healing characteristics of AC film capacitors, these components have less variation than DC electrolytic capacitors. Therefore, to compare the impact of variation of passive components on grid-tied single inverter and AC-stacked inverter system, the impact of variation of DC capacitor values are considered. This study has been conducted on a grid-tied system with three inverters shown in Figure 6.3. The boundary of robustness for this system is 51% which is higher than single inverter which was 39%. The reason for this fact is that, if in a AC-stacked inverter system a DC capacitor does not perform well, the impact on overall system robustness is less than a condition where we have a single inverter and one DC capacitor.

Table 6.1. Impact of DC capacitor variation on robustness of single grid-tied inverter

Standard Deviation	Efficiency	Power Factor	THD	MPPT	SIRI
0% (Ideal System)	98.14%	0.948	1.07%	99.9%	0.3882
20%	98.06%	0.947	9.74%	99.9%	0.3732
30%	98.11%	0.948	0.74%	99.8%	0.3389
37%	96.7%	0.948	0.70%	99.7%	0.1671
38%	96.06%	0.947	0.67%	99.7%	0.097
39%	95.36%	0.946	0.68%	99.7%	0.0306
40%	92.86%	0.945	0.68%	99.7%	-1

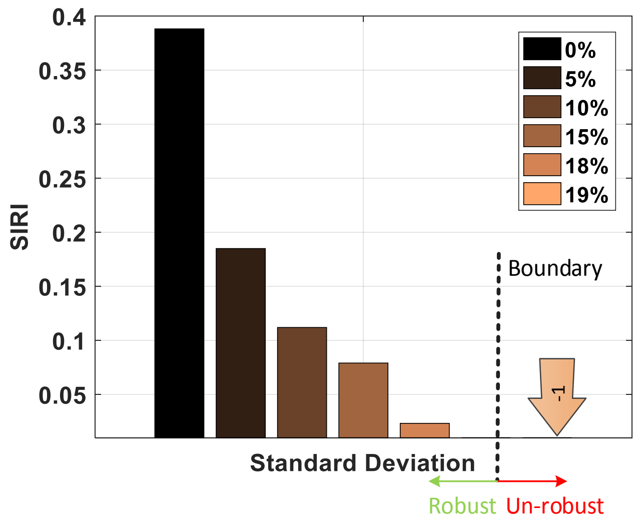

Figure 6.7. SIRI index for combined manufacturing inaccuracy in different standard deviations for grid-tied single PV inverter.

Table 6.2. Impact of AC filter variation on robustness

Standard Deviation	SIRI
0% (Ideal System)	0.3882
20%	0.3689
40%	0.311
50%	0.2751
70%	0.1983
82%	0.0751
83%	-1

Table 6.3. Impact of combined inaccuracy on robustness

Standard Deviation	SIRI
0% (Ideal System)	0.3882
5%	0.185
10%	0.112
15%	0.0791
18%	0.0233
19%	-1
20%	-1

6.5.2. Current Sensing Inaccuracies

In order to analyze the impact of current sensing inaccuracies on robust operation of string inverters and AC stacking PV inverters, two MATALB Simulink models are built based on schematics and control schemes presented in previous sections.

Table 6.4. Performance characteristics and SIRI index values for single gird-tied PV inverter system with different current sensing inaccuracies.

Standard Deviation	Efficiency	Power Factor	THD	MPPT	SIRI
0%	98.23%	0.9996	1.3%	99.93%	0.4282
1%	97.13%	0.9997	1.37%	99.65%	0.1211
5%	96.9%	0.9994	1.4%	99.56%	0.096
7%	96.37%	0.9993	1.6%	99.12%	0.0237
8%	96.09%	0.9992	1.6%	98.95%	-1

In an individual PV inverter system, the input voltage of the inverter is stabilized by a DC capacitor. The inverter switches at 40kHz and output voltage is filtered out by an LC filter. Table 6.4 presents the impact of increasing current sensing inaccuracies on robust operation of a single grid-tied PV inverter. As it can be seen in this table, increasing inaccuracies will reduce MPPT precision, and system efficiency. This system operates in robust region till 7% standard deviation, which is the boundary of robustness. For the inaccuracies more than 7%, the system enters in un-robust region where SIRI sets on -1. Figure 6.4 shows how increasing current sensing inaccuracies reduces the system robustness, which is represented by SIRI. Comparing Figure 6.8 and Figure 6.9, it can be concluded that by cascading the PV inverters and using a decentralized control approach, boundary of robustness is increased to 17% standard deviation. This happens because the current sensing inaccuracy has a direct impact on the MPPT accuracy of the PV inverter system. However, in AC-stacked architecture, (n-1) have been controlled by DC-bus voltage control and their MPPT operations are not affected by current sensing inaccuracies. Therefore, MPPT accuracy of whole structure could raise up and make the system more robust.

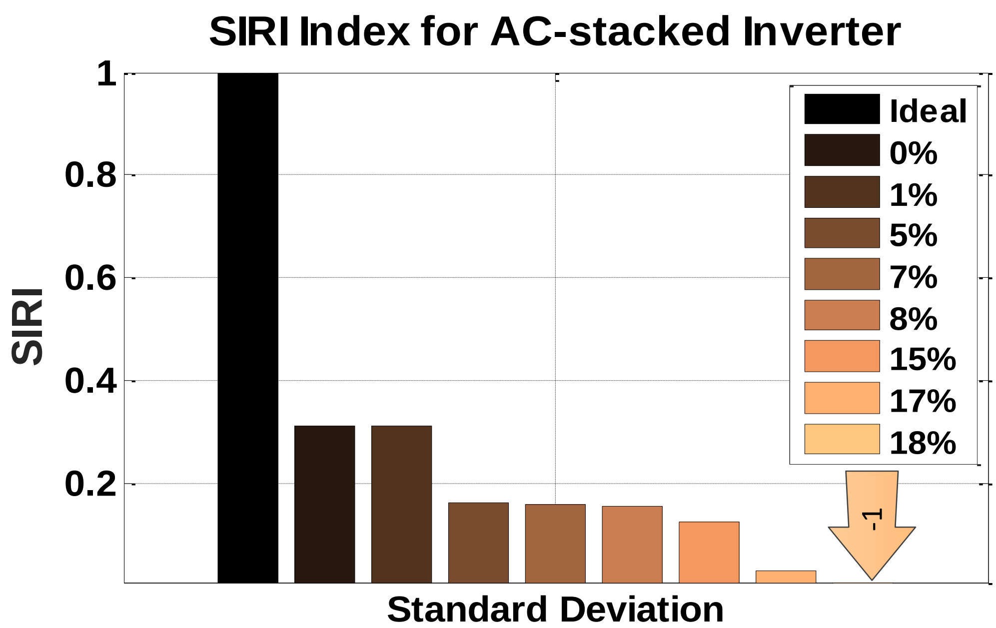

Figure 6.8. SIRI index for a single grid-tied PV inverter system with different current sensing inaccuracies.

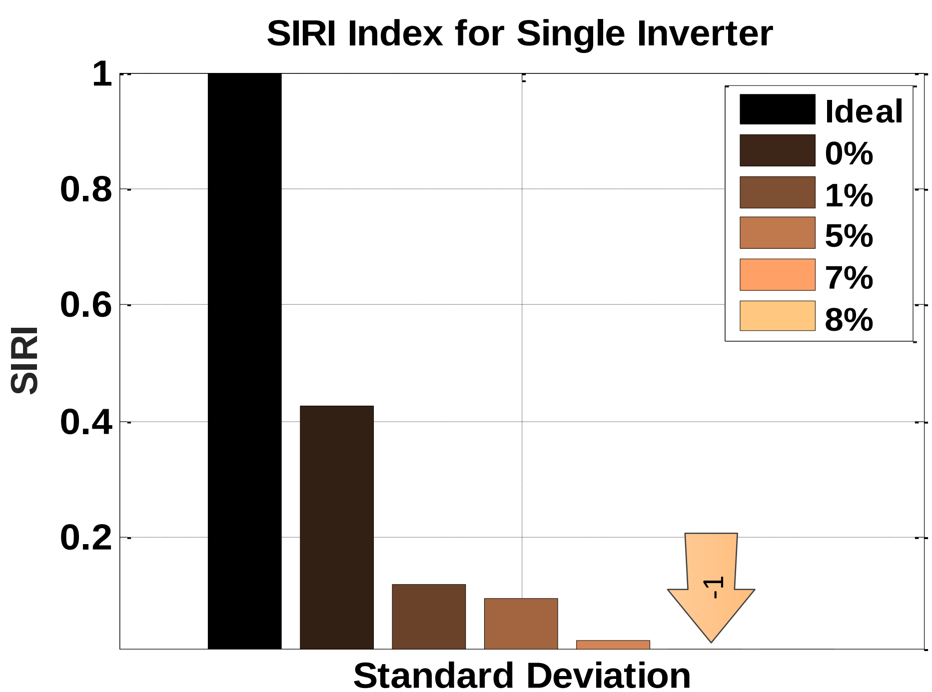

Figure 6.9. SIRI index for an AC-stacked grid-tied PV inverter system with different current sensing inaccuracies.

CHAPTER 7: RESULTS AND DISCUSSIONS

In this section, simulation, hardware-in-the-loop and experimental results are provided to examine the feasibility and effectiveness of proposed controllers and methods. Presented results consists of symmetrical nominal condition, asymmetric condition with partial shading, grid disturbances, reactive power controls, harmonics mitigation etc.

7.1. Nominal Condition

7.1.1. Simulation Results

The three-inverter system and decentralized controller scheme presented in the previous section is simulated in Simulink to show the feasibility of the decentralized control system. The schematic of this simulation is shown in Figure 7.1. In this AC-stacked PV inverter model, each inverter is connected to a *285W* PV module and the system is fully controlled by the designed decentralized controller architecture that was presented in Figure 3.5. The PV module is modelled based on Solar World SW 285W MONO PV module. The open circuit voltage and maximum power point voltage of PV panel are 39.7V and 31.3V under standard testing condition respectively. Short circuit current and maximum power point current of this PV module are 9.84A and 9.2A. Nominal values of passive components and operating point parameters for simulation were shown in Table 5.1. All the designed passive component values are based on the 40kHz switching frequency.

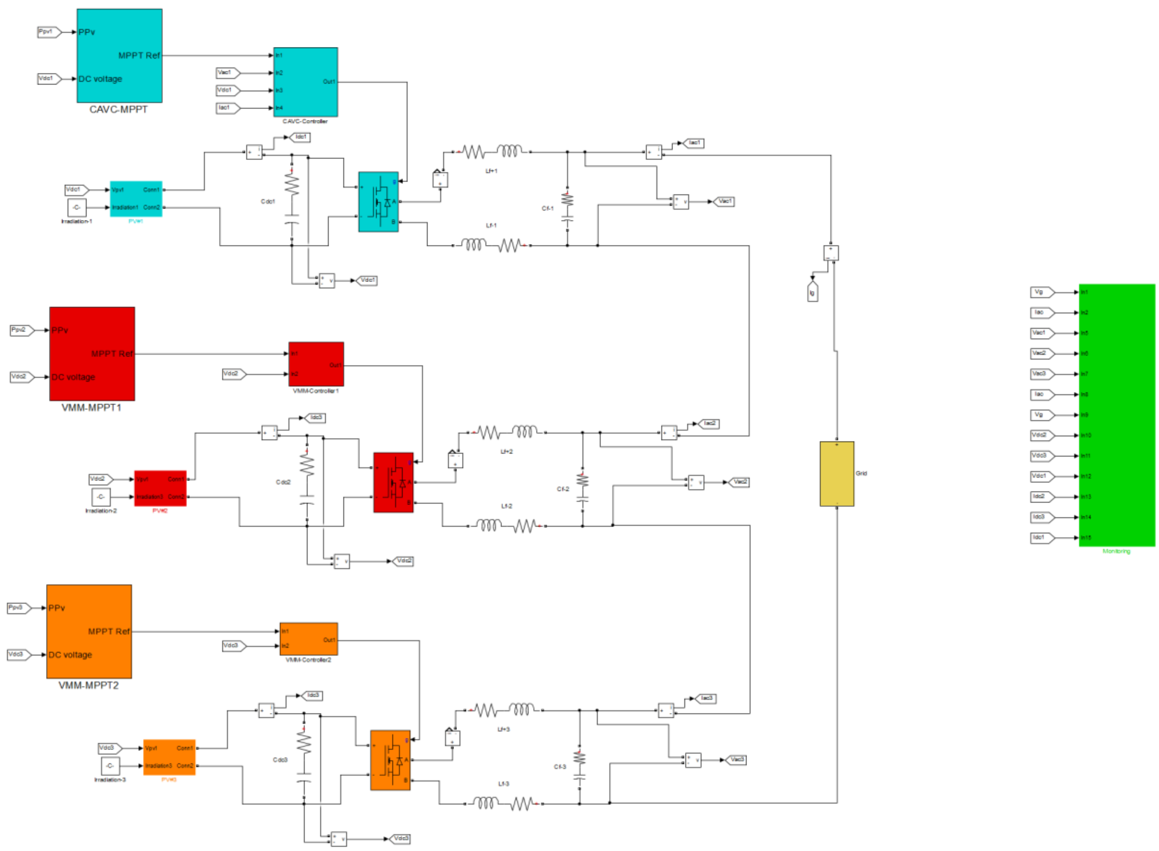

Figure 7.1. Simulation model of three-inverter AC-stacked PV inverter system

Figure 7. 2 illustrates normal operation of a grid-tied AC-stacked PV inverter system in symmetric condition. As can be seen in this figure, the output voltage of each inverter level is sinusoidal because of the low-pass filter at the output of each inverter. However, the output voltage of CAVC has higher THD content, since this inverter compensates for all the inaccuracies and steady state errors in the string to have the output current with minimum harmonics content. As the voltage compensator, CAVC compensates for the harmonics contents and other inaccuracies of the output voltages of VMM inverters to reduce the harmonics content of the string voltage and as a consequence has low THD in injected current. In this study, the THD content of output current is <2%. On the other

hand, Harmonics content of CAVC output voltage is around 8% and VMM inverters have THD less than 4.5% and the grid voltage is assumed to be pure sinusoidal.

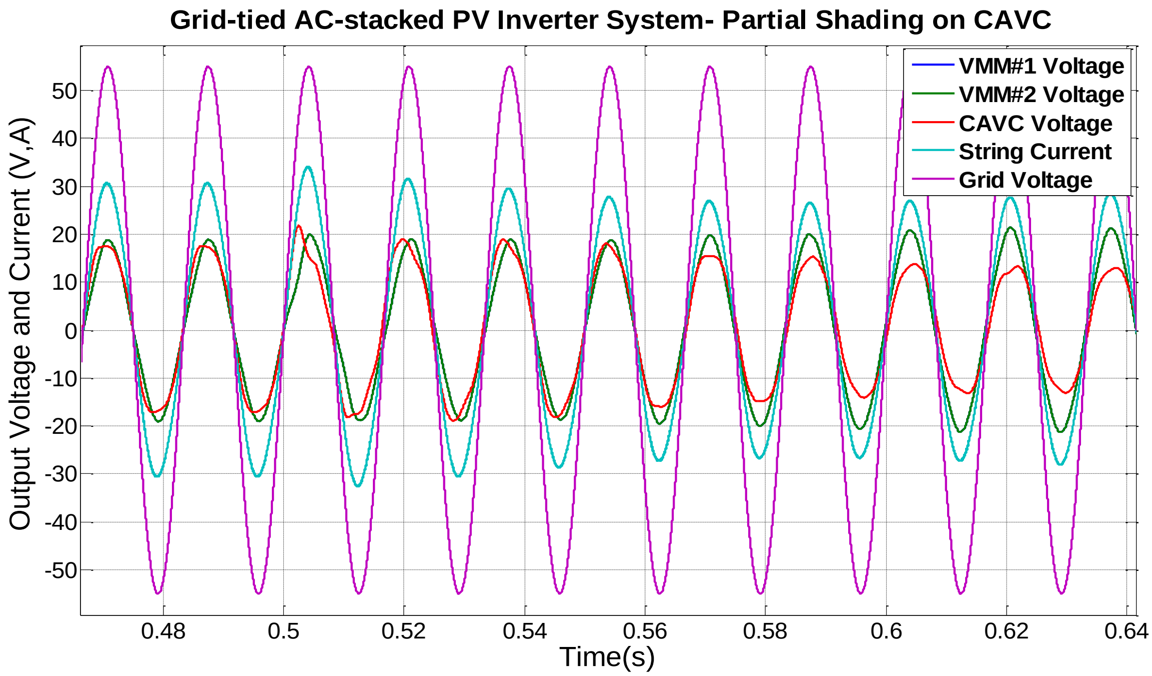

Figure 7. 2. Output voltages and current of AC-stacked PV inverter string in symmetric condition.

Figure 7.3 illustrates the DC-bus voltages and currents of inverters in a symmetric condition. This figure shows the transients of all inverters in startup situation and steady state MPPT operation, with CAVC compensating more for transients in the startup. Gradually, the system reaches the steady-state condition, and DC-link voltages are equal, meaning the PV modules are generating equal power in steady state at MPP.

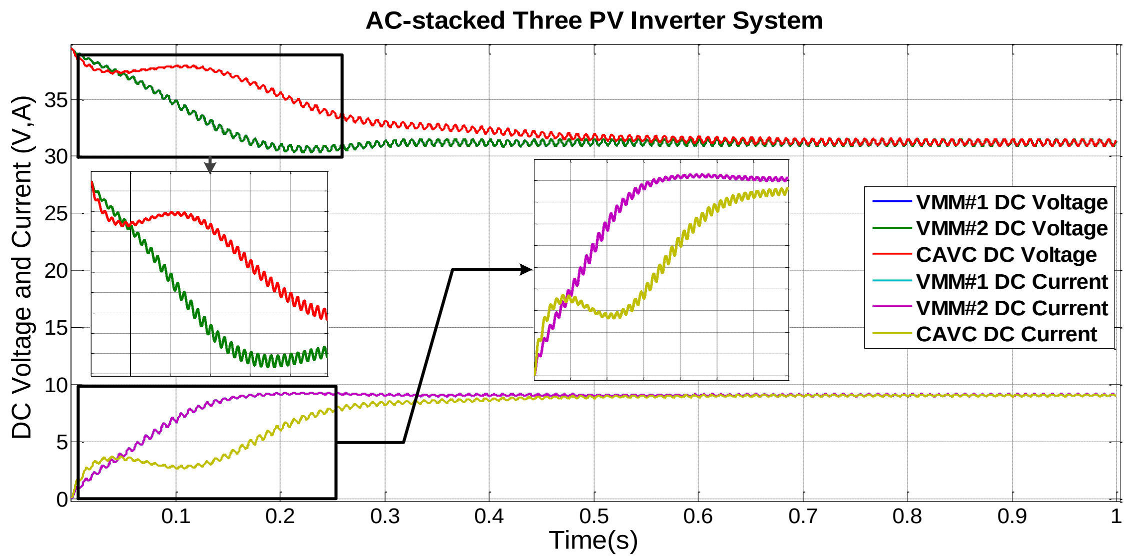

Figure 7.3. DC-side voltages and currents of PV inverters in symmetric condition

7.1.2. Experimental Results

To verify the effectiveness of the proposed PV string configuration and decentralized control method, a hardware test bed consisting of three PV inverters, three PV emulators and a grid emulator was built, which is shown in Figure 7.4. The nominal values of passive components and system parameters are the same as parameter values presented in Table 5.1, except PV emulator MPP voltage which is 28.5 V and PV emulator Power at MPP is 42W. Inverters' switching are controlled by a DSP using local measurement information. Grid voltage zero-cross information is detected in the interface box and it is sent to these control cards using a low frequency heartbeat signal. Similar to simulation, switching frequency of the experimental system is 40kHz.

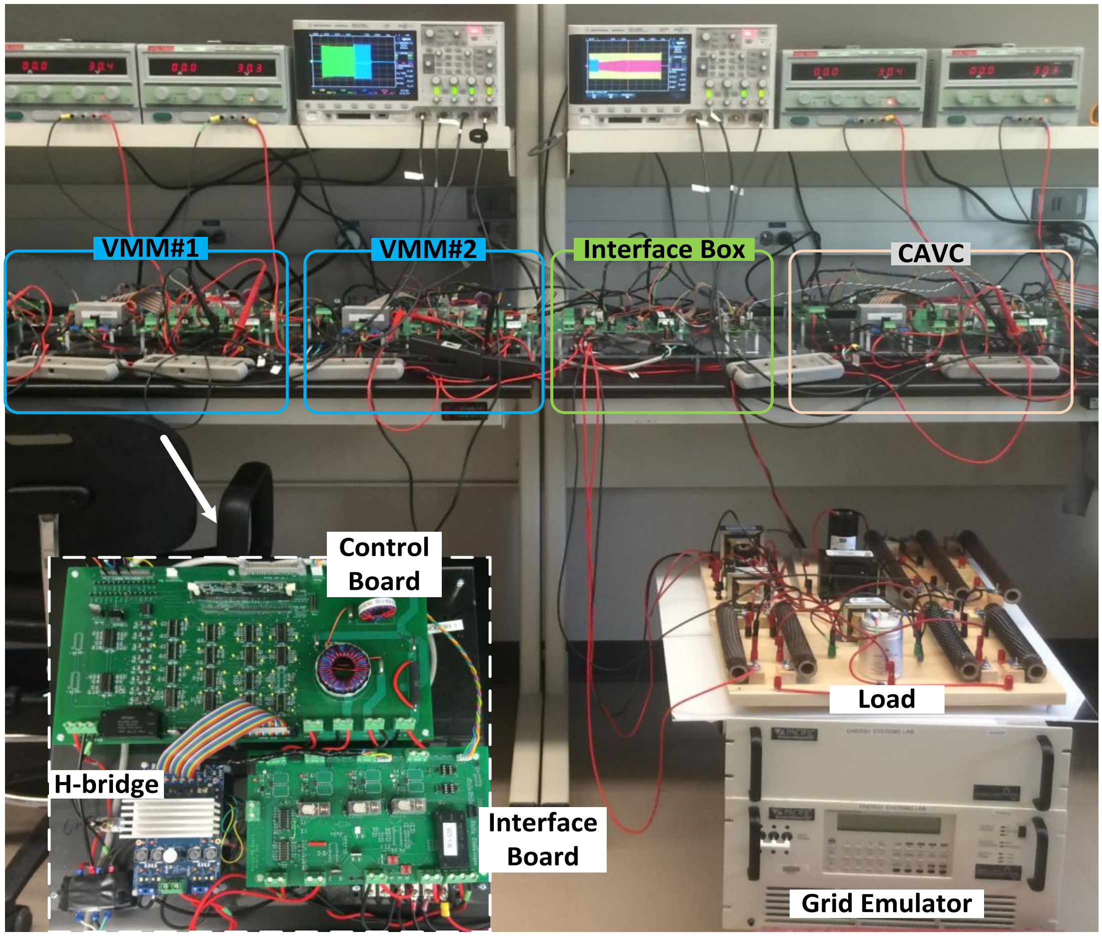

Figure 7.4. Lab-scale experimental setup grid-tied AC-stacked inverter system consisting three inverters.

Nominal operation of the AC-stacked PV inverter string system in unity power factor is shown in Figure 7.5. In this system, each scaled down PV emulator is working at 41W maximum power point. All three inverters are controlled by decentralized controllers explained in previous sections.

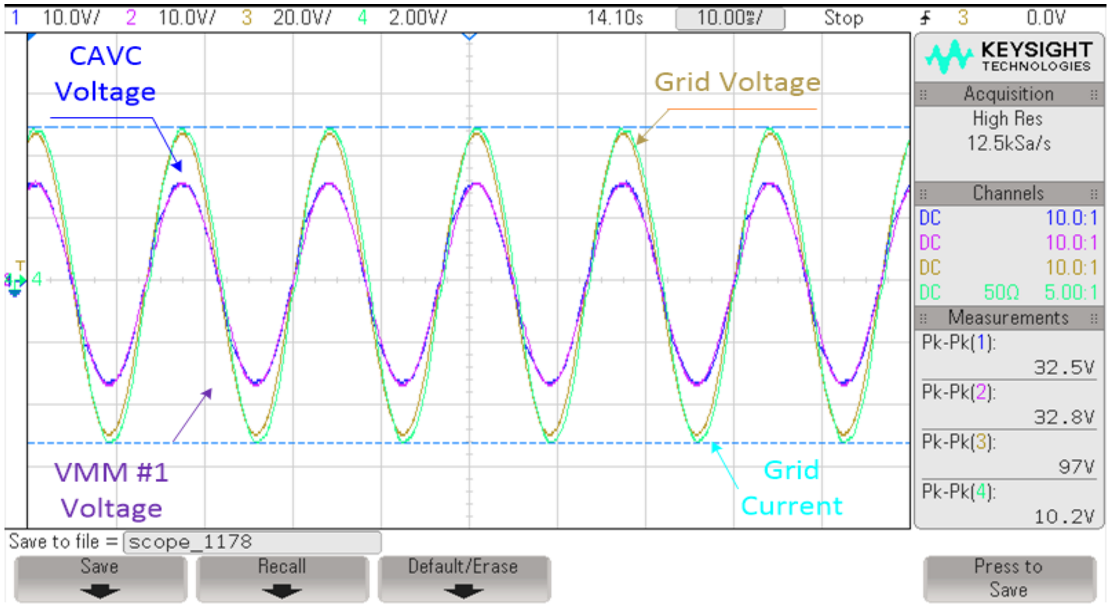

Figure 7.5. Steady-state symmetrical operation of lab-scaled grid-tied AC-stacked PV inverter test bed using decentralized control scheme in unity power factor.

7.2. Partial Shading

7.2.1. Simulation Results

In Figure 7.6.a, operation of the AC-stacked PV system with partial shading in one PV module is illustrated. In this scenario, at the time of 0.5s the irradiance of PV module #2 is reduced by 20%. As a consequence of this event, the string current is reduced and the share of output voltage for unshaded PV inverters is increased. To analyze the generated power of each PV module, the DC-side measurements are presented in Figure 7.6.b. This figure shows that the voltage compensator inverter reacts immediately to the shading event and other voltage mode inverters gradually increase their output voltage and after a transient time, the system reaches a new operating point where the DC-link voltages of the unshaded PV modules are equal.

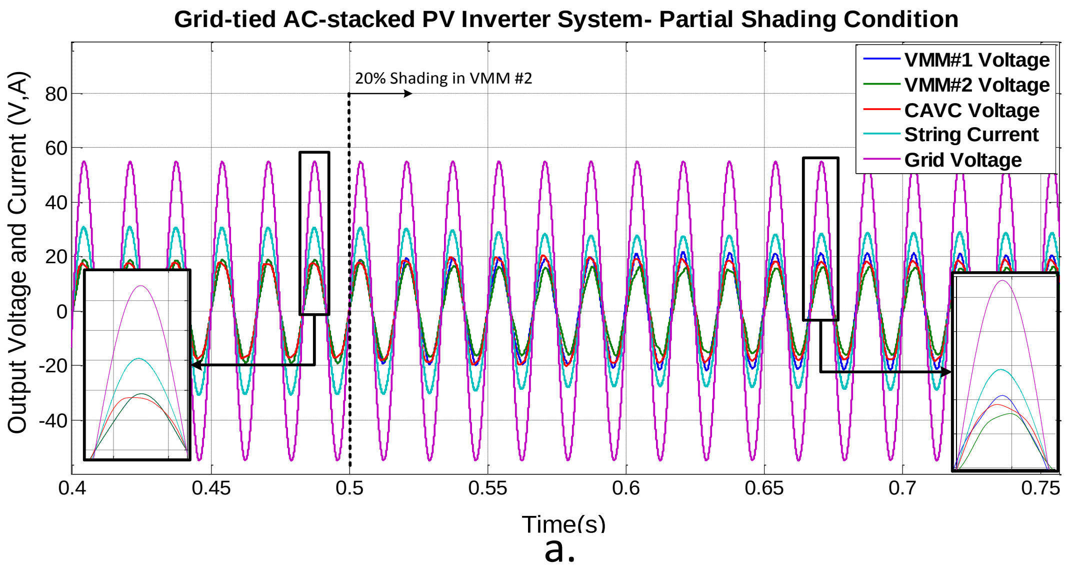

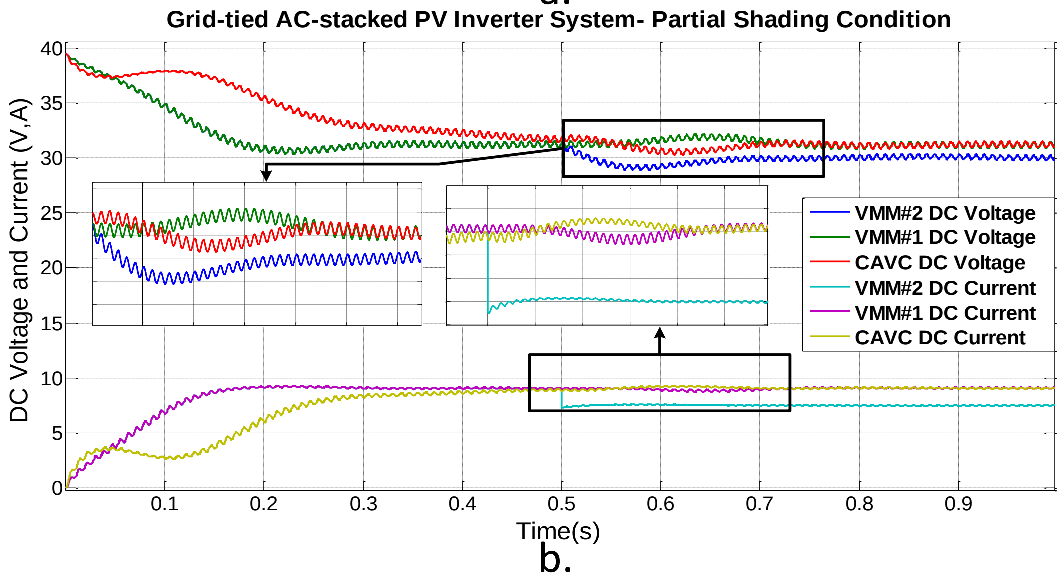

Figure 7.6. Steady state and transient operation of grid-tied AC-stacked PV inverter system in partial shading condition. a. Output voltages and current of AC-stacked PV inverter string in asymmetric condition under 20% shading one PV module. b. DC-side voltages and currents of PV inverters in asymmetric condition under 20% shading in one inverter.

To further analyze the system performance during partial shading, the 20% partial shading on CAVC inverter is shown in Figure 7.7. As can be seen in this figure, AC voltage share of CAVC inverter is reduced and output voltages of other inverters are increased to compensate for the voltage loss in the string.

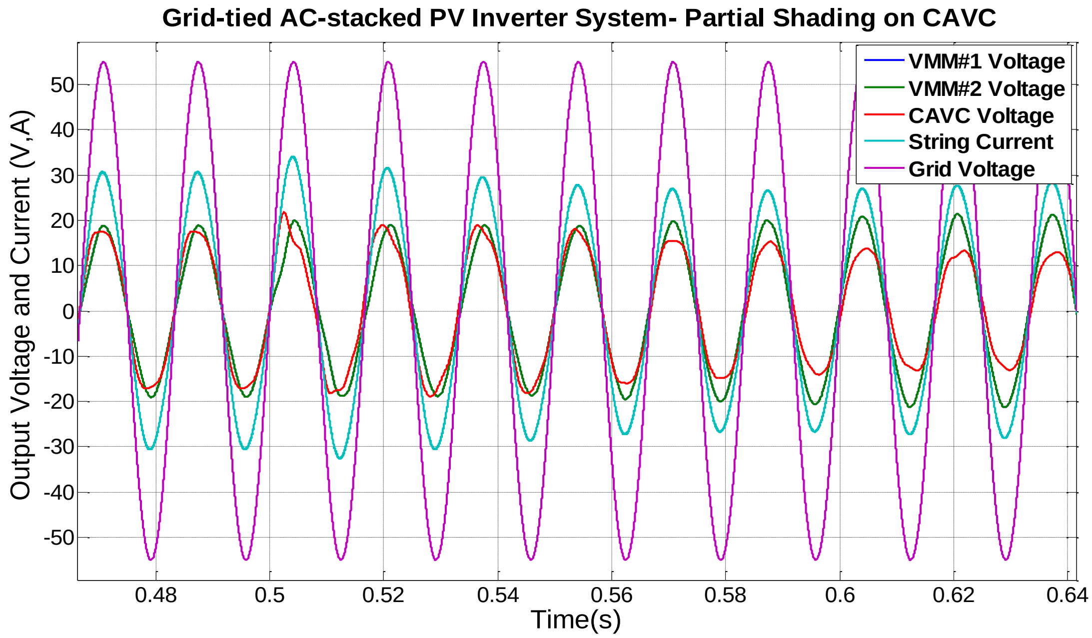

Figure 7.7. Steady state and transient operation of grid-tied AC-stacked PV inverter system in partial shading condition in CAVC inverter.

7.2.2. Experimental Results

Figure 7.8. shows the performance of the proposed decentralized control architecture during a 20% partial shading of one PV module. As can be seen in Figure 7.8.a, the system was operating in a symmetric condition before the shading occurred. When shading occurred, the output voltage of the shaded inverter dropped and therefore the injected current to the grid was reduced. CAVC, which is responsible for controlling the string current, temporarily compensated for the voltage drop of the shaded inverter and increased its output voltage. To maintain MPPT control operation the output current should be reduced. Because of reduced output current, the output voltage of the other unshaded inverter was increased gradually to share the voltage drop with the CAVC. Finally, after 450ms, the output current is reduced because of the power loss due to shading and the

voltage drop is divided between the two unshaded inverters (CAVC and VMM #1), the output voltage of these two inverters are increased.

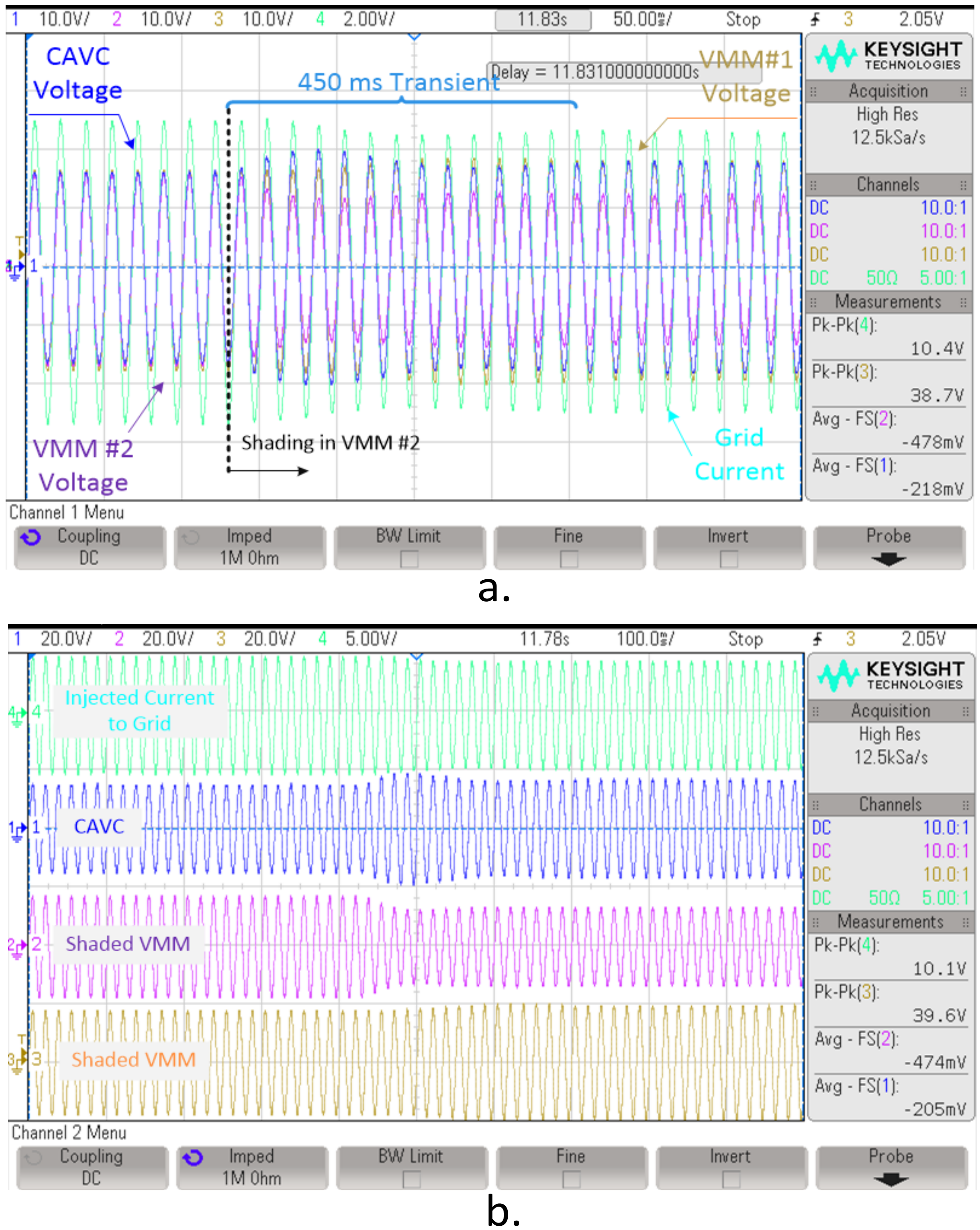

Figure 7.8. Performance of AC-stacked PV inverter system with the designed decentralized controller during partial shading occurred on VMM #2 (asymmetrical conditions).

In Figure 7.8.b these four traces are separated to clearly show the concept. All these tasks were done without any communications between inverters, showing the high reliability of this control scheme, which can operate in severe cases such as conditions of communications system shutdown.

7.3. Full Shading

Another study is two steps of full shading disturbances on all the inverters which is illustrated in Figure 7.9. In this study at time 0.4s the AC-stacked system faced a 20% shading which is shown in this figure. The decentralized controller after around 400ms transient operation reaches to the steady state. One cycle zoomed captures magnify the waveforms before and after shading disturbances. At 1.1s, the solar irradiance reduced by 20% again. As can be seen in all the three zoomed in waveforms, the AC voltage share of individual inverters remain constant during full shading but the output string current is reduced, which means the inverters share the voltage requirement for grid integration but due to shading the output power is reduced.

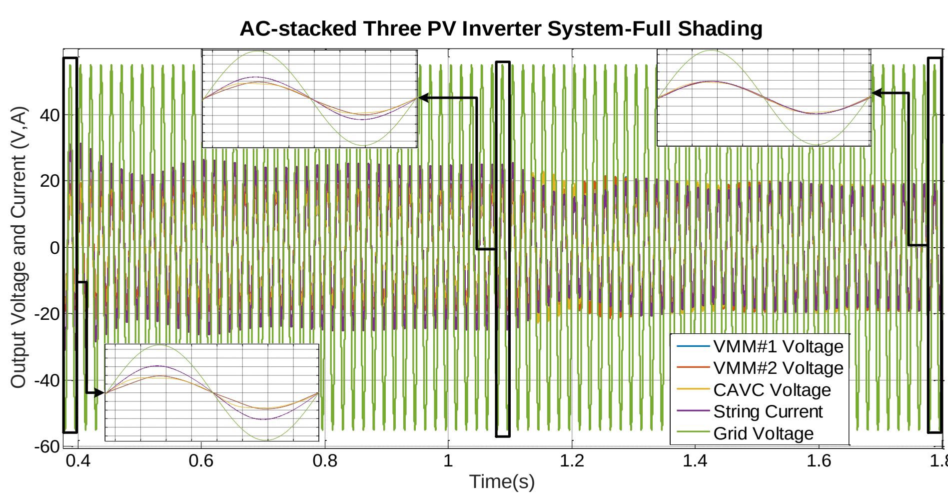

Figure 7.9. Steady state and transient operation of the grid-tied AC-stacked PV inverter system experiencing 30% full shading on all the inverters.

7.4. Grid Voltage Disturbance

7.4.1. Simulation Results

Finally, Figure 7. 10 shows the performance of the proposed decentralized control scheme during 10% voltage sag on grid. During this disturbance, CAVC reacts immediately to compensate for voltage drop, which causes CAVC loss of MPP operation for short period of time (100ms). Other inverters reduce their output voltages gradually and therefore DC-side voltages and currents come back to the operating point of the system before disturbance occurs, as can be seen in Figure 7. 10.

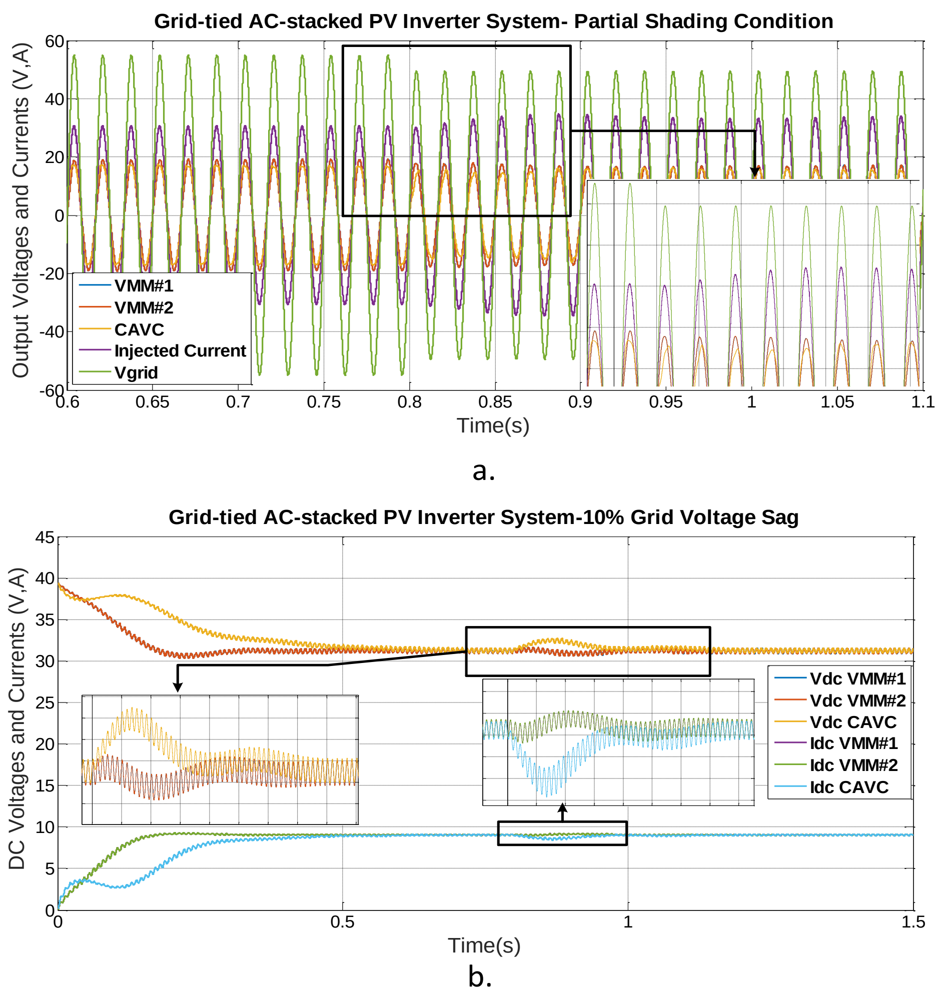

Figure 7. 10. Operation of grid-tied AC-stacked PV inverter system during 10% voltage sag on grid. a. Output voltages and current transient. b. DC-side voltages and currents of individual inverters.

7.4.2. Experimental Results

Another study is a voltage regulation operation on AC-stacked PV inverter to evaluate the feasibility of decentralized control scheme in abnormal conditions such as voltage sag. In this test, which is presented in Figure 7. 11, the system experimented a 10% voltage sag for the time period of 400ms. In this condition, CAVC immediately compensated for voltage drop and the output voltage of this inverter is reduced. To maintain MPP operation, this inverter increased the output current command. By increasing the output current, VMM inverters in the string also reduced their own output voltage to maintain MPP operation. As can be seen in this figure, gradually after 100ms, the system reached to the new operating point in which all inverters were operating at MPP but their output voltages were dropped and the string current was increased. This operation performed with no communication between inverters which verifies the feasibility and performance of fully decentralized control architecture presented in this thesis.

Finally, in order to see the active power control and MPPT operation of the decentralized AC-stacked PV inverter system, DC voltage dynamics of this system during grid voltage disturbance is provided in Figure 7. 12. As can be seen in this figure, DC voltages of CAVC and VMM inverters remain constant during this disturbance and after it is cleared, which shows that individual inverters are be able to maintain MPPT control and provide maximum power.

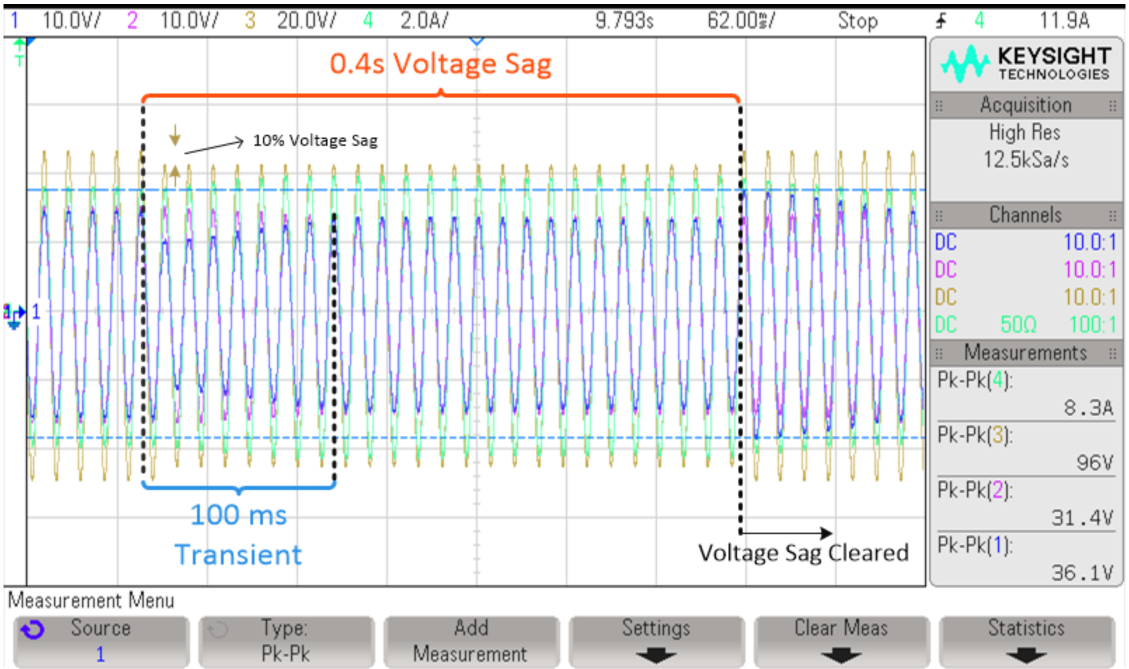

Figure 7. 11. Voltage Regulation of AC-stacked PV inverter string during 10% grid voltage sag.

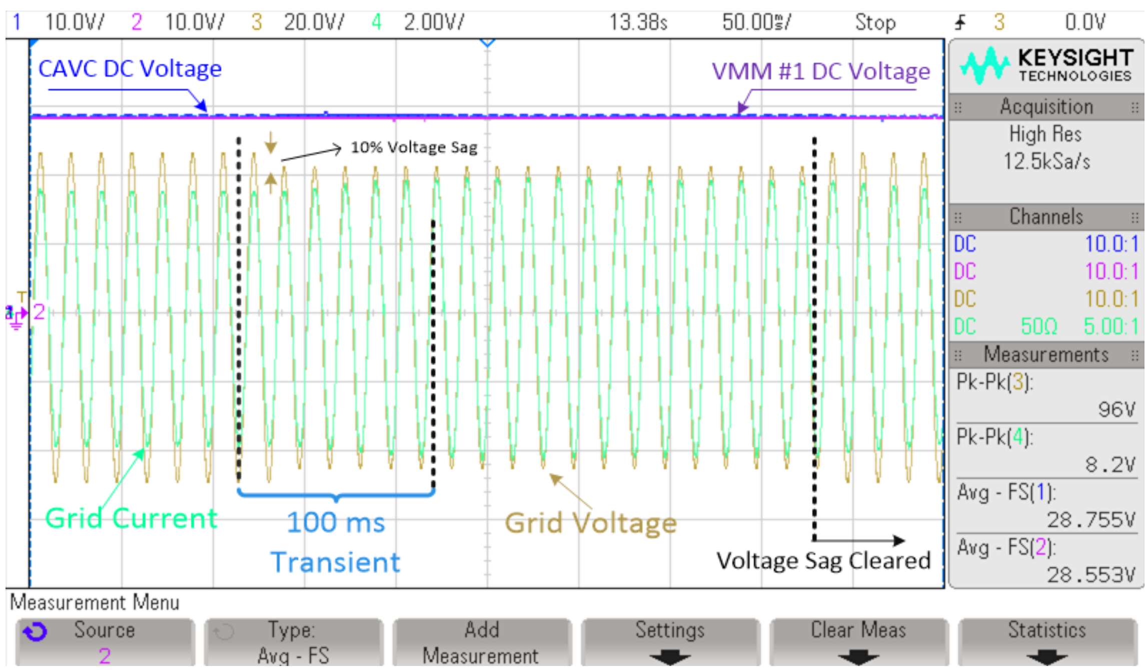

Figure 7. 12. DC voltage dynamic of AC-stacked PV inverter string during 10% grid voltage sag.

7.5. Single-member Phase Compensation

7.5.1 Simulation Results

In this section, first, I will provide a comparison between central and decentral reactive power control. As it is mentioned, central control of reactive power has the advantage of balanced system operation. However, it requires communication infrastructure which will increase the balance of system cost. On the other hand, the AC-stacked PV inverter system controlled with the decentralized controller has very small passive components, and the voltage drop across these passive components is negligible. Therefore, controlling the injected reactive power using the SmPC method, proposed in this paper, can provide the reactive power control capability with minimum communication requirements. In order to provide a comparison between central and decentral reactive power control for AC-stacked PV inverter system, a set of simulation results are provided here.

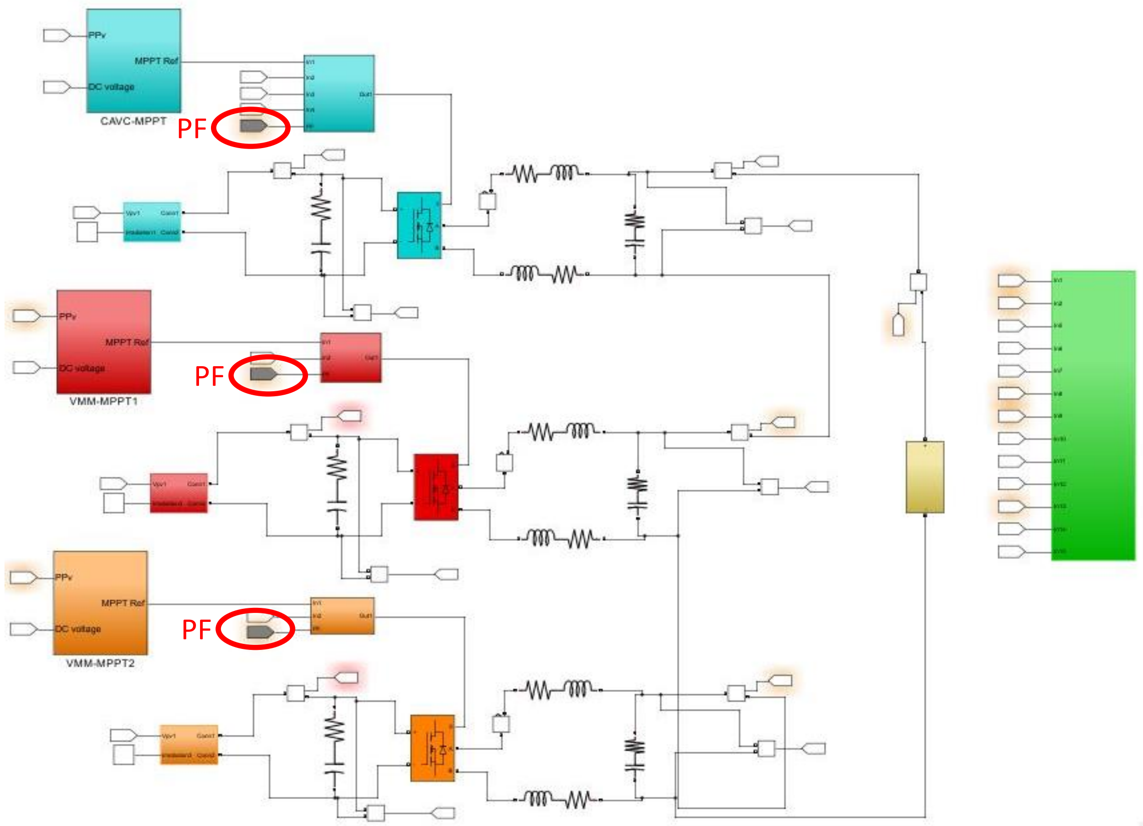

Figure 7. 13. Schematic of AC-stacked PV inverter system with central reactive power control.

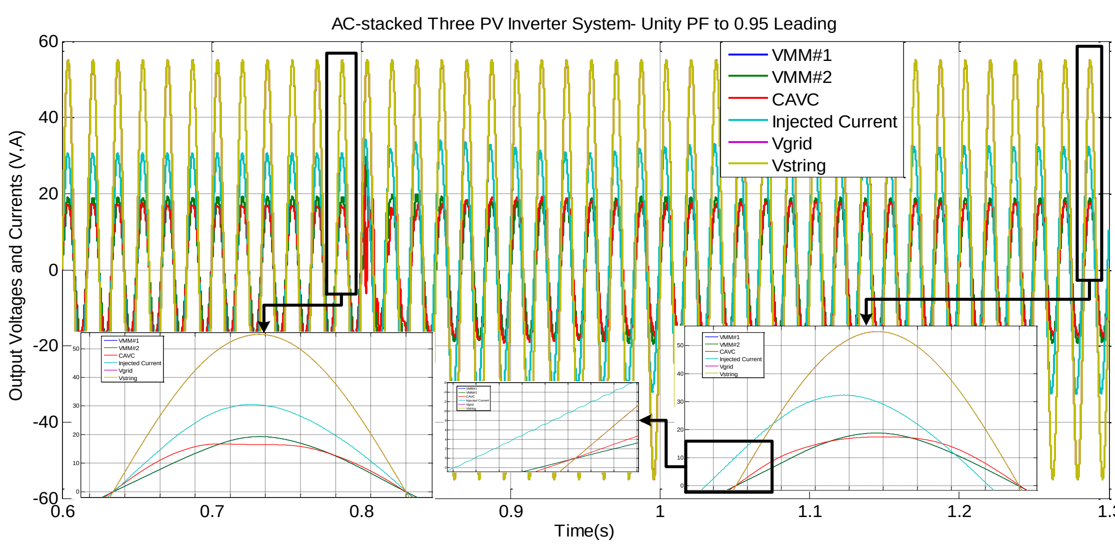

Figure 7.14. Central reactive power control results.

In Figure 7. 13, the schematic of central controlled reactive power scheme is shown. As can be seen in this figure, the power factor information has been sent to all the inverters in the string. Therefore, the system operates in the balanced condition, and output voltages of all individual inverters are in phase with each other as shown in Figure 7.14.

In Figure 7.14, the reactive power command sent to all inverter is changed from 1 to 0.95 lagging. As can be seen in the zoomed in the capture, output voltages of all inverters are in phase with each other and system operates in the balanced condition.

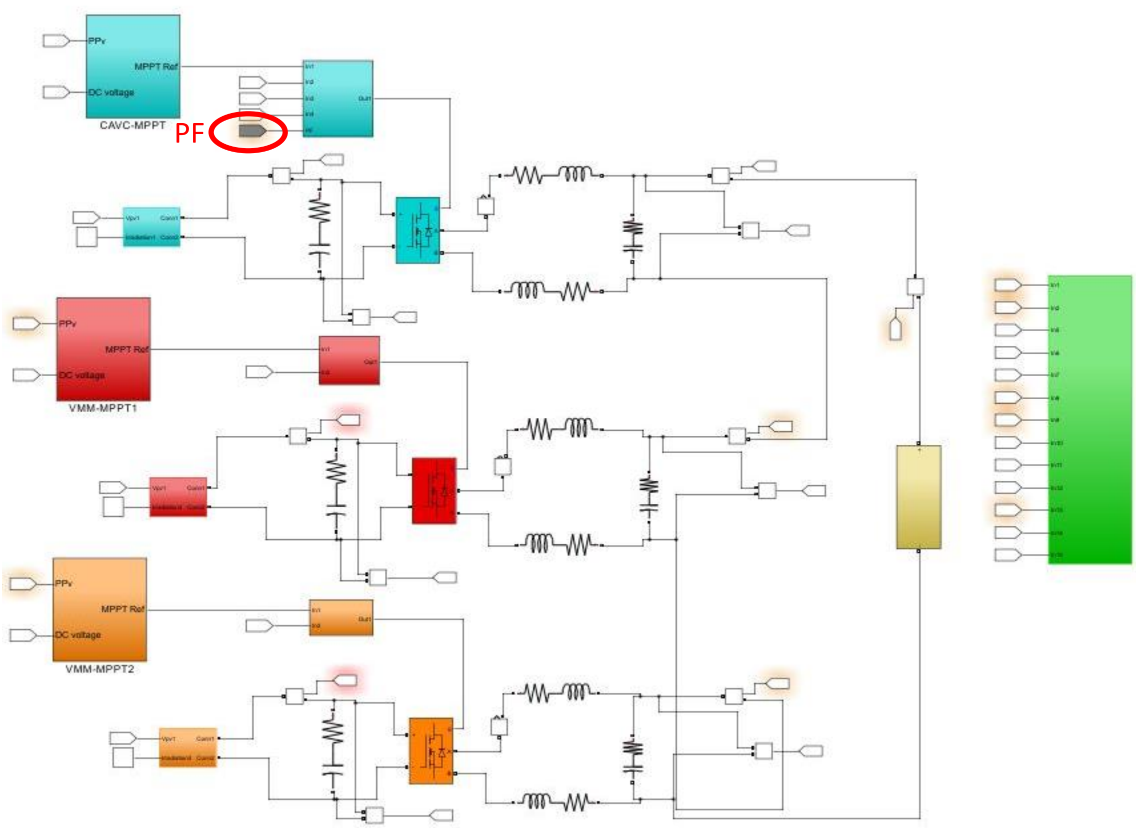

Figure 7.15. Schematic of AC-stacked PV inverter system with decentral reactive power control.

In Figure 7.15, schematic of decentral reactive power control method is shown. As can be seen in this figure, the power factor information has been sent only to one inverter which is CAVC. Therefore, the system is not balanced, and there is a small phase difference between the output voltage of CAVC and VMMs as shown in Figure 7.16. However, the difference between output voltages is very small due to small passive components in the string. Therefore, the unbalance condition in the system is negligible. By using the SmPC method, we can control the reactive power of AC-stacked PV inverter system with minimum communication requirements, which is very important specially in the string with a higher number of inverters.

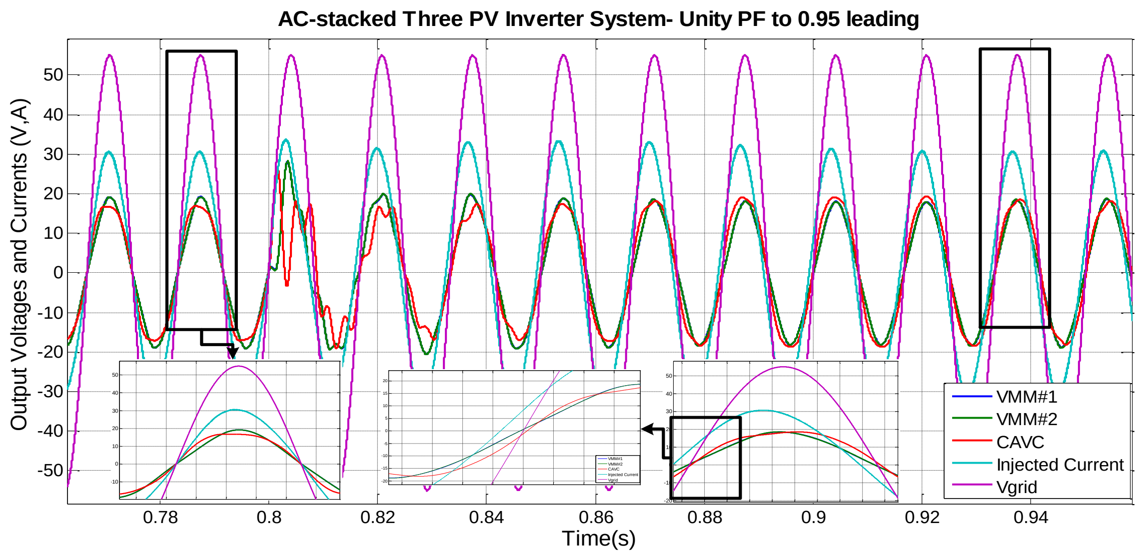

Figure 7.16. Reactive power control using only single member (CAVC) phase compensation.

In order to investigate the SmPC method better, more simulation results are provided in this part. In Figure 7.17, the operation of the AC-stacked PV system during reactive power command variation is shown. In this scenario, at the time of 0.8s after MPPT operation reaches to the steady states the PF command which is sent only to CAVC inverter is changed from unity to 0.95 lagging. As can be seen in Figure 7.17.a, both VMM inverters are exactly aligned with grid voltage which shows they only received grid voltage zero crossing information. On the other hand, CAVC output voltage is slightly phase shifted which is due to compensating for the voltage drop across interface inductor which is negligible. To analyze the generated power of each PV module, the DC-side measurements are presented in Figure 7.17.b. This figure shows that the voltage compensator inverter reacts immediately to the new command and deviates from MPPT operation for a short period of time and other inverters without any communications detect the reactive power variation from MPP power error and react accordingly. After around 200ms transient condition, DC voltages and currents come back to the initial values which means inverters after power factor variation still maintain MPPT operation.

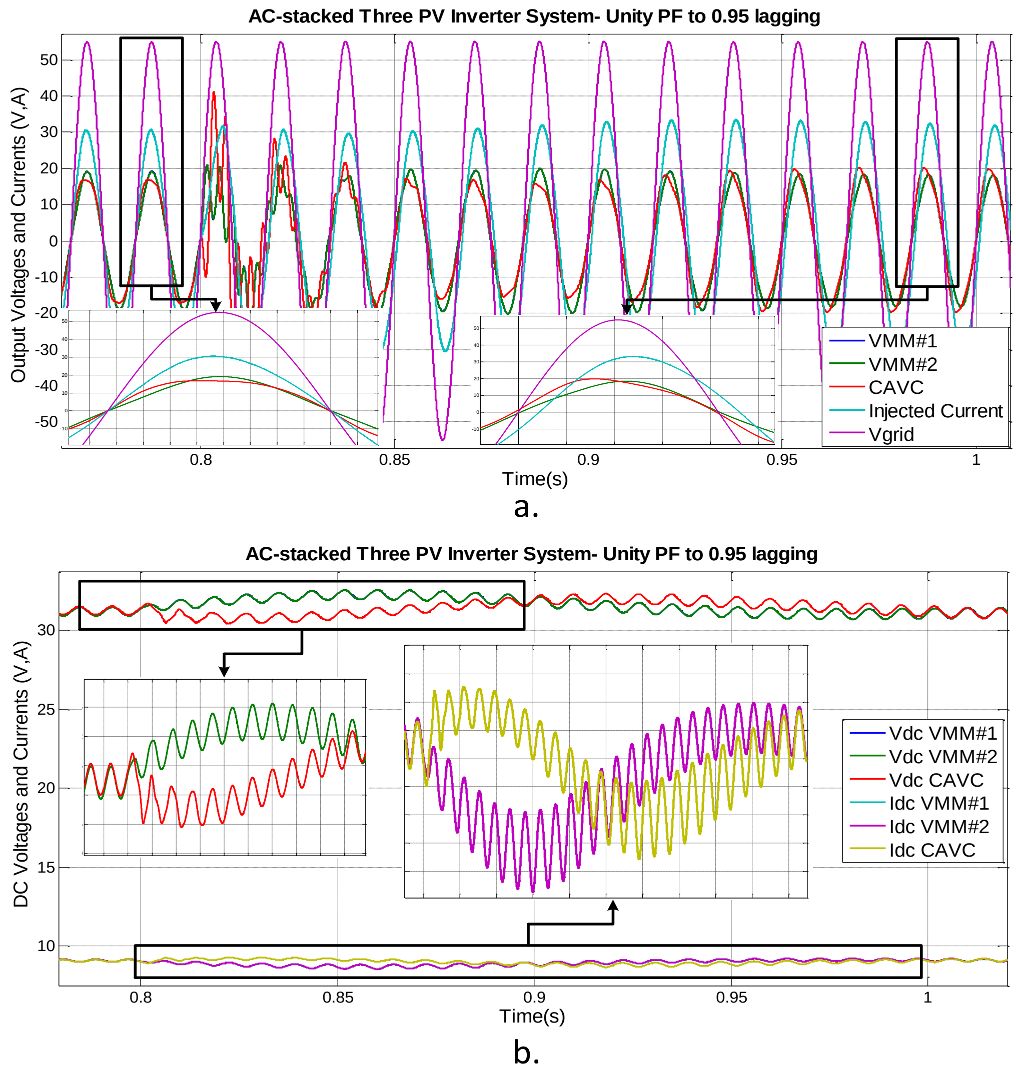

Figure 7.17. Reactive power control transient during command change from unity PF to 0.95 lagging. a. AC output voltages and current before, after and during reactive power control transient. b. DC currents and voltages before, after and during reactive power control transient.

Similar study but this time reactive power absorption command sent to CAVC. Figure 7.18.a shows the AC output before and after command changes and Figure 7.18.b illustrates the DC parameters. As we expect, comparing Figure 7.17.b and Figure 7.18.b shows that dynamic behavior of inverters in these two studies is in opposite directions. For instance, CAVC DC current is increased immediately after the command for lagging PF received but when the command for leading PF received, CAVC DC current is fallen immediately.

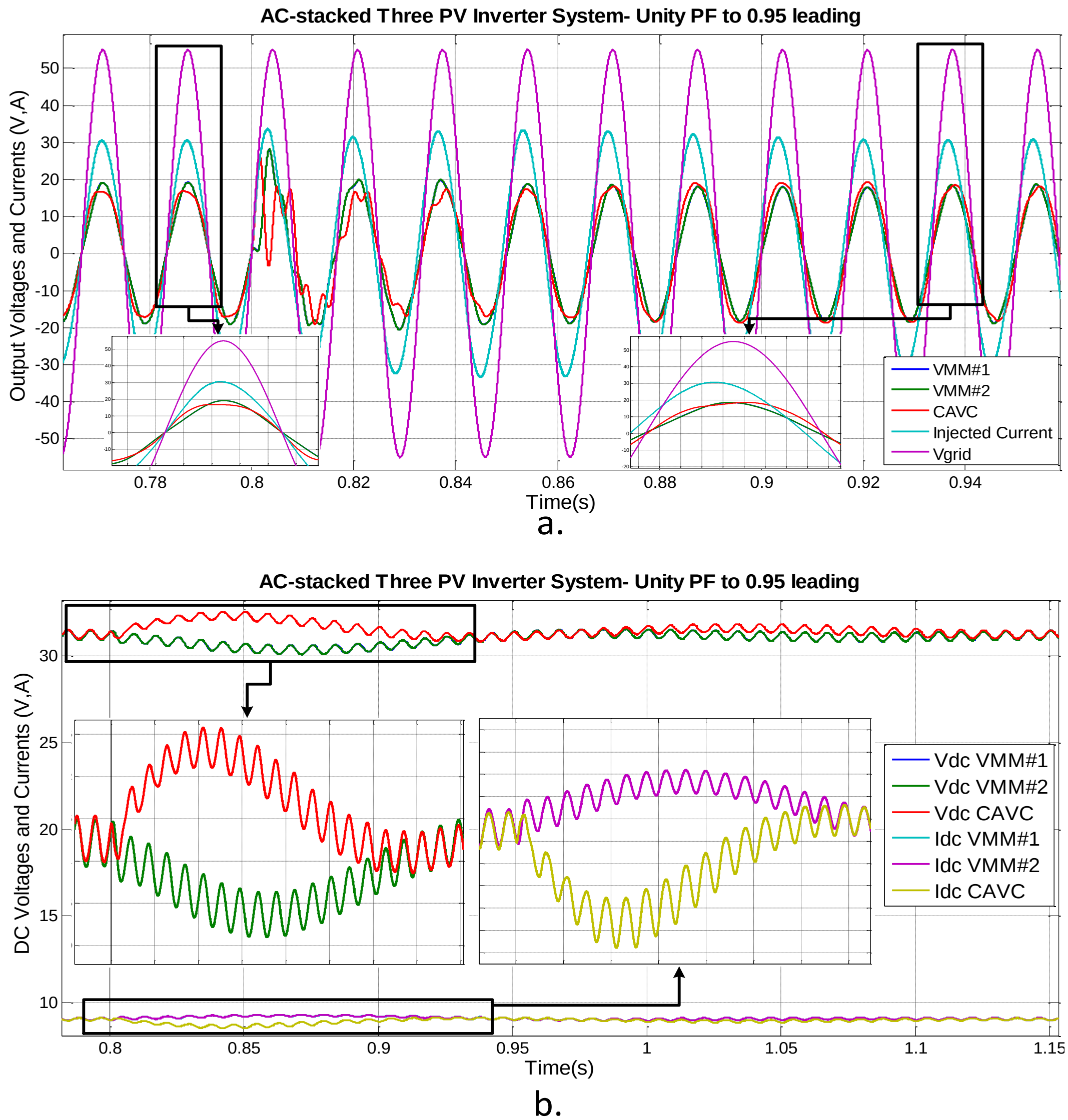

Figure 7.18. Reactive power control transient during command change from unity PF to 0.95 leading. a. AC output voltages and current before, after and during reactive power control transient. b. DC currents and voltages before, after and during reactive power control transient.

7.5.2 Experimental Results

To examine the effectiveness of the SmPC method, experimental results are provided in this section. The hardware test bed consisting three PV inverters which was introduced in the previous chapter is utilized for this study.

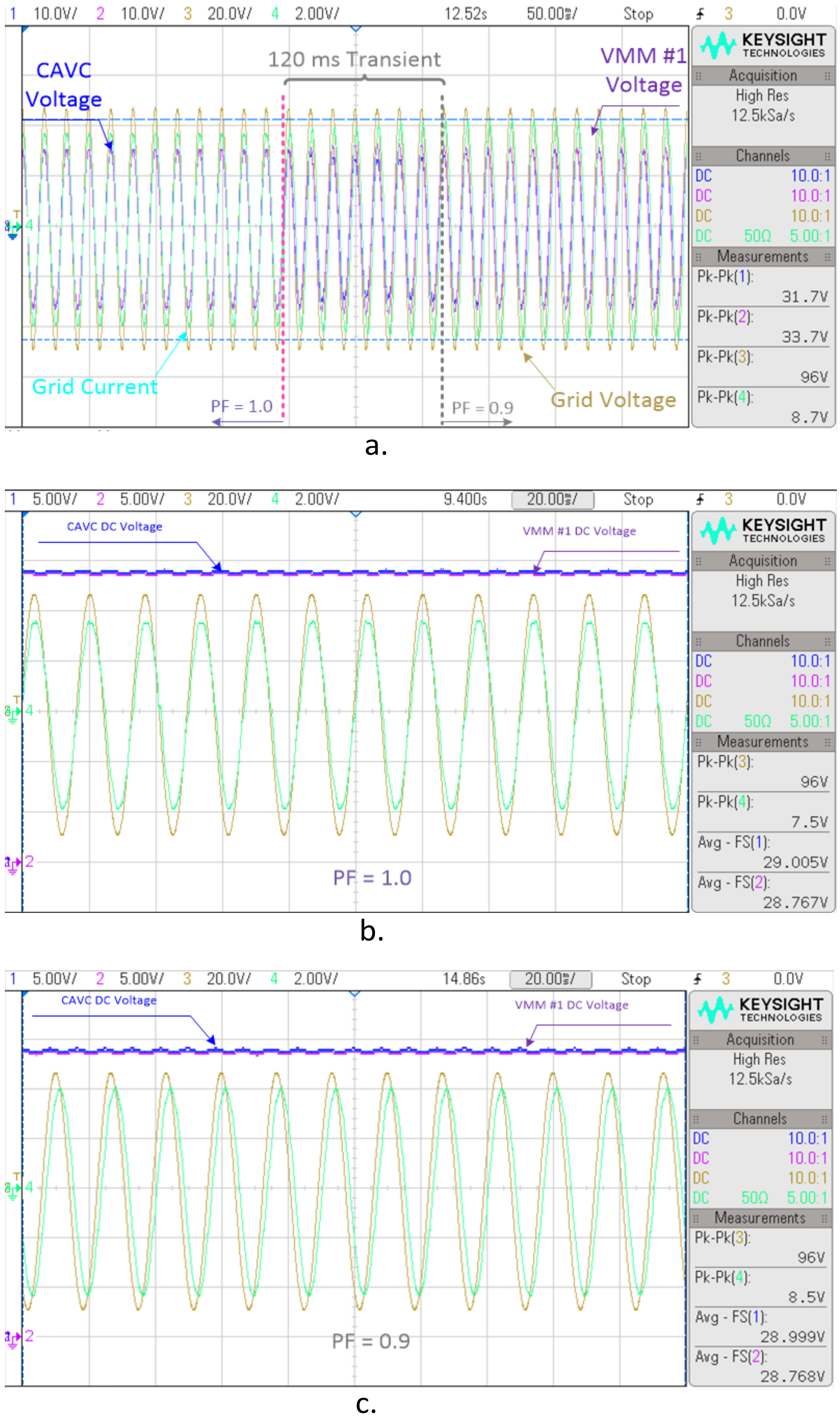

Figure 7.19. Reactive power control operation of AC-stacked PV inverter string. a. AC voltages and current transient b. Unity power factor before reactive power command received c. DC and AC parameters after PF changes.

Figure 7.19 shows the reactive power control operation of the AC-stacked PV inverter system. Figure 7.19.a shows the voltage transient during PF change. In this figure, PF is changed from 1 to 0.9 lagging. In order to maintain the Maximum Power Point Tracking (MPPT) operation, the current amplitude, is increased by CAVC. Initially, CAVC voltage drops around 12%, and after 120ms transient, the system reaches the steady state. Scope captures in Figure 7.19.b and Figure 7.19.c show that average DC voltages before and after PF change remain constant which means individual inverters can maintain the MPPT control and the string delivers maximum power to the grid in both reactive power support conditions. Moreover, an upper limit has been applied to the amplitude of output current in CAVC controller to limit the variation in reactive power during active power changing and avoid over current in the string.

Reactive power absorption operation is also tested by using decentralized control scheme and minimum communications. Figure 7.20.a shows the voltage transient during PF change from unity to 0.9 leading. Like the previous study, CAVC momentarily reacts to the new command and changes output current. Because of variation of output current other inverters change their output voltage to maintain MPPT operation. After 180ms transient, the system reaches to new operating point at 0.9 leading power factor.

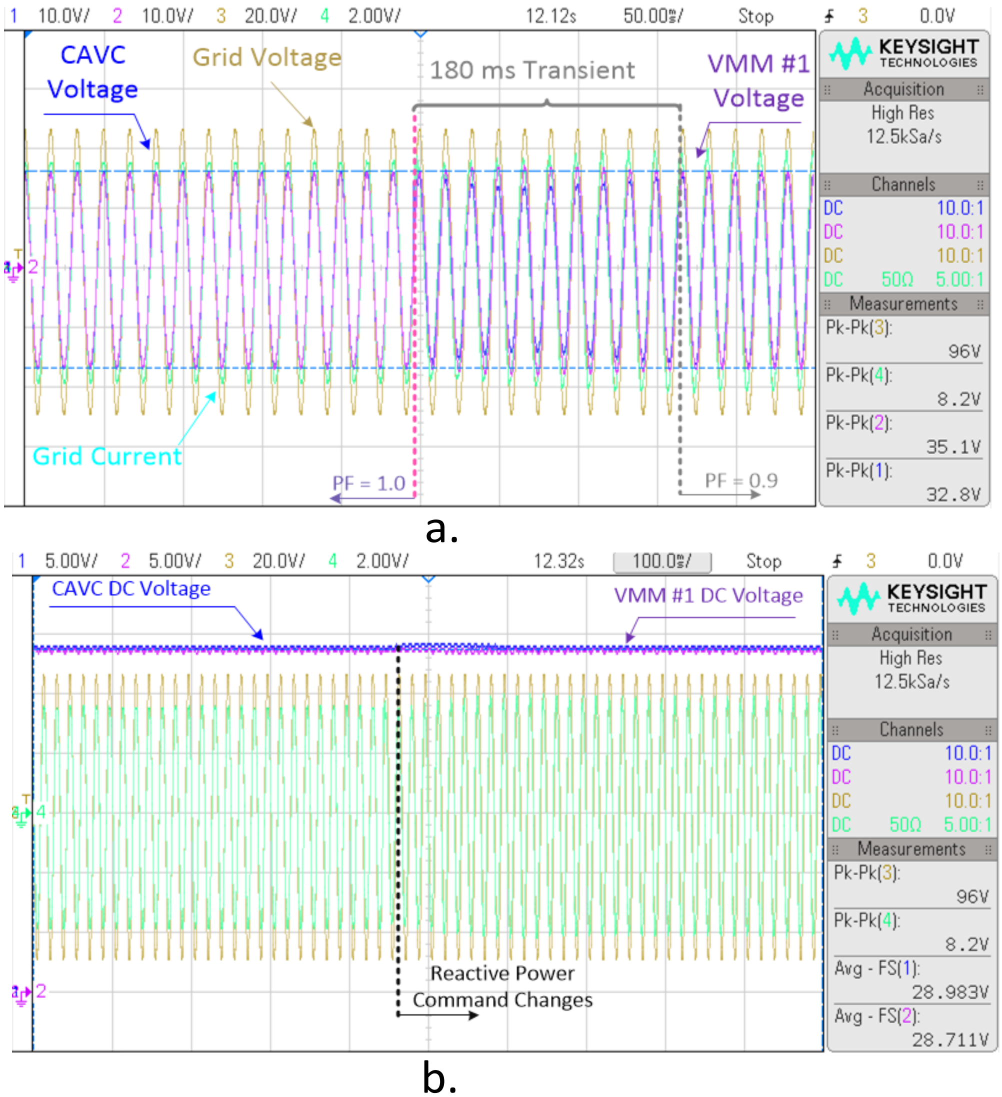

Figure 7.20. Reactive power control dynamic during command changes from unity power factor to 0.9 leading. a. AC voltages and current b. DC side voltages during power factor changes.

7.6 Background Harmonics Compensation

To verify the effectiveness of the proposed harmonics mitigation methods, CHIL test bed with a real-time power electronics simulator with 500ns time step and a 150MHz digital controller is built, as shown in Figure 7.21.

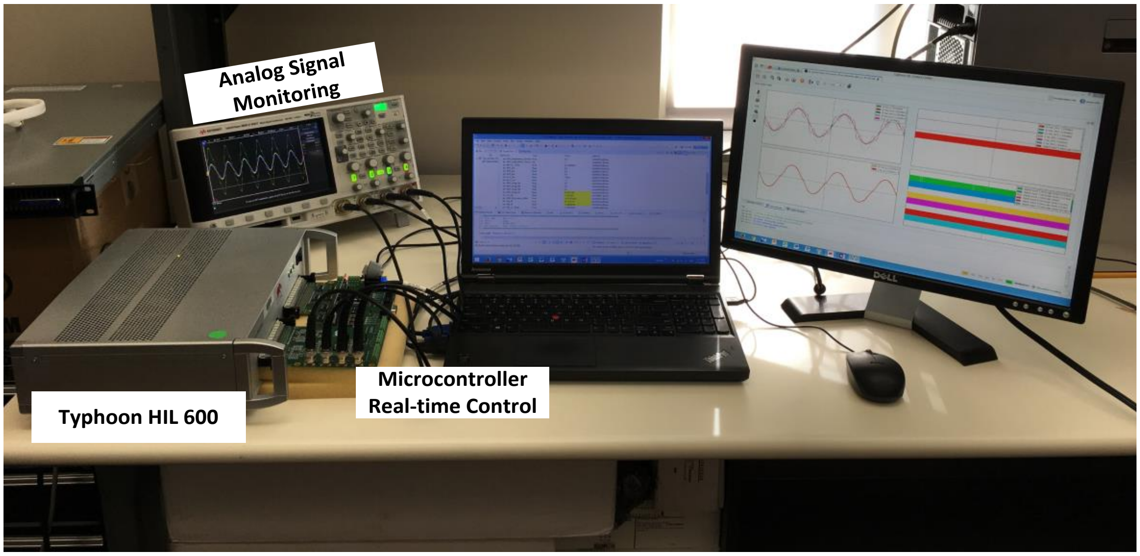

Figure 7.21. CHIL setup for testing grid-tied AC-stacked PV inverter system.

The CHIL experiment results of harmonics mitigation controls with different grid background harmonics in nominal operating condition of PV system, string PV power of 726W and string RMS current of 16.3A, are presented in Figure 7., Figure 7 and Table 7.1. When 8% of 5th and 7th grid background harmonics are added to the grid voltage, ≈9.5% and ≈6.5% of harmonics currents are caused respectively without harmonics mitigation. When 8% of 5th harmonics is injected and the SmHC harmonics mitigation control is applied, the duty cycle of CAVC is increased by 12% which is 41% of available operating margin $\left(\frac{12\%}{29\%}\times 100 = 41.4\%\right)$. By applying the AmHC harmonics mitigation control strategy, all the modular inverters participate in the harmonics current mitigation by using ≈4%-5% of additional duty cycle which is 13.8%-14.7% of available operating margin. As a result, the AmHC harmonics mitigation reduces the burden on the CAVC and increases the overall operating margin of the system during harmonics mitigation, which can be more significant when more modular inverters (VMMs) are stacked in series, and stabilizes the AC-stacked architecture.

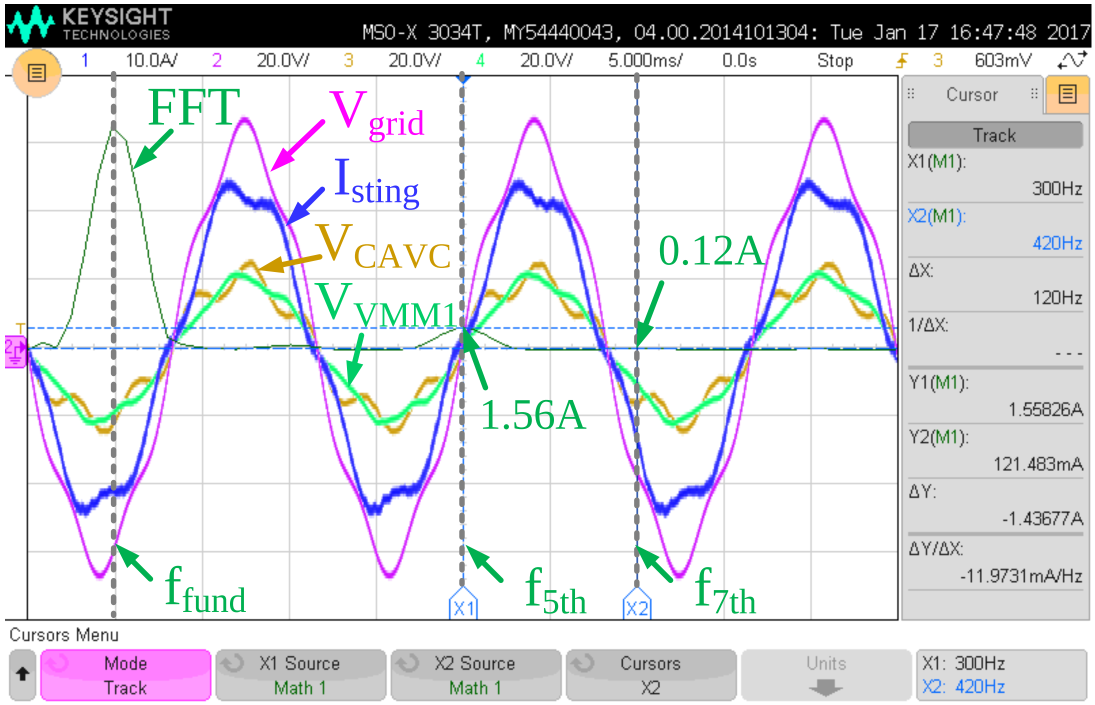

(a)

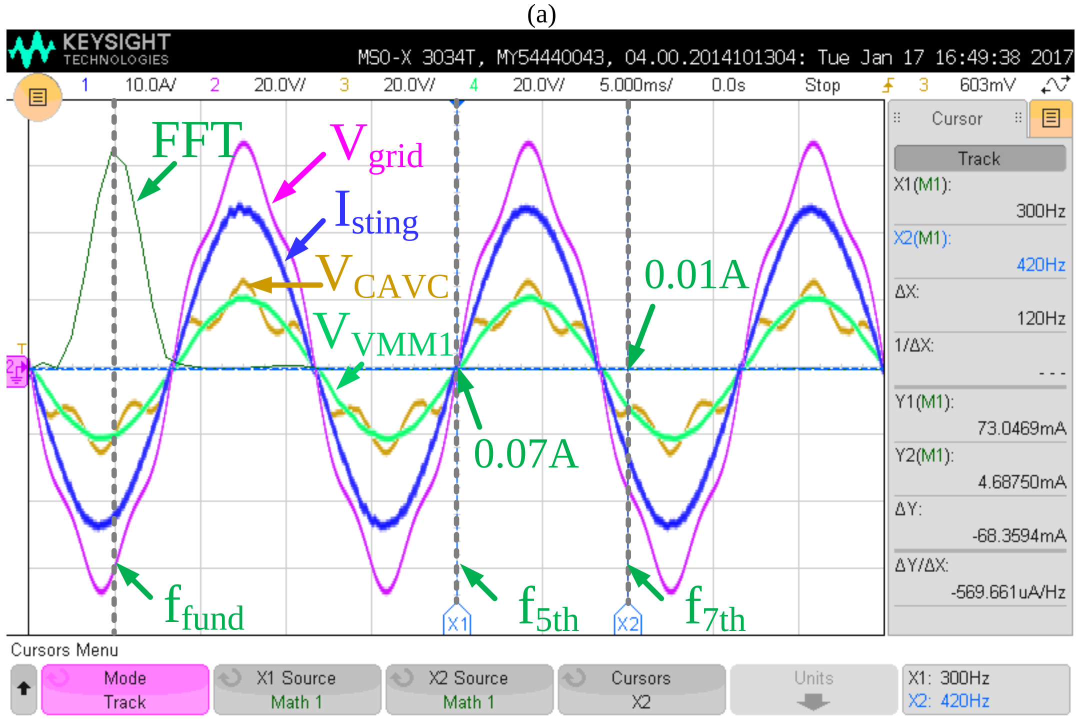

(b)

Figure 7.22. CHIL simulation results: Current, voltage, and FFT waveform in with a grid with 8% of 5^{th} harmonics. (PV1: 1000W/m2, PV2: 1000W/m2, PV3: 1000W/m2, PPV_total=726W and Istring_RMS=16.3A). a. HCVC control scheme with no harmonics compensation. b. HCVC control scheme with SmHC harmonics compensation strategy. c. HCVC control scheme with AmHC harmonics compensation strategy.

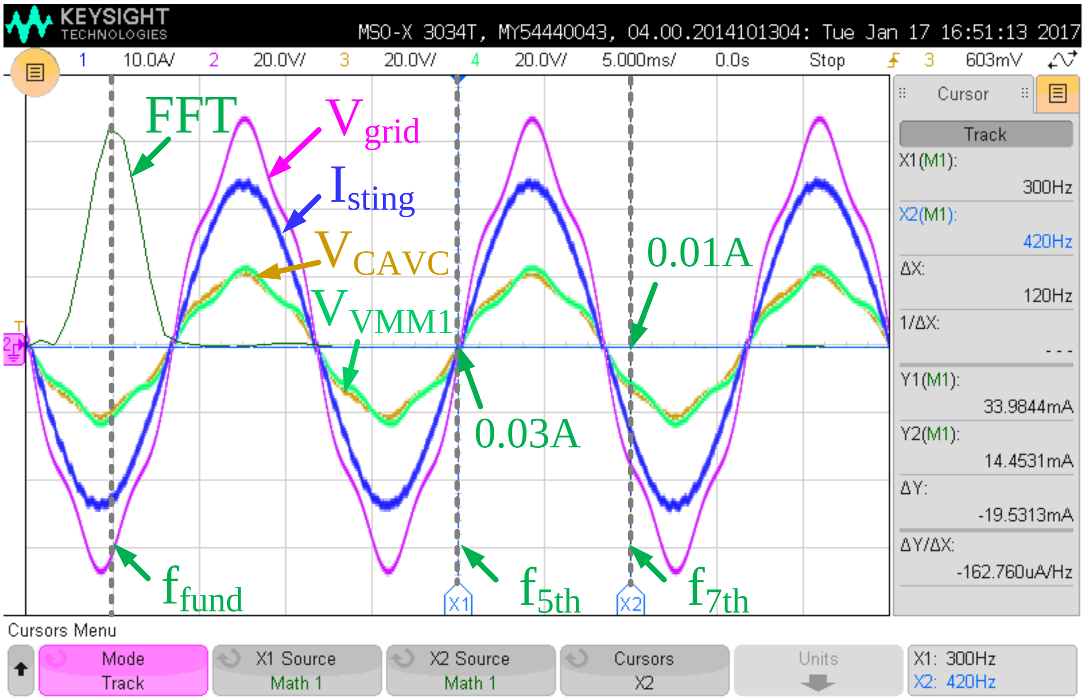

(c)

Figure 7.22, continued.

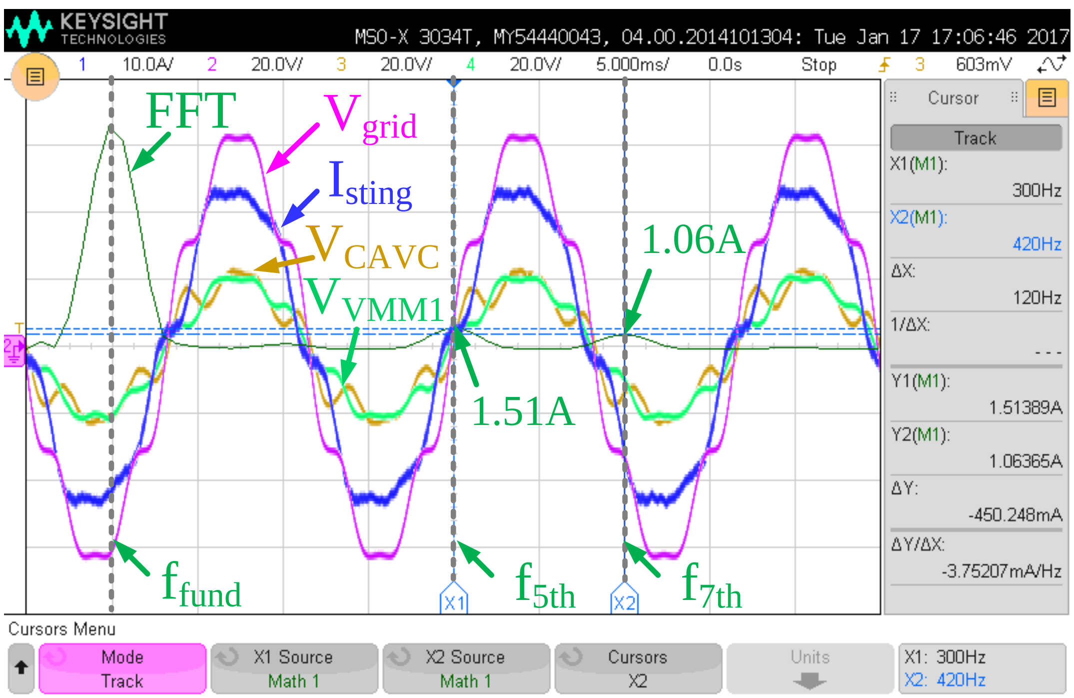

(a)

Figure 7.23. CHIL simulation results: Current, voltage, and FFT waveform in with a grid with 8% of 5^{th} and 7^{th} harmonics. (PV1: 1000W/m2, PV2: 1000W/m2, PV3: 1000W/m2, PPV_total=726W and Istring_RMS=16.3A). a. HCVC control scheme with no harmonics compensation. b. HCVC control scheme with SmHC harmonics compensation strategy. c. HCVC control scheme with AmHC harmonics compensation strategy.

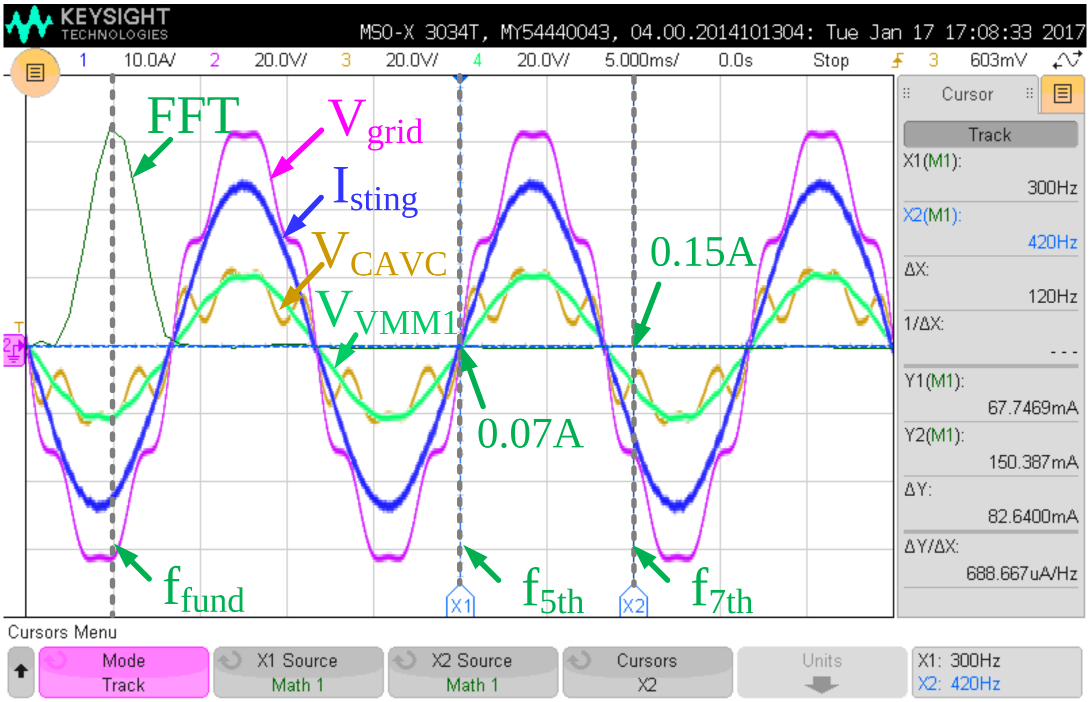

(b)

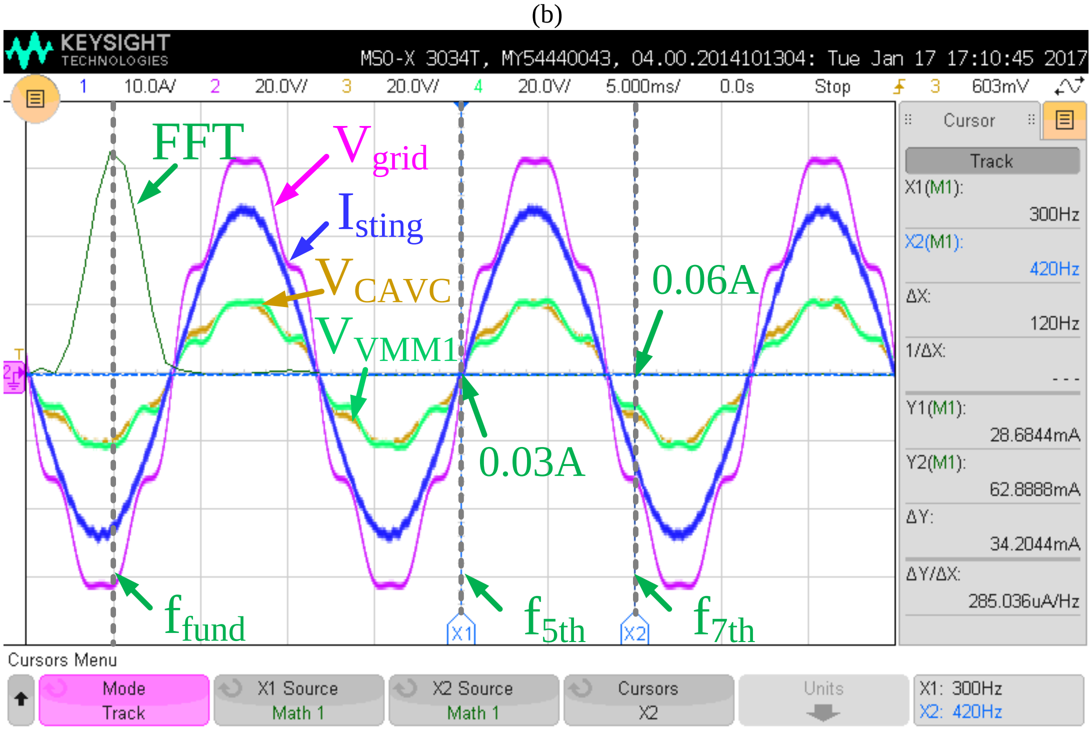

(c)

Figure 7. 23. Continued.

Table 7.1. Summary of CHIL simulation results: Duty cycle of modular inverters and current harmonics in different grid background harmonics conditions Nominal operating condition (PV1: 1000W/m2, PV2: 1000W/m2, PV3: 1000W/m2, PPV_total=726W and Istring_RMS=16.3A).

Case#	Detail conditions				Duty cycle			Operating margin			Harmonics-I_{string}	
	Grid Harmonics		Mitigation		CAVC	VMM1	VMM2	CAVC	VMM1	VMM2	5^{th} (%)	7^{th} (%)
	5^{th} (%)	7^{th} (%)	CAVC	VMMs								
1.1	-	-	-	-	0.71	0.66	0.66	29%	34%	34%	1.11	0.56
2.1	8	-	-	-	0.80	0.66	0.66	20% (-9%)	34% (-0%)	34% (-0%)	9.58	0.75
2.2	8	-	☑	-	0.83	0.67	0.66	17% (-12%)	33% (-1%)	34% (-0%)	0.45	0.03
2.3	8	-	☑	☑	0.75	0.71	0.71	25% (-4%)	29% (-5%)	29% (-5%)	0.21	0.09
3.1	-	8	-	-	0.79	0.66	0.66	21% (-8%)	34% (-0%)	34% (-0%)	1.14	6.78
3.2	-	8	☑	-	0.83	0.66	0.67	17% (-12%)	34% (-0%)	33% (-1%)	0.18	0.98
3.3	-	8	☑	☑	0.73	0.67	0.68	27% (-2%)	33% (-1%)	32% (-2%)	0.27	0.51
4.1	8	8	-	-	0.77	0.66	0.66	23% (-6%)	34% (-0%)	34% (-0%)	9.30	6.54
4.2	8	8	☑	-	0.78	0.67	0.67	22% (-7%)	33% (-1%)	33% (-1%)	0.42	0.92
4.3	8	8	☑	☑	0.75	0.69	0.69	25% (-4%)	31% (-3%)	31% (-3%)	0.18	0.39

In order to investigate the impact of higher voltage harmonics on the AC-stacked PV inverter system, two sets of experimental results are provided in Figure 7., Figure 7. and Table 7. 2. As can be seen, once larger amount of harmonics content is applied, bigger amount of harmonics current is occurred. Therefore, harmonics compensation consumes more of operating margin and it is more important to distribute the compensation among inverters to have more stability in the string. In Figure 7., the results for no compensation, SmHC and AmHC methods when the grid voltage is distorted by 30% 5^{th} harmonics.

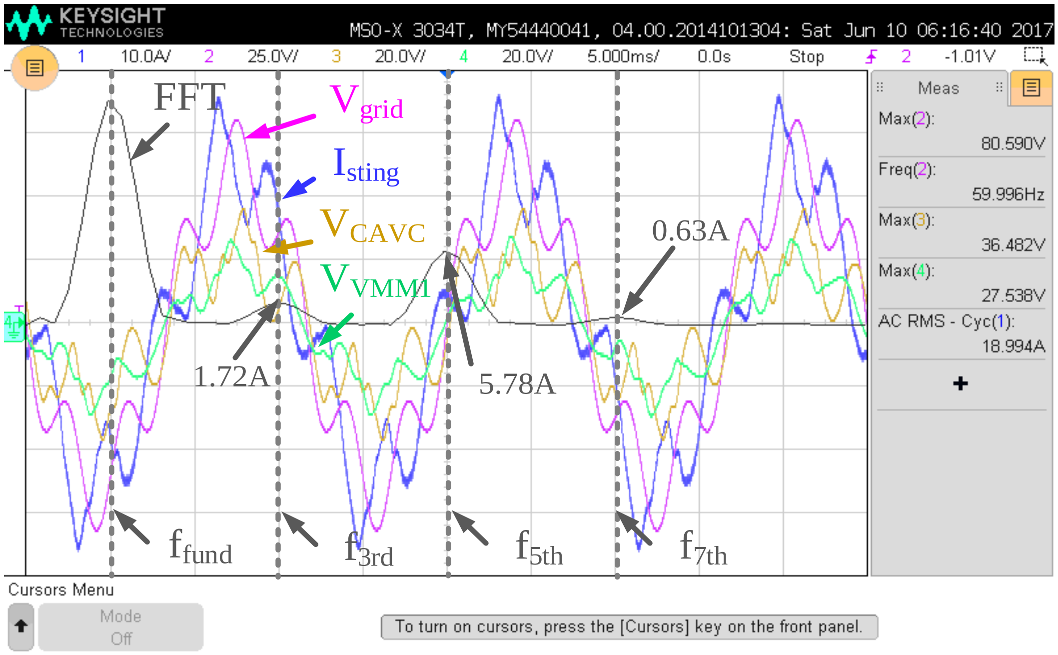

(a)

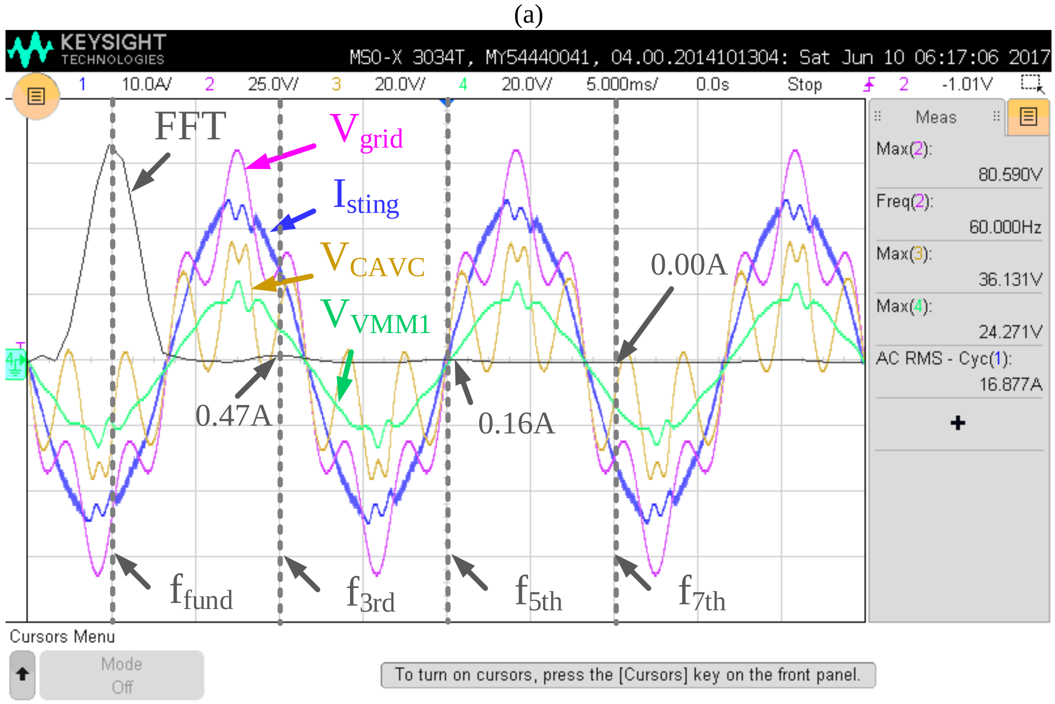

(b)

Figure 7.24. CHIL simulation results for 30% of 5th grid background harmonics. a. no harmonics mitigation. b. SmHC mitigation method. c. AmHC mitigation method.

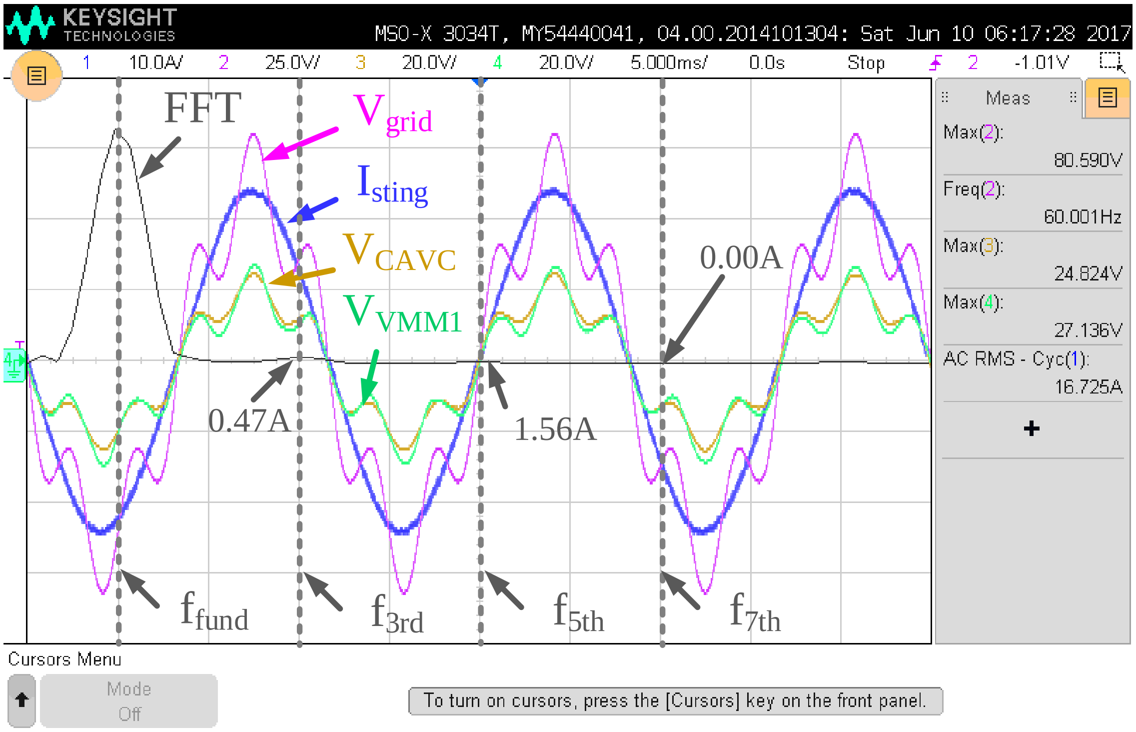

(c)

Figure 7.24. continued.

In this case, CAVC cannot compensate for all the required harmonics content because it reaches its maximum duty-cycle representing zero operating margin. Therefore, the output AC current has high harmonics content as it can be seen in Figure 7..b. The performance of the system with 30% 7th harmonics distortion is also presented in Figure 7.. Similar to 5th harmonics, in 7th harmonics also SmHC method cannot compensate for background harmonics and the output current is distorted, Figure 7..b.

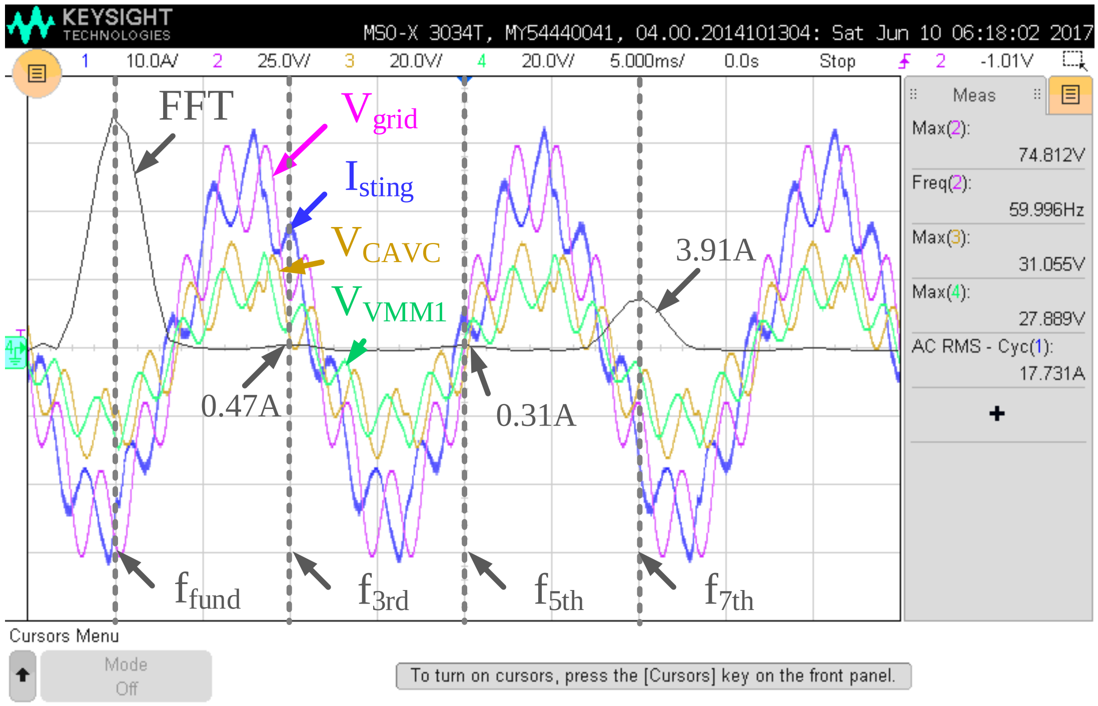

(a)

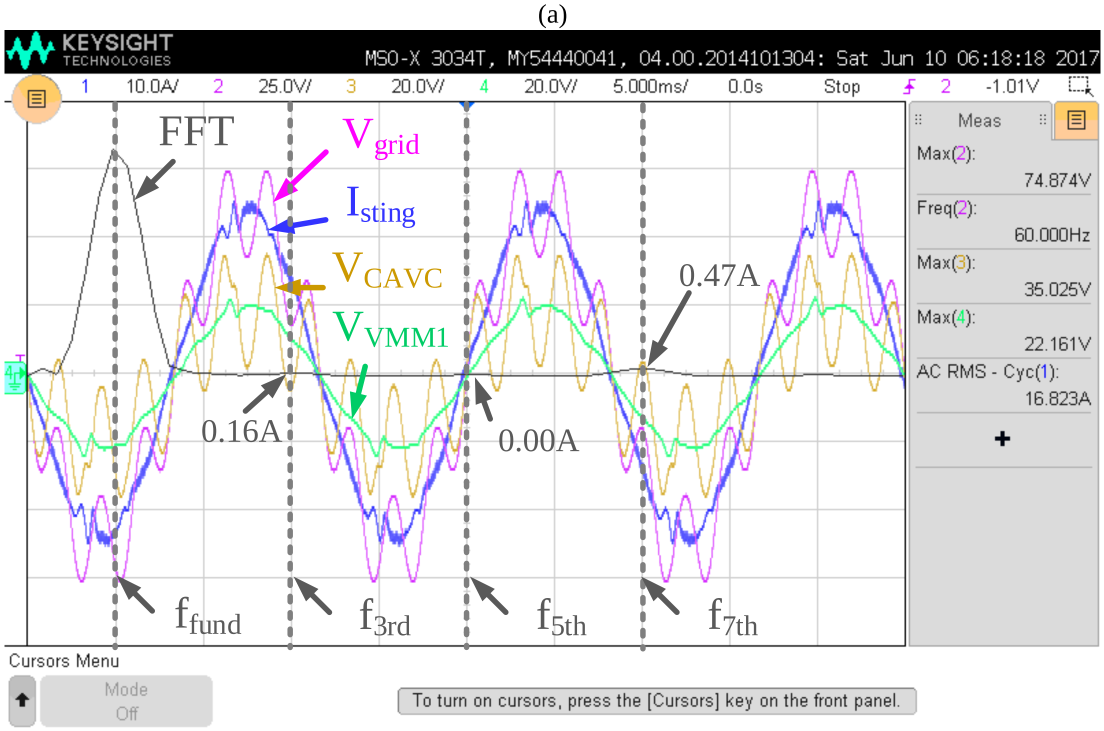

(b)

Figure 7.25. CHIL simulation results: 30% of 7th grid background harmonics. a. no harmonics mitigation. b. SmHC mitigation method. c. AmHC mitigation method.

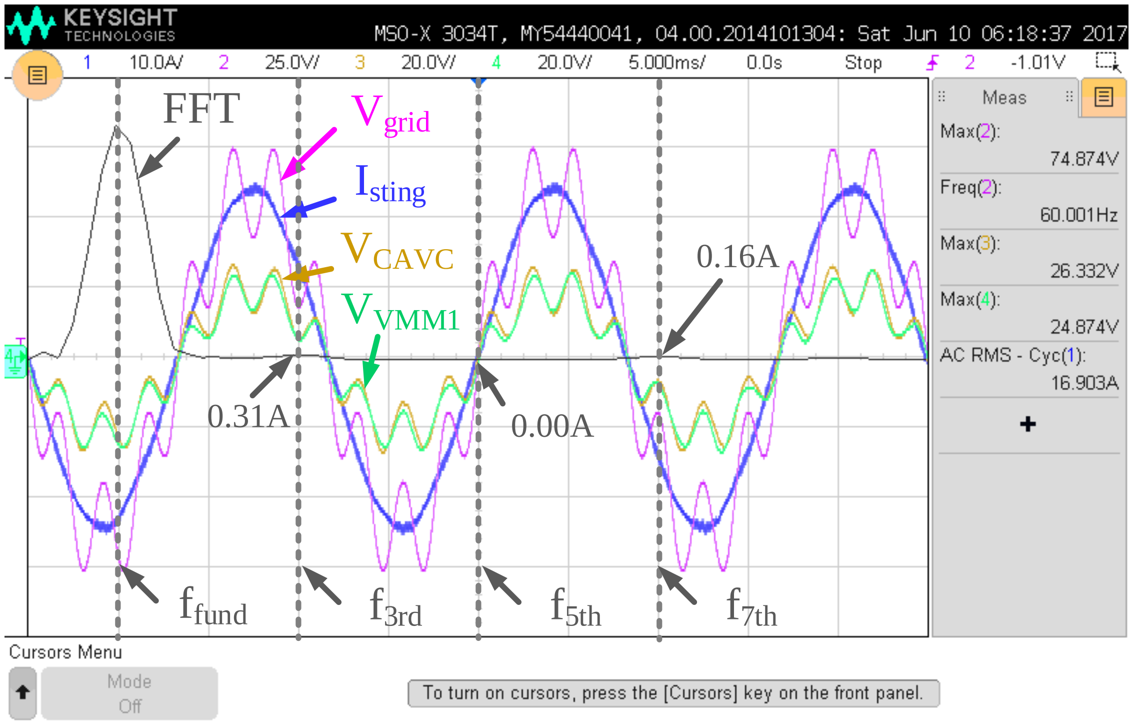

(c)

Figure 7.25. continued.

On the other hand, with AmHC method, all the inverter members can share their operating margin to mitigate the large harmonics content and provide high-quality AC current with low THD, see Figure 7..c and Figure 7..c. Detailed results information of inverters' duty-cycle, operating margin, and AC current harmonics is presented in Table 7. 2. The same study can be also applied to the 3rd harmonics or other higher order harmonics by adding selective harmonics mitigation for this frequency.

Table 7. 2. Summary of CHIL simulation results: Duty cycle of modular inverters and current harmonics in different grid background harmonics conditions.

Detail conditions				Duty cycle			Operating margin			Harmonics-I_{string}		
Grid Harmonics		Mitigation		CAVC	VMM1	VMM2	CAVC (%)	VMM 1 (%)	VMM 2 (%)	3rd (A)	5th (A)	7th (A)
5th (%)	7th (%)	CAVC	VMMs									
30	-	-	-	1.0	0.62	0.62	0	38	38	1.72	5.78	0.63
30	-	☑	-	1.0	0.67	0.67	0	33	33	0.47	0.16	0.00
30	-	☑	☑	0.83	0.83	0.83	17	17	17	0.47	1.56	0.00
-	30	-	-	1.0	0.63	0.63	0	37	37	0.47	0.31	3.91
-	30	☑	-	1.0	0.67	0.67	0	33	33	0.16	0.00	0.47
-	30	☑	☑	0.87	0.74	0.74	13	26	26	0.31	0.00	0.16

In order to show the impact of AmHC harmonics mitigation on operation of AC-stacked PV inverter architecture and have a better comparison between SmHC and AmHC methods, an asymmetrical condition is studied, where VMM2 experiences a severe shading $\left(0W/m^2\right)$, which causes increase of duty cycle on the CAVC and VMM1. The results of this study are analyzed and presented in Figure 7., Figure 7. and Table 7.3. Once VMM2 is lost which means loss of 33.3% of total PV output power, the most of operating margin is used up and the AC-stacked inverter architecture still requires available room to mitigate harmonics contents.

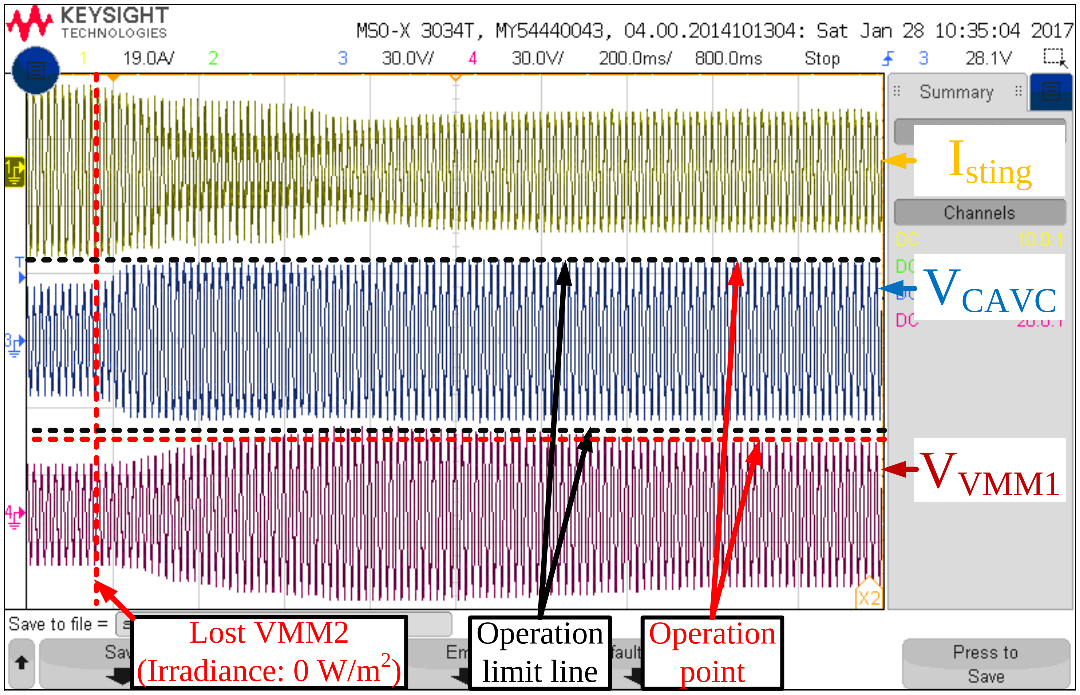

(a)

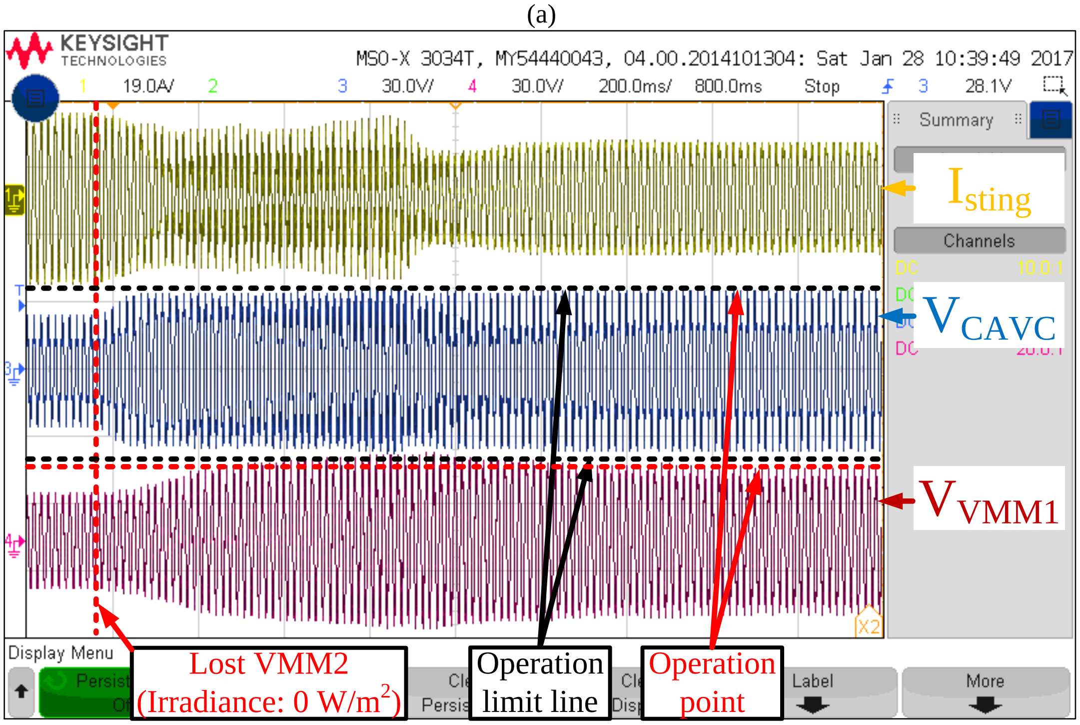

(b)

Figure 7.24. CHIL simulation results: Current, voltage, and FFT waveform in asymmetric operating condition Asymmetric operating condition (PV1: 1000W/m2, PV2: 1000W/m2, PV3: 0W/m2, PPV_total=477W and Istring_RMS=10.7A). Transient operation when one VMM2 is fully shaded. a. No harmonics compensation. b. SmHC method. c. AmHC method.

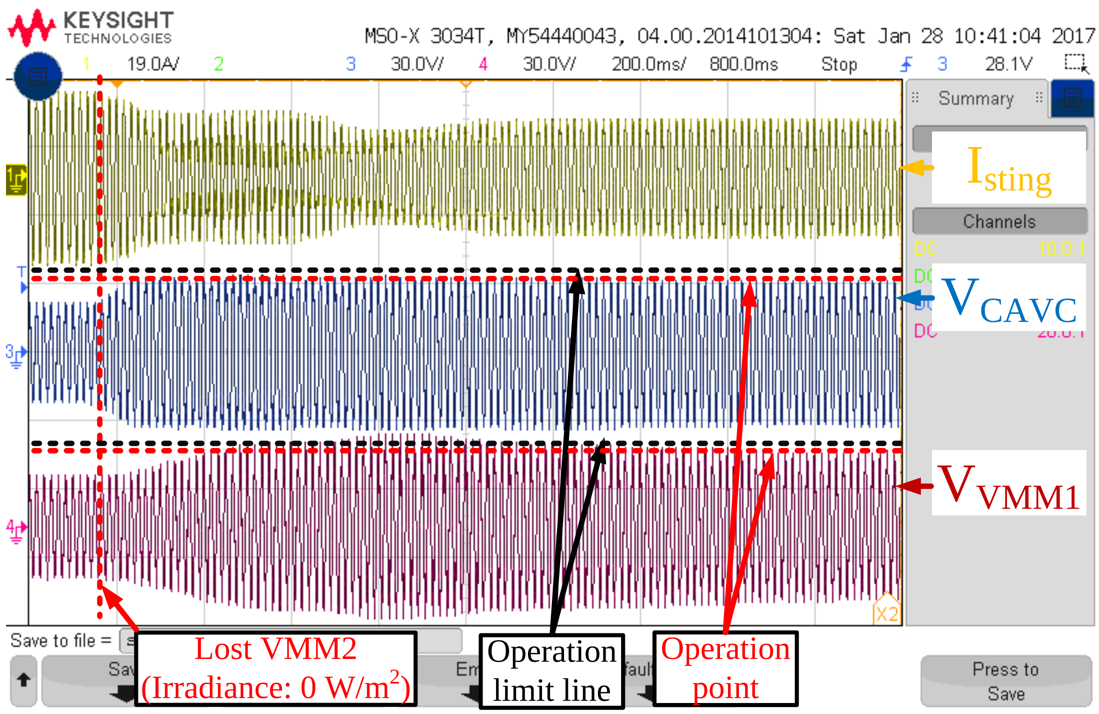

(c)

Figure 7.26. continued.

In SmHC harmonics mitigation strategy, CAVC reaches its limitation of available room for operation and generates extra harmonics contents such as 3rd, 9th, 17th, etc. which are not appeared in nominal operating condition. On the other hand, in the AmHC harmonics mitigation strategy, CAVC and VMM1 still provide high quality AC current while having stable operation within the limitation. These results with nominal and asymmetrical operation conditions demonstrate the effectiveness and feasibility of the proposed AmHC control algorithm.

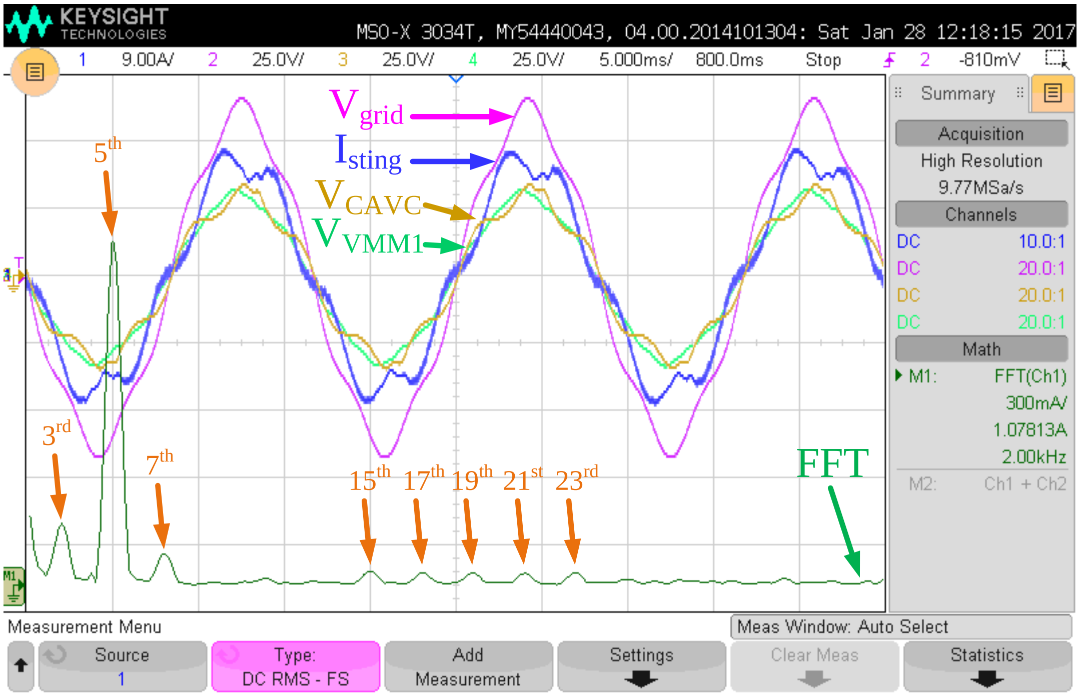

(a)

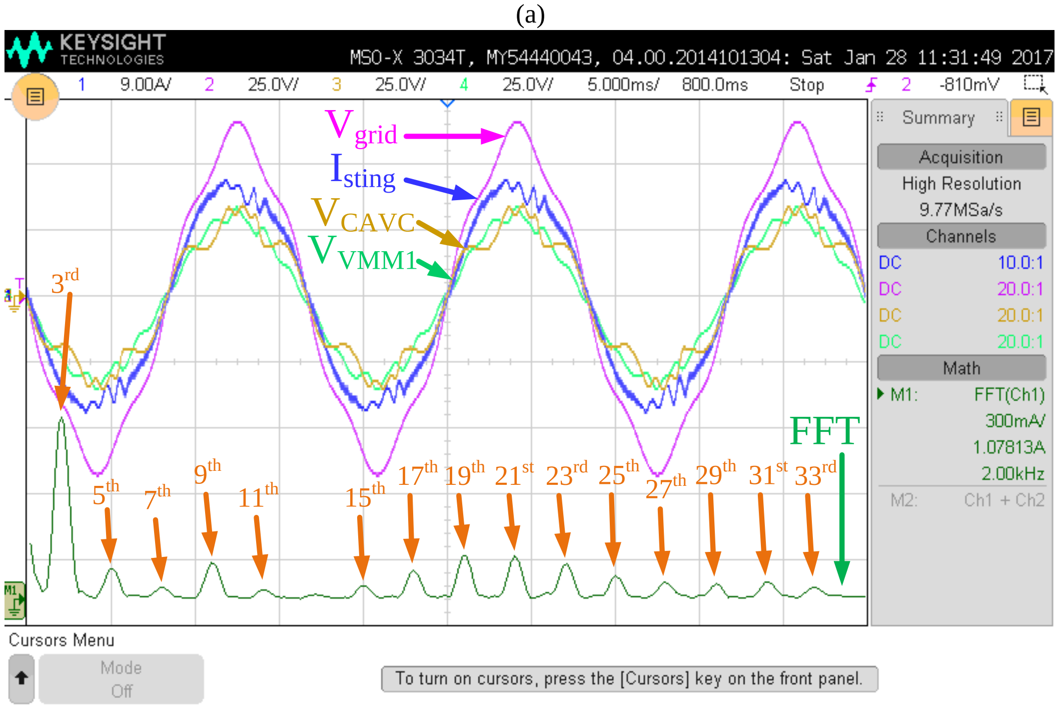

(b)

Figure 7.25. CHIL simulation results: Current, voltage, and FFT waveform in asymmetric operating condition Asymmetric operating condition (PV1: 1000W/m2, PV2: 1000W/m2, PV3: 0W/m2, PPV_total=477W and Istring_RMS=10.7A). steady state operation condition when one VMM2 is fully shaded. a. No harmonics compensation. b. SmHC method. c. AmHC method.

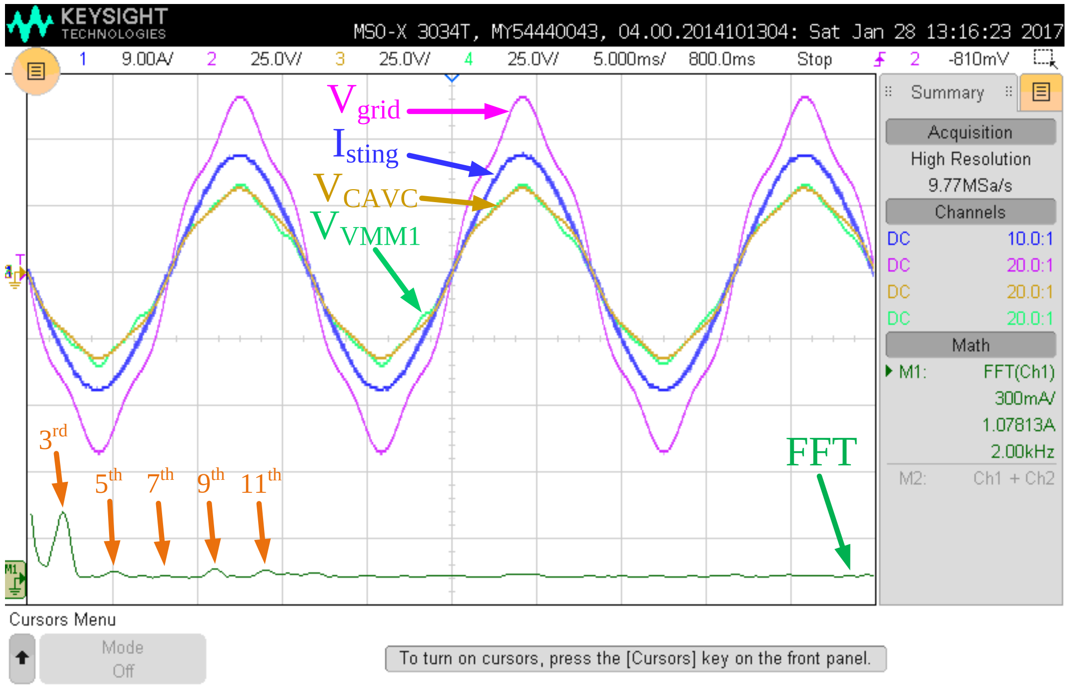

(c)

Figure 7.25. continued.

Table 7.3. Summary of CHIL results: String current harmonics in different operating condition Nominal operating condition (PV1: 1000W/m2, PV2: 1000W/m2, PV3: 1000W/m2, PPV_total=726W and Istring_RMS=16.3A) Asymmetric operating condition (PV1: 1000W/m2, PV2: 1000W/m2, PV3: 0W/m2, PPV_total=477W and Istring_RMS=10.7A).

Case #	Detail conditions				String current harmonics									
	Grid Harmonics	Mitigation		Operating condition	Orders of harmonics & magnitude (%)									
	5th (%)	CAVC	VMM		3rd	5th	7th	9th	17th	19th	21st	23rd	25th	27th
5.1	8	-	-	Nominal	1.9	9.3	0.5	0.3	0.1	0.1	0	0.2	0	0
5.2	8	☑	-	Nominal	1.7	0.4	0.1	0.4	0.1	0.1	0.1	0.1	0.1	0.1
5.3	8	☑	☑	Nominal	1.6	0.1	0.1	0.4	0.1	0.1	0.1	0.1	0.1	0.1
6.1	8	-	-	Asymmetric	3.0	14.4	1.8	0.1	0.4	0.4	0.2	0.2	0.4	0.3
6.2	8	☑	-	Asymmetric	7.6	1.3	0.5	1.5	1.2	1.8	1.8	1.4	0.9	0.7
6.3	8	☑	☑	Asymmetric	2.8	0.1	0.1	0.4	0	0	0	0	0.1	0

In order to study the impact of sudden changes in the harmonics content of the grid and the impact of such events on the proposed method, additional experiments and analysis are provided here. In Figure 7.25 and Figure 7.26 I investigated the impact of sudden change in the grid voltage harmonics content for 5th and 7th harmonics. As can be seen in these two studies when we have a significant change in the harmonics content of grid voltage from 10% to 20%, the proposed AmHC method, presented in this manuscript, can be able to mitigate the impact of background harmonics of this sudden change. Of course, the system experiences a transient time which is around 2s till the controller compensates for the new harmonics content as can be seen in these figures.

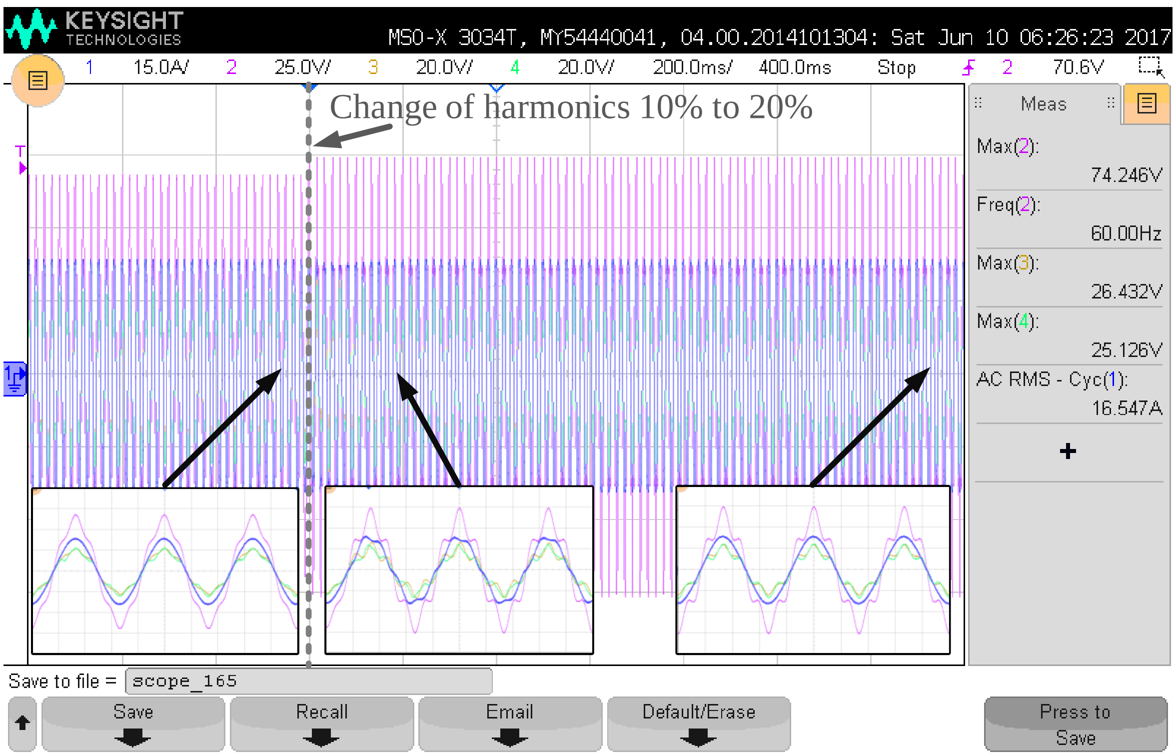

Figure 7.25. CHIL simulation results: Transient state response of AmHC mitigation when a sudden change 10% to 20% of 5th grid background harmonics is applied.

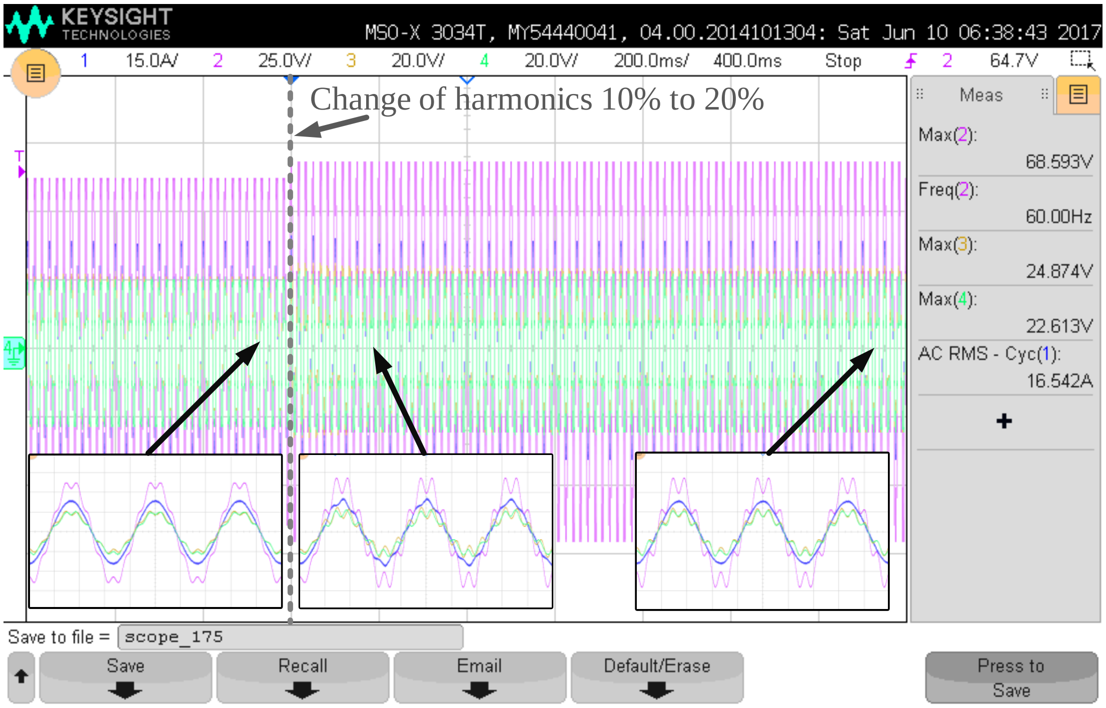

Figure 7.26. CHIL simulation results: Transient state response of AmHC mitigation when a sudden change 10% to 20% of 7th grid background harmonics is applied.

Finally, the impact of grid disturbances is studied in this part. Grid voltage disturbances can be controlled with minimum communication requirements using the control strategy presented in previous sections. However, grid voltage disturbances can affect the operating margin of the inverter members. If the disturbance is voltage swell, the inverters should increase their modulation indices to provide required voltage for grid integration. Therefore, operating margin of the system will be reduced. On the other side, during voltage sag, due to decrease in the amplitude of grid voltage, the modulation indices of inverters will be reduced and the operating margin of inverter will be increased. These experiments and the detailed results are provided in Figure 7. and Table 7.4. where the CHIL simulation results with grid voltage disturbances; 89~111% of the nominal grid voltage are provided.

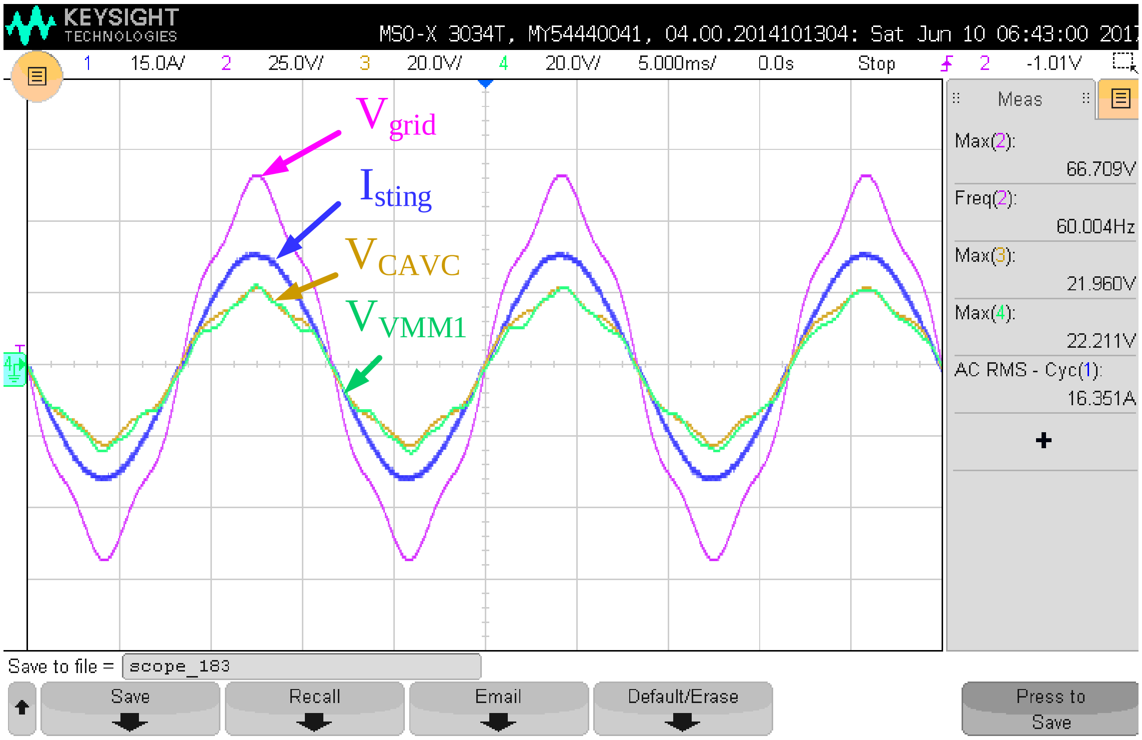

(a)

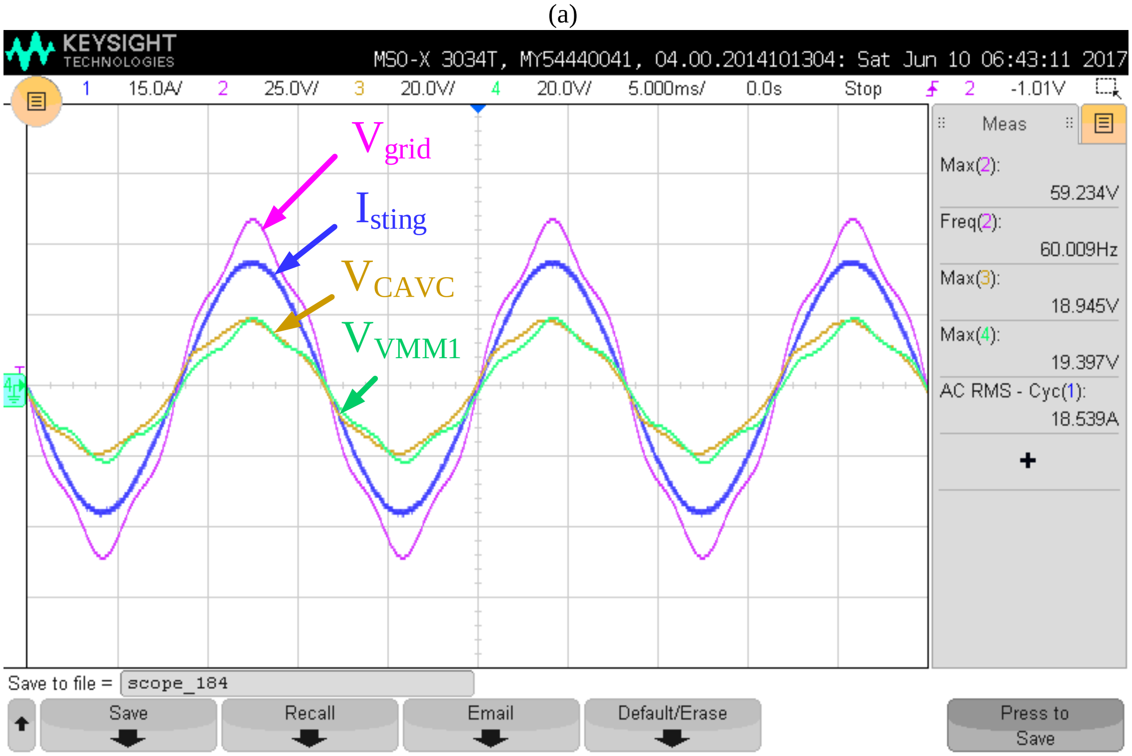

(b)

Figure 7.30. CHIL simulation results: Effect of grid voltage disturbances with 8% of 5th grid background harmonics in AmHC mode. a. Grid voltage 45Vrms. b. Grid voltage 40Vrms. c. Grid voltage 50Vrms.

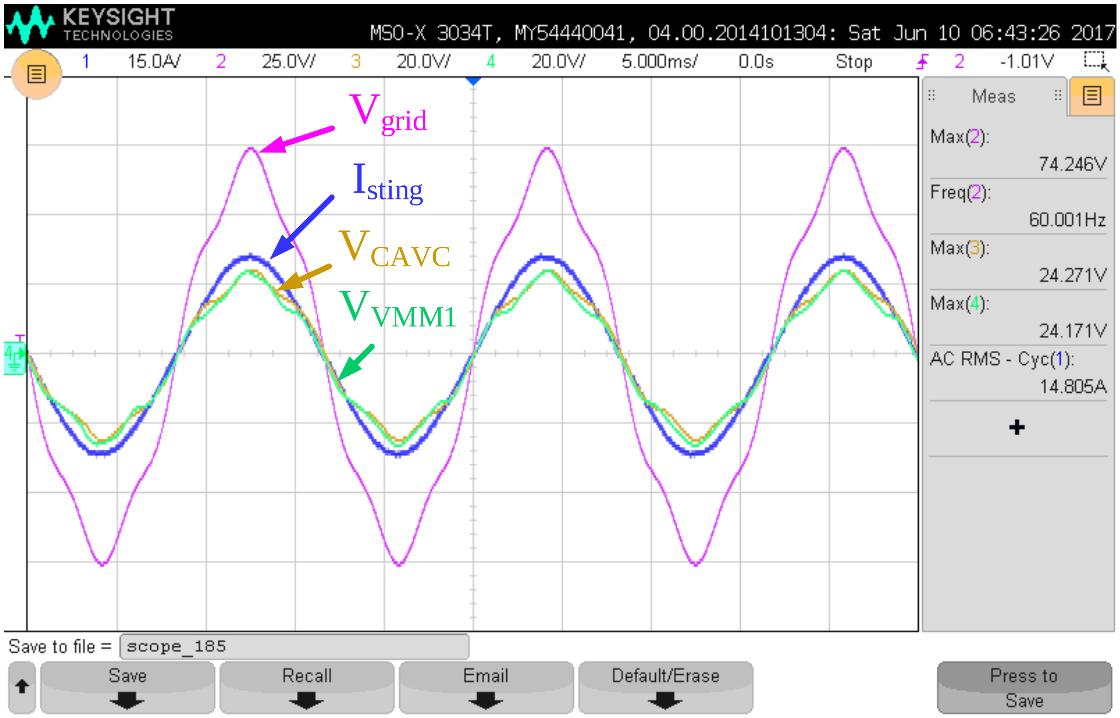

(c)

Figure 7.30. continued.

Table 7.4. Summary of CHIL simulation results: Duty cycle of modular inverters in AmHC mode with different grid disturbances.

Detail conditions				Duty cycle			Operating margin		
Grid Harmonics & Disturbances			Fundamental frequency tracking	CAVC	VMM1	VMM2	CAVC (%)	VMM1 (%)	VMM2 (%)
5^{th} (%)	Voltage (V)	Frequency (Hz)							
8	45	60	-	0.76	0.71	0.71	24	29	29
8	40	60	-	0.68	0.64	0.65	32	36	35
8	50	60	-	0.84	0.79	0.79	16	21	21
8	45	59.3	-	0.80	0.68	0.68	20	32	32
8	45	60.5	-	1.00	0.72	0.72	0	28	28
8	45	59.3	☑	0.73	0.71	0.71	27	29	29
8	45	60.5	☑	0.74	0.71	0.71	26	29	29

Also, grid frequency disturbances affect the performance of selective PR controllers. Since the PR controllers can only compensate the selective harmonics contents and require the fundamental frequency information, the PR controller cannot cover the different harmonics contents when the mismatch between the grid frequency and the PR controller frequency is occurred. To improve the performance of the PR controllers with the grid frequency disturbances, fundamental frequency tracking control can be adopted to the proposed control system. Figure and Figure show the CHIL simulation results with grid frequency disturbances; 59.3~60.5Hz.

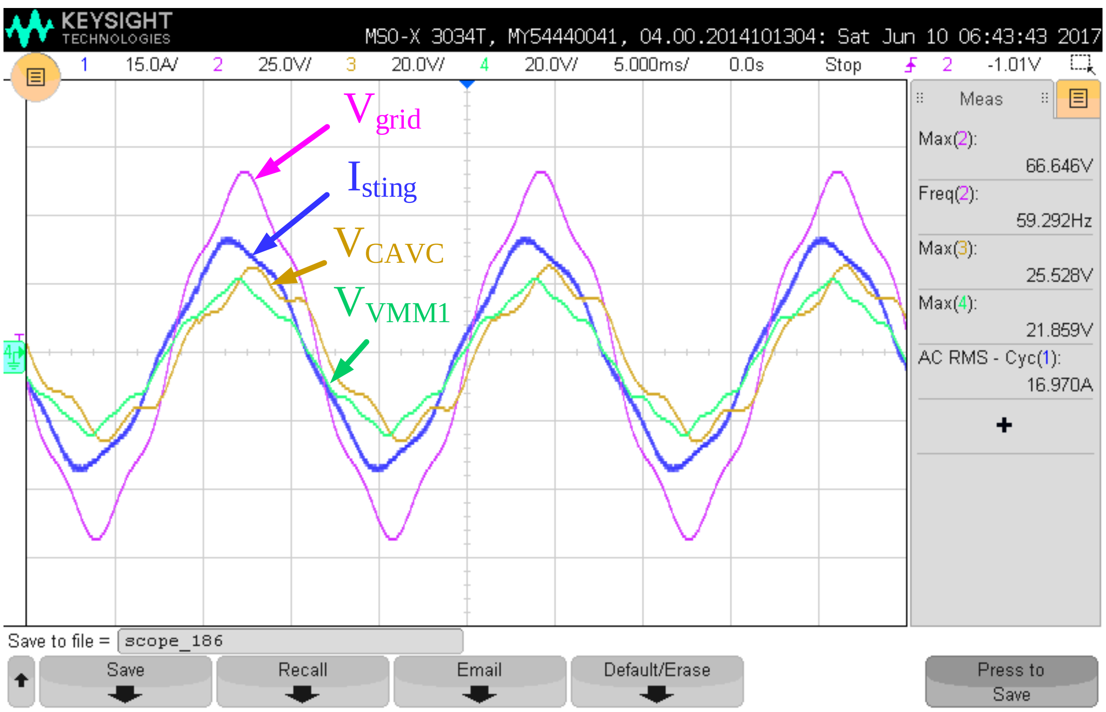

(a)

Figure 7.31. CHIL simulation results: Effect of grid frequency disturbances (59.3Hz) with 8% of 5th grid background harmonics in AmHC mode. a. No fundamental frequency tracking. b. With fundamental frequency tracking.

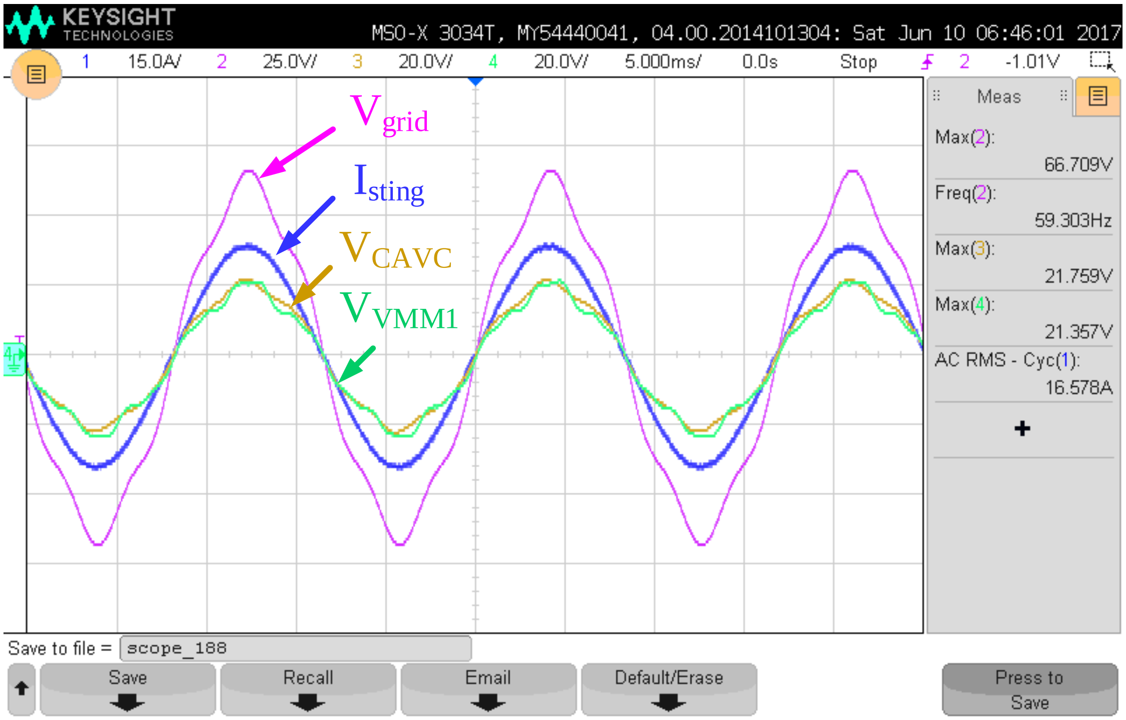

(b)

Figure 7.31. continued.

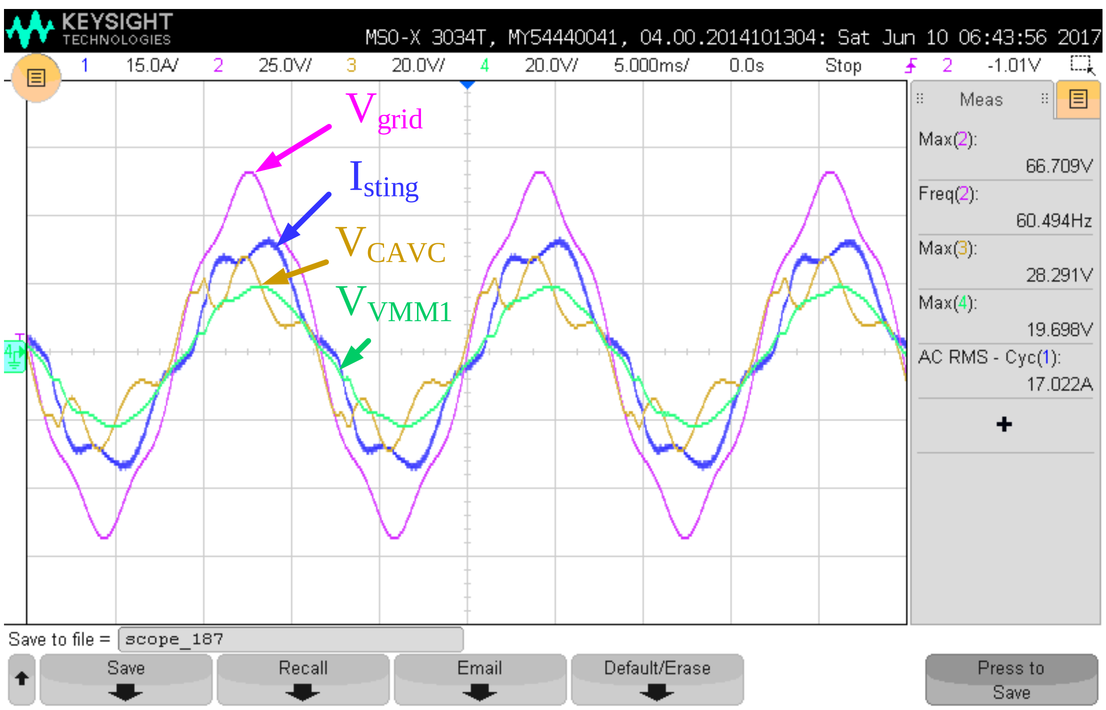

(a)

Figure 7.32. CHIL simulation results: Effect of grid frequency disturbances (60.5Hz) with 8% of 5th grid background harmonics in AmHC mode. a. No fundamental frequency tracking. b. With fundamental frequency tracking.

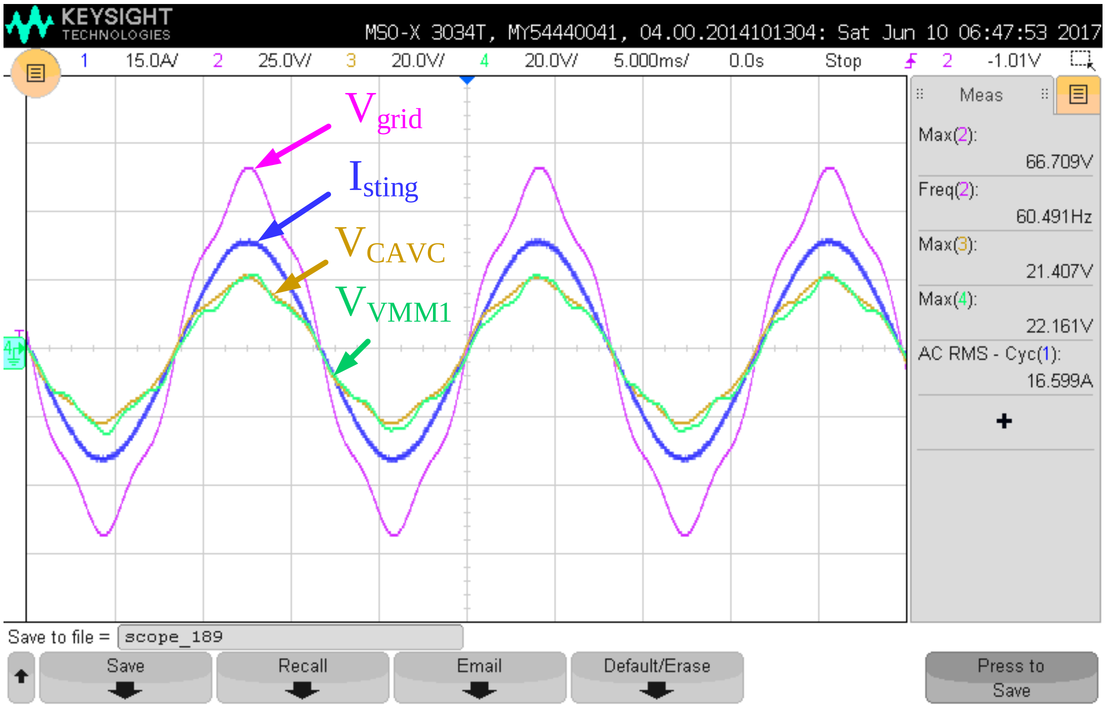

(b)

Figure 7.32. continued.

CHAPTER EIGHT: CONCLUSION AND FUTURE WORK

8.1 Conclusion

This research presented an advanced decentralized control algorithm for new AC-stacked PV inverter architecture. In this research, for the first time, the feasibility of fully decentralized control scheme for grid-tied AC-stacked architecture was analyzed. Using Relative Gain Array approach the strength of inter-connection between inputs and outputs of this system was calculated and the best pairing sets for decentralized control system were determined. The proposed Hybrid Current/Voltage Control (HCVC) method, proposed in the thesis, controlled the AC-stacked PV inverter system with four stages of decentralized controller by utilizing local measurements and no communication between inverters.

In order to satisfy the requirements of modern power networks with high penetrated distributed generations, different smart inverter functionalities were designed in this dissertation. Reactive power control algorithm that was introduced in this research which was called Single-member Phase Compensation (SmPC), is a decentralized controller which was verified to be able to control the output reactive power of the inverter string with only on inverter.

Another smart function, which was studied in this thesis was the impact of distorted grid voltage on the performance of the current controllers of PV inverters. Utilizing output impedance approach and frequency domain analysis, two novel strategies were proposed which were called, Single-member Harmonics Compensation (SmHC) and All-member Harmonics Compensation (AmHC). Effectiveness of the proposed methods and advantages of AmHC method was verified using mathematical modeling and analysis.

Controller robustness analysis is another critical study which was provide in this research. Robustness analysis and the impact of inaccuracies and variations of components on the performance of controllers are very important in the process of control implementation, especially for decentralized control systems. Smart Inverter Robustness Index (SIRI), proposed in this thesis, is a comprehensive approach for robustness evaluation of grid-tied PV inverters consisting the four main characteristics of grid-connected PV inverters such as conversion efficiency, maximum power point tracking accuracy, power factor compliance and total harmonics distortion. Using SIRI index, the impact of stacking PV inverters and decentralized controller system on the robustness of grid-tied PV inverter systems were analyzed considering sensing inaccuracies and passive components variations due to manufacturing inaccuracies, aging and environmental conditions.

The feasibility and effectiveness of control and methods which were proposed in this thesis were verified through several modeling, and simulation approaches and Controller Hardware-in-the-Loop (CHiL) test-bed and experimental results. All the analysis and results verified the advanced advantages of control methods introduced in this research compared with traditional central or pseudo-central control schemes.

8.2 Future Work

- Studying the feasibility of the other possible decentralized controllers such as overlapping decomposition methods.
- Studying the stability of the overlapping decomposition controller and comparing it with the proposed decentralized controller in this research.
- Design and implementation of decentralized controller for three-phase grid-tied AC-stacked PV inverter system for high power PV power plants.
- Studying the possibility of the balanced reactive power control methods with minimum communication requirements.
- Design and implementing of the other smart inverter functions such as Low Voltage Ride-Through (LVRT) with decentralized control strategies.
- Design and development of a frequency control method for performing the off-line operation with disconnected grid and for islanded networks with decentralized control scheme.
- Stability analysis of the proposed control method in an asymmetric system with different PV panels with different characteristics and analytical study for determining the best inverter member for CAVC assignment.
- Studying the impact of other inaccuracies such as communication inaccuracies, conversion inaccuracies etc. on the robust operation of the AC-stacked PV inverter systems.
- Development of state estimation method for predicting the system states in high distorted environment and designing a self-healing algorithm for improving the robustness of PV inverters with high inaccuracies.

REFERENCES

[1] R. Renewable Energy Policy Network for thr 21st Centure, "Renewables and global status report 2016," 2016.

[2] Y. Yongheng, W. Huai, and F. Blaabjerg, "Reactive Power Injection Strategies for Single-Phase Photovoltaic Systems Considering Grid Requirements," *Industry Applications, IEEE Transactions on,* vol. 50, pp. 4065-4076, 2014.

[3] T. Stetz, F. Marten, and M. Braun, "Improved Low Voltage Grid-Integration of Photovoltaic Systems in Germany," *Sustainable Energy, IEEE Transactions on,* vol. 4, pp. 534-542, 2013.

[4] Y. Yongheng, P. Enjeti, F. Blaabjerg, and W. Huai, "Suggested grid code modifications to ensure wide-scale adoption of photovoltaic energy in distributed power generation systems," in *Industry Applications Society Annual Meeting, 2013 IEEE*, 2013, pp. 1-8.

[5] B. Mohammad Hasan, N. Nouri, A. Nasiri, and H. Seifoddini, "Development of an economical model for a hybrid system of grid, PV and Energy Storage Systems," in *2015 International Conference on Renewable Energy Research and Applications (ICRERA)*, 2015, pp. 1108-1113.

[6] A. Cagnano, E. De Tuglie, M. Liserre, and R. A. Mastromauro, "Online Optimal Reactive Power Control Strategy of PV Inverters," *Industrial Electronics, IEEE Transactions on,* vol. 58, pp. 4549-4558, 2011.

[7] R. Langella, A. Testa, J. Meyer, M. F, x00F, ller, *et al.*, "Experimental-Based Evaluation of PV Inverter Harmonic and Interharmonic Distortion Due to Different Operating Conditions," *IEEE Transactions on Instrumentation and Measurement,* vol. PP, pp. 1-13, 2016.

[8] A. Marzoughi and H. Imaneini, "Optimal selective harmonic elimination for cascaded H-bridge-based multilevel rectifiers," *IET Power Electronics,* vol. 7, pp. 350-356, 2014.

[9] H. Hu, Q. Shi, Z. He, J. He, and S. Gao, "Potential Harmonic Resonance Impacts of PV Inverter Filters on Distribution Systems," *IEEE Transactions on Sustainable Energy,* vol. 6, pp. 151-161, 2015.

[10] M. Moosavi, S. Farhangi, H. Iman-Eini, and A. Haddadi, "An LCL-based interface connecting photovoltaic back-up inverter to load and grid," in *Power Electronics, Drive Systems and Technologies Conference (PEDSTC), 2013 4th*, 2013, pp. 465-470.

[11] I. Mazhari, H. Jafarian, B. Parkhideh, S. Trivedi, and S. Bhowmik, "Locking frequency band detection method for grid-tied PV inverter islanding protection," in *Energy Conversion Congress and Exposition (ECCE), 2015 IEEE*, 2015, pp. 1976-1981.

[12] I. Stoyanova, M. Biglarbegian, and A. Monti, "Cooperative energy management approach for short-term compensation of demand and generation variations," in *2014 IEEE International Systems Conference Proceedings*, 2014, pp. 559-566.

[13] S. B. Kjaer, J. K. Pedersen, and F. Blaabjerg, "A review of single-phase grid-connected inverters for photovoltaic modules," *IEEE Transactions on Industry Applications,* vol. 41, pp. 1292-1306, 2005.

[14] G. R. Walker and P. C. Sernia, "Cascaded DC-DC converter connection of photovoltaic modules," *IEEE Transactions on Power Electronics,* vol. 19, pp. 1130-1139, 2004.

[15] N. A. Rahim and J. Selvaraj, "Multistring Five-Level Inverter With Novel PWM Control Scheme for PV Application," *IEEE Transactions on Industrial Electronics,* vol. 57, pp. 2111-2123, 2010.

[16] S. M. Tayebi, C. Jourdan, and I. Batarseh, "Dynamic Dead-Time Optimization and Phase Skipping Control Techniques for Three-Phase Microinverter Applications," *IEEE Transactions on Industrial Electronics,* vol. 63, pp. 7523-7532, 2016.

[17] H. Hu, S. Harb, N. H. Kutkut, Z. J. Shen, and I. Batarseh, "A Single-Stage Microinverter Without Using Eletrolytic Capacitors," *IEEE Transactions on Power Electronics,* vol. 28, pp. 2677-2687, 2013.

[18] S. M. Chen, T. J. Liang, and K. R. Hu, "Design, Analysis, and Implementation of Solar Power Optimizer for DC Distribution System," *IEEE Transactions on Power Electronics,* vol. 28, pp. 1764-1772, 2013.

[19] S. Bhowmik, "Systems and methods for solar photovoltaic energy collection and conversion," ed: Google Patents, 2013.

[20] E. Villanueva, P. Correa, J. Rodriguez, and M. Pacas, "Control of a Single-Phase Cascaded H-Bridge Multilevel Inverter for Grid-Connected Photovoltaic Systems," *Industrial Electronics, IEEE Transactions on*, vol. 56, pp. 4399-4406, 2009.

[21] B. Xiao, L. Hang, J. Mei, C. Riley, L. M. Tolbert, and B. Ozpineci, "Modular Cascaded H-Bridge Multilevel PV Inverter With Distributed MPPT for Grid-Connected Applications," *IEEE Transactions on Industry Applications*, vol. 51, pp. 1722-1731, 2015.

[22] S. Kouro, B. Wu, Moya, E. Villanueva, P. Correa, J. Rodr, *et al.*, "Control of a cascaded H-bridge multilevel converter for grid connection of photovoltaic systems," in *Industrial Electronics, 2009. IECON '09. 35th Annual Conference of IEEE*, 2009, pp. 3976-3982.

[23] S. Daher, J. Schmid, and F. L. M. Antunes, "Multilevel Inverter Topologies for Stand-Alone PV Systems," *IEEE Transactions on Industrial Electronics*, vol. 55, pp. 2703-2712, 2008.

[24] H. Jafarian, I. Mazhari, B. Parkhideh, S. Trivedi, D. Somayajula, R. Cox, *et al.*, "Design and implementation of distributed control architecture of an AC-stacked PV inverter," in *Energy Conversion Congress and Exposition (ECCE), 2015 IEEE*, 2015, pp. 1130-1135.

[25] I. Mazhari, H. Jafarian, J. Enslin, S. Bhowmik, and B. Parkhideh, "Locking Frequency Band Detection Method for Islanding Protection of Distribution Generation," *IEEE Journal of Emerging and Selected Topics in Power Electronics*, vol. PP, pp. 1-1, 2017.

[26] R. Yousefian, A. Sahami, and S. Kamalasadan, "Hybrid energy function based real-time optimal wide-area transient stability controller for power system stability," in *2015 IEEE Industry Applications Society Annual Meeting*, 2015, pp. 1-8.

[27] M. Davoudi, "Increasing Hosting Capacity of Distribution Systems For Renewable Distributed Generation By Means of Network Reconfiguration," The University of North Carolina at Charlotte, 2017.

[28] L. Liming, L. Hui, and X. Yaosuo, "Control strategies for utility-scale cascaded photovoltaic system," in *Energy Conversion Congress and Exposition (ECCE), 2013 IEEE*, 2013, pp. 2391-2397.

[29] H. Jafarian, S. Bhowmik, and B. Parkhideh, "Hybrid Current/Voltage-mode Control Scheme for Distributed AC-stacked PV Inverter with Low Bandwidth Communication Requirements," *IEEE Transactions on Industrial Electronics,* vol. PP, pp. 1-1, 2017.

[30] M. Coppola, F. D. Napoli, P. Guerriero, D. Iannuzzi, S. Daliento, and A. D. Pizzo, "An FPGA-Based Advanced Control Strategy of a GridTied PV CHB Inverter," *IEEE Transactions on Power Electronics,* vol. 31, pp. 806-816, 2016.

[31] J. Chavarr, x00Ed, D. Biel, F. Guinjoan, C. Meza, and J. Negroni, "Energy-Balance Control of PV Cascaded Multilevel Grid-Connected Inverters Under Level-Shifted and Phase-Shifted PWMs," *IEEE Transactions on Industrial Electronics,* vol. 60, pp. 98-111, 2013.

[32] G. Petrone, G. Spagnuolo, R. Teodorescu, M. Veerachary, and M. Vitelli, "Reliability Issues in Photovoltaic Power Processing Systems," *IEEE Transactions on Industrial Electronics,* vol. 55, pp. 2569-2580, 2008.

[33] P. Cortes, S. Kouro, F. Barrios, and J. Rodriguez, "Predictive control of a single-phase cascaded h-bridge photovoltaic energy conversion system," in *Power Electronics and Motion Control Conference (IPEMC), 2012 7th International*, 2012, pp. 1423-1428.

[34] J. E. a. B. P. • H. Jafarian, "On Reactive Power Injection Control of Distributed Grid-tied AC-stacked PV Inverter Architecture," in *Energy Conversion Congress and Exposition (ECCE)*, Milwaukee, 2016, p. in press.

[35] A. Dell'Aquila, M. Liserre, V. G. Monopoli, and P. Rotondo, "Overview of PI-based solutions for the control of the dc-buses of a single-phase H-bridge multilevel active rectifier," in *Applied Power Electronics Conference and Exposition, 2004. APEC '04. Nineteenth Annual IEEE,* 2004, pp. 836-842 vol.2.

[36] T. Zhao, G. Wang, S. Bhattacharya, and A. Q. Huang, "Voltage and Power Balance Control for a Cascaded H-Bridge Converter-Based Solid-State Transformer," *IEEE Transactions on Power Electronics,* vol. 28, pp. 1523-1532, 2013.

[37] L. Zhang, K. Sun, Y. Xing, L. Feng, and H. Ge, "A Modular Grid-Connected Photovoltaic Generation System Based on DC Bus," *IEEE Transactions on Power Electronics,* vol. 26, pp. 523-531, 2011.

[38] O. Alonso, P. Sanchis, E. Gubia, and L. Marroyo, "Cascaded H-bridge multilevel converter for grid connected photovoltaic generators with independent maximum power point tracking of each solar array," in *Power Electronics Specialist Conference, 2003. PESC '03. 2003 IEEE 34th Annual*, 2003, pp. 731-735 vol.2.

[39] G. Grandi, C. Rossi, D. Ostojic, and D. Casadei, "A New Multilevel Conversion Structure for Grid-Connected PV Applications," *IEEE Transactions on Industrial Electronics*, vol. 56, pp. 4416-4426, 2009.

[40] G. Grandi, D. Ostojic, and D. Casadei, "A novel DC voltage regulation scheme for dual-inverter grid-connected photovoltaic plants," in *Advanced Electromechanical Motion Systems & Electric Drives Joint Symposium, 2009. ELECTROMOTION 2009. 8th International Symposium on*, 2009, pp. 1-6.

[41] G. Grandi and D. Ostojic, "Dual-inverter-based MPPT algorithm for grid-connected photovoltaic systems," in *Clean Electrical Power, 2009 International Conference on*, 2009, pp. 393-398.

[42] Q. Huang, M. Wang, W. Yu, and A. Q. Huang, "Power-weighting-based multiple input and multiple output control strategy for single-phase PV cascaded H-bridge multilevel grid-connected inverter," in *Applied Power Electronics Conference and Exposition (APEC), 2015 IEEE*, 2015, pp. 2148-2153.

[43] B. Xiao, F. Filho, and L. M. Tolbert, "Single-phase cascaded H-bridge multilevel inverter with nonactive power compensation for grid-connected photovoltaic generators," in *Energy Conversion Congress and Exposition (ECCE), 2011 IEEE*, 2011, pp. 2733-2737.

[44] S. Wang, J. Zhao, and C. Shi, "Research on a three-phase cascaded inverter for grid-connected photovoltaic systems," in *Advanced Power System Automation and Protection (APAP), 2011 International Conference on*, 2011, pp. 543-548.

[45] A. Eskandari, V. Javadian, H. Iman-Eini, and M. Yadollahi, "Stable operation of grid connected Cascaded H-Bridge inverter under unbalanced insolation conditions," in *Electric Power and Energy Conversion Systems (EPECS), 2013 3rd International Conference on*, 2013, pp. 1-6.

[46] B. Xiao, K. Shen, J. Mei, F. Filho, and L. M. Tolbert, "Control of cascaded H-bridge multilevel inverter with individual MPPT for grid-connected photovoltaic

generators," in *Energy Conversion Congress and Exposition (ECCE), 2012 IEEE*, 2012, pp. 3715-3721.

[47] Y. Liu, B. Ge, H. Abu-Rub, and F. Z. Peng, "An Effective Control Method for Three-Phase Quasi-Z-Source Cascaded Multilevel Inverter Based Grid-Tie Photovoltaic Power System," *IEEE Transactions on Industrial Electronics*, vol. 61, pp. 6794-6802, 2014.

[48] B. Xiao, L. Hang, C. Riley, L. M. Tolbert, and B. Ozpineci, "Three-phase modular cascaded H-bridge multilevel inverter with individual MPPT for grid-connected photovoltaic systems," in *Applied Power Electronics Conference and Exposition (APEC), 2013 Twenty-Eighth Annual IEEE*, 2013, pp. 468-474.

[49] B. Xiao and L. M. Tolbert, "Efficiency improved and current balanced three-phase modular cascaded H-bridge multilevel PV inverter for grid-connected applications," in *Energy Conversion Congress and Exposition (ECCE), 2014 IEEE*, 2014, pp. 4661-4669.

[50] S. A. Khajehoddin, A. Bakhshai, and P. Jain, "The Application of the Cascaded Multilevel Converters in Grid Connected Photovoltaic Systems," in *Electrical Power Conference, 2007. EPC 2007. IEEE Canada*, 2007, pp. 296-301.

[51] S. Dongsen, G. Baoming, F. Z. Peng, A. R. Haitham, B. Daqiang, and L. Yushan, "A new grid-connected PV system based on cascaded H-bridge quasi-Z source inverter," in *Industrial Electronics (ISIE), 2012 IEEE International Symposium on*, 2012, pp. 951-956.

[52] L. Liu, H. Li, and Y. Xue, "A coordinated active and reactive power control strategy for grid-connected cascaded photovoltaic (PV) system in high voltage high power applications," in *Applied Power Electronics Conference and Exposition (APEC), 2013 Twenty-Eighth Annual IEEE*, 2013, pp. 1301-1308.

[53] C. Boonmee and Y. Kumsuwan, "Control of single-phase cascaded H-bridge multilevel inverter with modified MPPT for grid-connected photovoltaic systems," in *Industrial Electronics Society, IECON 2013 - 39th Annual Conference of the IEEE*, 2013, pp. 566-571.

[54] L. Liu, H. Li, Y. Xue, and W. Liu, "Decoupled Active and Reactive Power Control for Large-Scale Grid-Connected Photovoltaic Systems Using Cascaded Modular

Multilevel Converters," *IEEE Transactions on Power Electronics,* vol. 30, pp. 176-187, 2015.

[55] S. Skogestad and I. Postlethwaite, *Multivariable feedback control: analysis and design*: Wiley, 1996.

[56] S. Skogestad and I. Postlethwaite, *Multivariable Feedback Control: Analysis and Design*: John Wiley \& Sons, 2005.

[57] E. Bristol, "On a new measure of interaction for multivariable process control," *Automatic Control, IEEE Transactions on,* vol. 11, pp. 133-134, 1966.

[58] A. K. Swain, M. J. Neath, U. K. Madawala, and D. J. Thrimawithana, "A Dynamic Multivariable State-Space Model for Bidirectional Inductive Power Transfer Systems," *IEEE Transactions on Power Electronics,* vol. 27, pp. 4772-4780, 2012.

[59] J. E. Espinoza, J. R. Espinoza, and L. A. Moran, "A systematic controller-design approach for neutral-point-clamped three-level inverters," *IEEE Transactions on Industrial Electronics,* vol. 52, pp. 1589-1599, 2005.

[60] Y. Pipelzadeh, N. R. Chaudhuri, B. Chaudhuri, and T. C. Green, "System stability improvement through optimal control allocation in voltage source converter-based high-voltage direct current links," *IET Generation, Transmission & Distribution,* vol. 6, pp. 811-821, 2012.

[61] M. Veerachary, "Two-Loop Controlled Buck–SEPIC Converter for Input Source Power Management," *IEEE Transactions on Industrial Electronics,* vol. 59, pp. 4075-4087, 2012.

[62] J.-W. Chang and C.-C. Yu, "The relative gain for non-square multivariable systems," *Chemical Engineering Science,* vol. 45, pp. 1309-1323, 1990/01/01 1990.

[63] W. Hu, W. J. Cai, and G. Xiao, "Relative gain array for MIMO processes containing integrators and/or differentiators," in *Control Automation Robotics & Vision (ICARCV), 2010 11th International Conference on*, 2010, pp. 231-235.

[64] X. Liang, "Emerging Power Quality Challenges Due to Integration of Renewable Energy Sources," *IEEE Transactions on Industry Applications,* vol. 53, pp. 855-866, 2017.

[65] T. Caldognetto, P. Tenti, A. Costabeber, and P. Mattavelli, "Improving Microgrid Performance by Cooperative Control of Distributed Energy Sources," *IEEE Transactions on Industry Applications,* vol. 50, pp. 3921-3930, 2014.

[66] J. H. R. Enslin and P. J. M. Heskes, "Harmonic interaction between a large number of distributed power inverters and the distribution network," *IEEE Transactions on Power Electronics*, vol. 19, pp. 1586-1593, 2004.

[67] X, P. A. Gray, and P. W. Lehn, "New Metric Recommended for IEEE Standard 1547 to Limit Harmonics Injected Into Distorted Grids," *IEEE Transactions on Power Delivery,* vol. 31, pp. 963-972, 2016.

[68] F. Wang, J. L. Duarte, M. A. M. Hendrix, and P. F. Ribeiro, "Modeling and Analysis of Grid Harmonic Distortion Impact of Aggregated DG Inverters," *IEEE Transactions on Power Electronics,* vol. 26, pp. 786-797, 2011.

[69] H. S. Goh, M. Armstrong, and B. Zahawi, "The effect of grid operating conditions on the current controller performance of grid connected photovoltaic inverters," in *2009 13th European Conference on Power Electronics and Applications*, 2009, pp. 1-8.

[70] Y. A. R. I. Mohamed, "Mitigation of Dynamic, Unbalanced, and Harmonic Voltage Disturbances Using Grid-Connected Inverters With <formula formulatype="inline"> <img src="/images/tex/749.gif" alt="LCL"> </formula> Filter," *IEEE Transactions on Industrial Electronics,* vol. 58, pp. 3914-3924, 2011.

[71] Y. Jia, J. Zhao, and X. Fu, "Direct Grid Current Control of LCL-Filtered Grid-Connected Inverter Mitigating Grid Voltage Disturbance," *IEEE Transactions on Power Electronics,* vol. 29, pp. 1532-1541, 2014.

[72] Y. Chen, A. Luo, Z. Shuai, and S. Xie, "Robust predictive dual-loop control strategy with reactive power compensation for single-phase grid-connected distributed generation system," *Power Electronics, IET,* vol. 6, pp. 1320-1328, 2013.

[73] T. Erika and D. G. Holmes, "Grid current regulation of a three-phase voltage source inverter with an LCL input filter," *IEEE Transactions on Power Electronics,* vol. 18, pp. 888-895, 2003.

[74] H. Jafarian, B. Parkhideh, J. Enslin, R. Cox, and S. Bhowmik, "On reactive power injection control of distributed grid-tied AC-stacked PV inverter architecture," in *2016 IEEE Energy Conversion Congress and Exposition (ECCE)*, 2016, pp. 1-6.

[75] M. Yilmaz and P. T. Krein, "Review of the Impact of Vehicle-to-Grid Technologies on Distribution Systems and Utility Interfaces," *IEEE Transactions on Power Electronics*, vol. 28, pp. 5673-5689, 2013.

[76] X. Wu, X. Li, X. Yuan, and Y. Geng, "Grid Harmonics Suppression Scheme for <italic>LCL</italic>-Type Grid-Connected Inverters Based on Output Admittance Revision," *IEEE Transactions on Sustainable Energy*, vol. 6, pp. 411-421, 2015.

[77] X. Wang, X. Ruan, S. Liu, and C. K. Tse, "Full Feedforward of Grid Voltage for Grid-Connected Inverter With LCL Filter to Suppress Current Distortion Due to Grid Voltage Harmonics," *IEEE Transactions on Power Electronics*, vol. 25, pp. 3119-3127, 2010.

[78] W. Li, X. Ruan, D. Pan, and X. Wang, "Full-Feedforward Schemes of Grid Voltages for a Three-Phase <formula formulatype="inline"> <img src="/images/tex/749.gif" alt="LCL"> </formula>-Type Grid-Connected Inverter," *IEEE Transactions on Industrial Electronics*, vol. 60, pp. 2237-2250, 2013.

[79] T. Abeyasekera, C. M. Johnson, D. J. Atkinson, and M. Armstrong, "Suppression of line voltage related distortion in current controlled grid connected inverters," *IEEE Transactions on Power Electronics*, vol. 20, pp. 1393-1401, 2005.

[80] M. Liserre, R. Teodorescu, and F. Blaabjerg, "Stability of photovoltaic and wind turbine grid-connected inverters for a large set of grid impedance values," *IEEE Transactions on Power Electronics*, vol. 21, pp. 263-272, 2006.

[81] T. Geury, S. Pinto, and J. Gyselinck, "Current source inverter-based photovoltaic system with enhanced active filtering functionalities," *IET Power Electronics*, vol. 8, pp. 2483-2491, 2015.

[82] W. H. Ko and J. C. Gu, "Impact of Shunt Active Harmonic Filter on Harmonic Current Distortion of Voltage Source Inverter-Fed Drives," *IEEE Transactions on Industry Applications*, vol. 52, pp. 2816-2825, 2016.

[83] W. Huai, M. Ke, and F. Blaabjerg, "Design for reliability of power electronic systems," in *IECON 2012 - 38th Annual Conference on IEEE Industrial Electronics Society*, 2012, pp. 33-44.

[84] A. Pigazo, M. Liserre, F. Blaabjerg, and T. Kerekes, "Robustness analysis of the efficiency in PV inverters," in *Industrial Electronics Society, IECON 2013 - 39th Annual Conference of the IEEE*, 2013, pp. 7015-7020.

[85] N. C. Sintamarean, F. Blaabjerg, W. Huai, F. Iannuzzo, and P. de Place Rimmen, "Reliability Oriented Design Tool For the New Generation of Grid Connected PV-Inverters," *Power Electronics, IEEE Transactions on,* vol. 30, pp. 2635-2644, 2015.

[86] D. Ricchiuto, M. Liserre, T. Kerekes, R. Teodorescu, and F. Blaabjerg, "Robustness analysis of active damping methods for an inverter connected to the grid with an LCL-filter," in *Energy Conversion Congress and Exposition (ECCE), 2011 IEEE*, 2011, pp. 2028-2035.

[87] H. Jedtberg, A. Pigazo, M. Liserre, and G. Buticchi, "Analysis of the Robustness of Transformerless PV Inverter Topologies to the Choice of Power Devices," *IEEE Transactions on Power Electronics,* vol. 32, pp. 5248-5257, 2017.

[88] M. Biglarbegian, N. Shah, I. Mazhari, J. Enslin, and B. Parkhideh, "Design and evaluation of high current PCB embedded inductor for high frequency inverters," in *2016 IEEE Applied Power Electronics Conference and Exposition (APEC)*, 2016, pp. 2998-3003.

[89] M. Biglarbegian, N. Shah, I. Mazhari, and B. Parkhideh, "Design considerations for high power density/efficient PCB embedded inductor," in *Wide Bandgap Power Devices and Applications (WiPDA), 2015 IEEE 3rd Workshop on*, 2015, pp. 247-252.

[90] H. Jedtberg, A. Pigazo, and M. Liserre, "Robustness evaluation of transformerless PV inverter topologies," in *Control and Modeling for Power Electronics (COMPEL), 2014 IEEE 15th Workshop on*, 2014, pp. 1-5.

[91] M. Martino, C. Citro, K. Rouzbehi, and P. Rodriguez, "Efficiency Analysis of Single-Phase Photovoltaic Transformer-less Inverters," in *International Conference on Renewable Energies and Power Quality (ICREPQ), 2012*, 2012.

[92] J. Selvaraj and N. A. Rahim, "Multilevel Inverter For Grid-Connected PV System Employing Digital PI Controller," *Industrial Electronics, IEEE Transactions on,* vol. 56, pp. 149-158, 2009.

[93] Y. Yongheng, Z. Keliang, and F. Blaabjerg, "Harmonics suppression for single-phase grid-connected PV systems in different operation modes," in *Applied Power Electronics Conference and Exposition (APEC), 2013 Twenty-Eighth Annual IEEE*, 2013, pp. 889-896.

[94] A. Kulkarni and V. John, "Mitigation of Lower Order Harmonics in a Grid-Connected Single-Phase PV Inverter," *Power Electronics, IEEE Transactions on,* vol. 28, pp. 5024-5037, 2013.

[95] H. Jafarian, B. Parkhideh, and S. Bhowmik, "A novel comparative robustness index for evaluating the performance of grid-tied PV inverters," in *2016 IEEE 43rd Photovoltaic Specialists Conference (PVSC)*, 2016, pp. 1254-1259.

[96] B. P. Hamidreza Jafarian, Shibashis Bhowmik, "A Novel Comparative Robustness Index for Evaluating the Performance

of Grid-tied PV inverters," in *Photovoltaic Specialists Conference (PVSC),*, Portland, 2016, p. In press.

[97] D. Yang, D. D. C. Lu, G. M. L. Chu, and X. Weidong, "Closed-Form Solution of Time-Varying Model and Its Applications for Output Current Harmonics in Two-Stage PV Inverter," *Sustainable Energy, IEEE Transactions on,* vol. 6, pp. 142-150, 2015.

[98] A. Driesse, S. Harrison, and P. Jain, "Evaluating the Effectiveness of Maximum Power Point Tracking Methods in Photovoltaic Power Systems using Array Performance Models," in *Power Electronics Specialists Conference, 2007. PESC 2007. IEEE*, 2007, pp. 145-151.

[99] M. Jantsch, M. Real, H. Häberlin, C. Whitaker, K. Kurokawa, G. Blässer*, et al.*, "Measurement of PV maximum power point tracking performance," in *14th European photovoltaic solar energy conference and exhibition*, Barcelona, 1997.

[100] "IEEE Recommended Practices and Requirements for Harmonic Control in Electrical Power Systems," *IEEE Std 519-1992,* pp. 1-112, 1993.

[101] "IEEE Recommended Practice and Requirements for Harmonic Control in Electric Power Systems," *IEEE Std 519-2014 (Revision of IEEE Std 519-1992)*, pp. 1-29, 2014.

[102] G. Fishman, *Monte Carlo Concepts, Algorithms, and Applications*: Springer, 1996.

[103] A. Pregelj, M. Begovic, and A. Rohatgi, "Impact of inverter configuration on PV system reliability and energy production," in *Photovoltaic Specialists Conference, 2002. Conference Record of the Twenty-Ninth IEEE*, 2002, pp. 1388-1391.

[104] C. Bailey, T. Tilford, and H. Lu, "Reliability Analysis for Power Electronics Modules," in *2007 30th International Spring Seminar on Electronics Technology (ISSE)*, 2007, pp. 12-17.

[105] M. Keramat and R. Kielbasa, "Modified Latin Hypercube Sampling Monte Carlo (MLHSMC) Estimation for Average Quality Index," *Analog Integr. Circuits Signal Process.*, vol. 19, pp. 87-98, 1999.

[106] J. F. Swidzinski, M. Keramat, and K. Chang, "A novel approach to efficient yield estimation for microwave integrated circuits," in *Circuits and Systems, 1999. 42nd Midwest Symposium on*, 1999, pp. 367-370 vol. 1.

[107] Y. Bae, T. K. Vu, and R. Y. Kim, "Implemental Control Strategy for Grid Stabilization of Grid-Connected PV System Based on German Grid Code in Symmetrical Low-to-Medium Voltage Network," *IEEE Transactions on Energy Conversion*, vol. 28, pp. 619-631, 2013.